TTI: 2/3-18-88-1175-1

DYNAMIC ANALYSIS OF FALLING-WEIGHT DEFLECTOMETER DATA

RESEARCH REPORT 1175-1

COOPERATIVE RESEARCH PROGRAM

TEXAS TRANSPORTATION INSTITUTE
THE TEXAS A&M UNIVERSITY SYSTEM
COLLEGE STATION, TEXAS

STATE DEPARTMENT OF HIGHWAYS
AND PUBLIC TRANSPORTATION

in cooperation with the
U.S. Department of Transportation
Federal Highway Administration

TECHNICAL REPORT STANDARD TITLE PAGE

1. Report No.	2. Government Accession No.	3. Recipient's Catalog No.
TX-89/1175-1		

4. Title and Subtitle	5. Report Date
Dynamic Analysis of Falling-Weight Deflectometer Data	September 1988
	6. Performing Organization Code Research Report 1175-1
7. Author(s) Allen H. Magnuson	8. Performing Organization Report No.
9. Performing Organization Name and Address Texas Transportation Institute The Texas A&M University System College Station, Texas 77843-3135	10. Work Unit No. 11. Contract or Grant No. Study No. 2/3-18-88-1175
12. Sponsoring Agency Name and Address Texas State Department of Highways and Public Transportation; Transportation Planning Division P.O. Box 5051 Austin, Texas 78763	13. Type of Report and Period Covered Interim - September 1987 - September 1988 14. Sponsoring Agency Code

15 Supplementary Notes

Research performed in cooperation with and for the U.S. Department of Transportation, Federal Highway Administration

16. Abstract

Falling-Weight Deflectometer data from three in-service pavement sections has been used to analyze dynamic response characteristics. The analyzed data will be used later in the project along with computer predictions of pavement response to back-calculate engineering properties of pavements. The pavements had thicknesses of 1.5 in., 9 in., and 12 in., and two load levels were tested. The full pulse data is presented for the dropweight force and all seven surface displacement sensors. The analysis was performed in the frequency domain using frequency response functions computed from the pulse data. The frequency response functions were computed by dividing the Fast Fourier Transform (FFT) of the displacements by the FFT of the force. Magnitude and phase angles of the frequency response functions are presented. An undesirable oscillation was present in the frequency response functions. This was attributed to a discontinuity in the displacement pulses resulting from zero-packing in the FFT Program. The pulses have a non-zero "tail" value at the end of the 60 msec sample period which causes the discontinuity. The pulse "tail" may be due to drift, permanent deformation of the pavement, or premature truncation before the transient response has died out. A linear correction to the pulses that eliminated the discontinuity was applied to one test case. This eliminated the undesirable oscillation, giving the responses a more regular behavior similar to predicted theoretical responses. This correction should facilitate comparison studies of computed versus measured FWD responses.

17. Key Words	18. Distribution Statement
Non-Destructive Testing of Pavements, Non-Destructive Evaluation of Pavements, Falling-Weight Deflectometer, Dynamic Analysis of Pavements, Asphaltic Concrete Pavements	No restrictions. This document is available to the public through the National Technical Information Service 5285 Port Royal Road Springfield, Virginia 22161

19. Security Classif. (of this report)	20. Security Classif. (of this page)	21. No. of Pages	22. Price
Unclassified	Unclassified	90	

Form DOT F 1700.7 (8-69)

DYNAMIC ANALYSIS OF FALLING-WEIGHT DEFLECTOMETER DATA

by

Allen H. Magnuson

Research Report 1175-1

Research Study No. 2/3-18-88-1175

Sponsored by

Texas State Department of Highways and Public Transportation

Maintenance and Operations Division

and

In Cooperation With The U.S. Department of Transportation

and Federal Highway Administration

Texas Transportation Institute
Texas A&M University
College Station, Texas 77843

September 1988

METRIC (SI*) CONVERSION FACTORS

APPROXIMATE CONVERSIONS TO SI UNITS

Symbol	When You Know	Multiply By	To Find	Symbol
LENGTH				
in	inches	2.54	millimetres	mm
ft	feet	0.3048	metres	m
yd	yards	0.914	metres	m
mi	miles	1.61	kilometres	km
AREA				
in²	square inches	645.2	millimetres squared	mm²
ft²	square feet	0.0929	metres squared	m²
yd²	square yards	0.836	metres squared	m²
mi²	square miles	2.59	kilometres squared	km²
ac	acres	0.395	hectares	ha
MASS (weight)				
oz	ounces	28.35	grams	g
lb	pounds	0.454	kilograms	kg
T	short tons (2000 lb)	0.907	megagrams	Mg
VOLUME				
fl oz	fluid ounces	29.57	millilitres	mL
gal	gallons	3.785	litres	L
ft³	cubic feet	0.0328	metres cubed	m³
yd³	cubic yards	0.0765	metres cubed	m³

NOTE: Volumes greater than 1000 L shall be shown in m³.

TEMPERATURE (exact)

°F	Fahrenheit temperature	5/9 (after subtracting 32)	Celsius temperature	°C

APPROXIMATE CONVERSIONS TO SI UNITS

Symbol	When You Know	Multiply By	To Find	Symbol
LENGTH				
mm	millimetres	0.039	inches	in
m	metres	3.28	feet	ft
m	metres	1.09	yards	yd
km	kilometres	0.621	miles	mi
AREA				
mm²	millimetres squared	0.0016	square inches	in²
m²	metres squared	10.764	square feet	ft²
km²	kilometres squared	0.39	square miles	mi²
ha	hectores (10 000 m²)	2.53	acres	ac
MASS (weight)				
g	grams	0.0353	ounces	oz
kg	kilograms	2.205	pounds	lb
Mg	megagrams (1 000 kg)	1.103	short tons	T
VOLUME				
mL	millilitres	0.034	fluid ounces	fl oz
L	litres	0.264	gallons	gal
m³	metres cubed	35.315	cubic feet	ft³
m³	metres cubed	1.308	cubic yards	yd³

TEMPERATURE (exact)

°C	Celsius temperature	9/5 (then add 32)	Fahrenheit temperature	°F

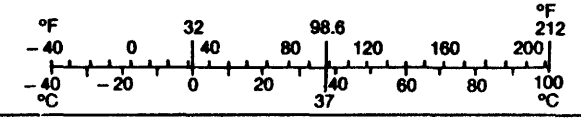

These factors conform to the requirement of FHWA Order 5190.1A.

* SI is the symbol for the International System of Measurements

ABSTRACT

Falling-Weight Deflectometer data from three in-service pavement sections has been used to analyze dynamic response characteristics. The analyzed data will be used later in the project along with computer predictions of pavement response to back-calculate engineering properties of pavements. The pavements had thicknesses of 1.5 in., 9 in., and 12 in., and two load levels were tested. The full pulse data is presented for the dropweight force and all seven surface displacement sensors. The analysis was performed in the frequency domain using frequency response functions computed from the pulse data. The frequency response functions were computed by dividing the Fast Fourier Transform (FFT) of the displacements by the FFT of the force. Magnitude and phase angles of the frequency response functions are presented. An undesirable oscillation was present in the frequency response functions. This was attributed to a discontinuity in the displacement pulses resulting from zero-packing in the FFT program. The pulses have a non-zero "tail" value at the end of the 60 msec sample period which causes the discontinuity. The pulse "tail" may be due to drift, permanent deformation of the pavement, or premature truncation before the transient response has died out. A linear correction to the pulses that eliminated the discontinuity was applied to one test case. This eliminated the undesirable oscillation, giving the responses a more regular behavior similar to predicted theoretical responses. This correction should facilitate comparison studies of computed versus measured FWD responses.

DISCLAIMER

The contents of this report reflect the views of the author who is responsible for the opinions, findings, and conclusions herein. The contents do not necessarily reflect the official views or policies of the Federal Highway Administration or the Texas State Department of Highways and Public Transportation. This report does not constitute a standard, specification, or regulation.

ACKNOWLEDGEMENTS

The author wishes to express thanks to Mr. R. Briggs of the Texas State Department of Highways and Public Transportation for supporting this research project, for his guidance and encouragement and for useful suggestions on modifications of the draft copy of the report.

The author also wishes to acknowledge the contributions of other members of the TTI staff: Dr. R.L. Lytton for helpful suggestions and for encouragement and support; Mr. F. Germann for acquiring the Dynatest FWD data, Mr. P. Chan for developing the FFT and frequency-response program listed in Appendix A and Mr. V.S. Torpunuri for performing the data analysis computations and preparing the data plots.

TABLE OF CONTENTS

LIST OF FIGURES

LIST OF TABLES

CHAPTER I

INTRODUCTION

Background

This study is part of the Texas State Department of Highways and Public Transportation Project 2/3-18-88-1175 entitled "Development of Dynamic Analysis techniques for Falling-Weight Deflectometer Data." The report has been written in preparation for Task 2 of this project: "Measurement and Verification of Deflection and Surface Wave Data."

Task 1 of the Project 1175 called for selection of pavement sections for nondestructive test measurements. Thirty highway sections were selected under this task. The sections are from Districts 1, 8, 11, and 21 and the TTI pavement Test Facility. The sections selected make maximum use of data from related studies. Most sites are monitored under Projects 1123, 1159, 473, and NCHRP 10-27. The locations of the test sites are shown in Figure 1. The characteristics of the in-service highway sections are shown in Table 1 where the pavement type and subgrade conditions, as well as special cases, are indicated. Special cases include rock ledge subgrade and cement-stabilized base sections.

Dynamic data from all these sites will be acquired using the Falling-Weight Deflectometer system which consists of the dropweight apparatus and a series of geophones mounted on a trailer as shown in Figure 2. The trailer is towed by a van containing electronic apparatus (computer and associated peripheral devices) for data acquisition, remote operation of the test and data analysis and display. During testing, the dropweights are raised by a hydraulic piston and released remotely by the operator in the van. At a given test site, the geophones are raised and lowered hydraulically. The test operation, including data acquisition and analysis, is performed remotely by the operator in the van. Because the whole operation is automated, great quantities of data can be acquired in a short time. Normally, only the peak values of the dropweight force and deflection are measured and recorded. The peak values are assumed to represent a static deflection basin. The peak values are used for the backcalculation analysis which assumes the pavement is a layered linear elastic (static) solid. However, the full-time history of the force and deflection pulses can be recorded if desired for dynamic analysis. This report will show how the full-time history can be analyzed and interpreted for dynamic analysis purposes.

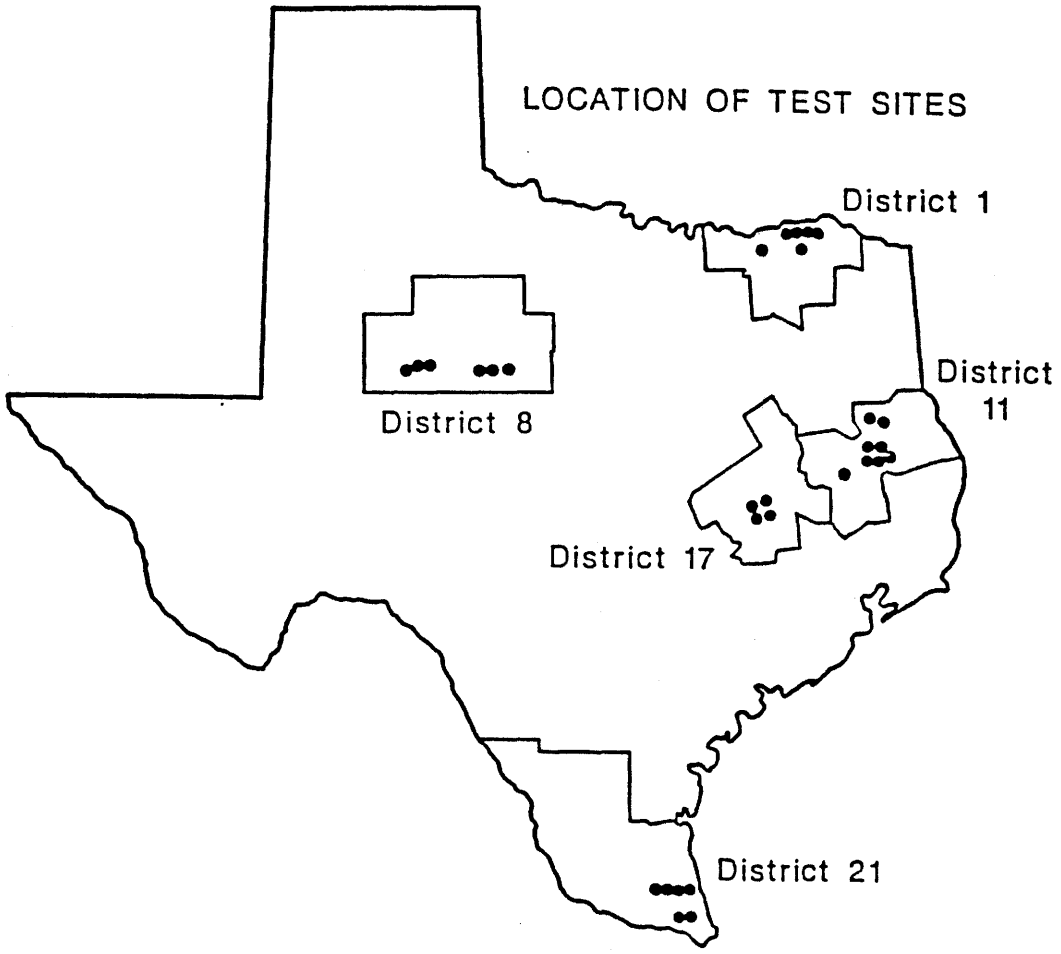

Figure 1. Location of Monitored Highway Sites Selected for Dynamic Analysis Using Falling-Weight Deflectometer Data

TABLE 1.

Pavement Sections Selected for Dynamic Analysis Using the Falling-Weight Deflectometer.

Subgrade Conditions		Pavement Type		
		Surface Treated (Thin)	Medium (2"-5")Thick A.C. on Granular Base	Thick (6" or more) A.C. on Granular Base
Clay	wet	8.6, 21.2	21.4	8.5, 11.1, 21.5
Clay	dry	1.3, 11.3, 11.4	1.2, 1.5, 21.6	1.1, 1.4
Sand	wet	21.1	8.2	21.3
Sand	dry	1.6, 8.1, 11.5	(8.3)	11.2, (8.4)
Shallow Bedrock			8.3	8.4
Cement Stabilized Base		11.9	11.8	11.7

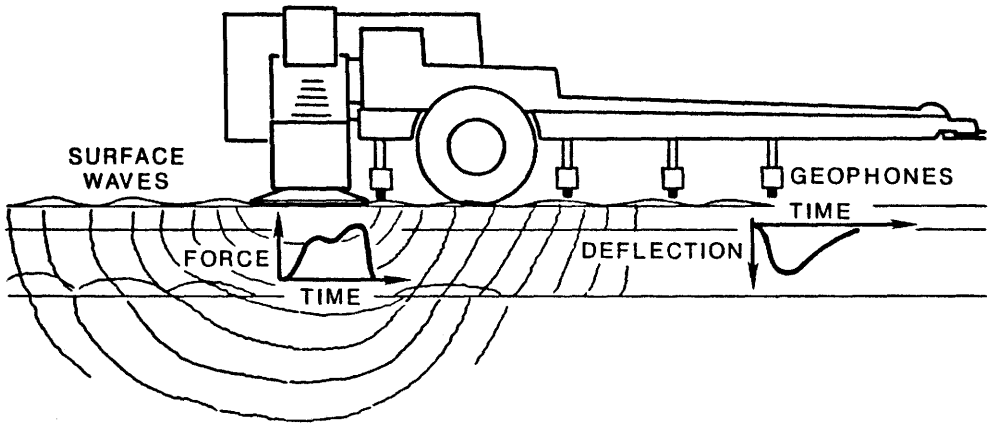

Figure 2. Schematic Diagram of the Dynatest Falling-Weight Deflectometer

The FWD nondestructive test data to be collected for this project includes the complete load impulse and geophone response signals, making available for the first time masses of pavement data that can, if analyzed properly, give useful information on the dynamic response of pavements. This research builds on the extensive past and ongoing work at TTI on pavement technology, design, research, testing, and evaluation, (Lytton, Roberts, and Stoffels, 1986; Lytton, 1988).

The overall approach or strategy of this research project is to extend or build on existing methods of extracting pavement properties from FWD data. Current practice is to use elastic (static) models to extract information on the properties of pavements, e.g, back-calculating elastic moduli for each layer (Uzan, Lytton, and Germann, 1988). Full use is not being made of the data which contains information on the dynamic properties of the pavement layers. Visco-elastic behavior such as creep and relaxation is exhibited in the pavement layers. To extract this information, new techniques must be developed that use analytical models of the dynamic properties. This is the ultimate objective of Project 1175. The work of Magnuson (1988) is the first step in developing a fast, efficient predictive computer program for pavement dynamics including viscoelastic effects. Successful completion of the project should result in new methods for:

1. More accurate determination of surface layer moduli,
2. Determination of layer thicknesses by data analysis rather than by labor-intensive core sampling and laboratory analysis,
3. Development of an improved structural index,
4. Prediction of remaining life of pavements, and
5. Possible in situ measurement of the rutting properties of pavements, using the FWD as a pavement evaluation tool.

Monitored sections from District 1 were chosen for a pilot study of FWD dynamic analysis. (See Table 1). The characteristics of the pavement section selected for the pilot study are given in Table 2. This study is based primarily on State Highways 19 and 24 having a 9-inch thick asphaltic concrete pavement. For comparison purposes, data is also presented for a thin (1.5 inch) pavement from Farm-to-Market road 79 and a thick (12-inch) pavement from State Highway 82.

Table 2. Description of Analyzed Pavement Sections (District 1)

Section	County	Pavement Section	Route	Location and/or Mile Post	Surface	Base	Subbase	Subgrade	Groundwater
1.1	Lamar	Thick	State 19 & 24	Paris, Texas to Sulphur River	9" AC	7" Crushed Stone	10" Lime-Treated Clay	Clay	No
1.4	Lamar	Thick	State 82	East of Loop 271	12" AC	22" Sandy S/G	---	Clay	No
1.6	Lamar	Thin	FM 79	0.7 miles East of Pine Creek	1.5" AC	6" Flex	6" Lime-treated Material	Silty Sand	No

Objectives

The major objectives of this study were to introduce dynamic pavement analysis methods to the highway engineering community and to prepare the way for the upcoming large-scale data acquisition and analysis effort. Other related objectives are to:

1. Present proposed standardized procedures for reducing and presenting data for use in subsequent comparison studies of computed versus measured FWD responses. In the comparison studies, key engineering properties related to pavement life and performance will be extracted by an iterative back-calculation procedure.
2. Develop a computerized system for data analysis and plotting.
3. Demonstrate how the dynamic response data looks and how to interpret it.
4. Point out any problems in analyzing data and present ways to resolve them.

CHAPTER II

DYNAMIC ANALYSIS OF PAVEMENTS

The purpose of this chapter is to introduce some "linear systems" concepts that are helpful in understanding pavement dynamics. The system concept involves a transformation of an input into an output. The system can be described or characterized by how it transforms the input into the output; that is, the system can be treated as an unknown "black box": where only the input and output are known.

The system description can be done in the time domain or in the frequency domain. The most direct approach is to use the time domain. However, the frequency domain characterization provides more insight into specific phenomena occurring within the system; therefore, it is a better "diagnostic" or analysis tool. The system concept will be described briefly here as it applies to pavement dynamics in both the time and frequency domains. The system approach is described in many books, for example Bendat and Piersol (1971), Bendat and Piersol (1980) and Lee (1960).

The FWD provides both input and output data to characterize the pavement section as a system. The input (excitation or forcing function) is the force, and the output or responses are each of the surface deflections, as shown in Figure 3a. The output for a linear system, z(t), is related to the input, F(t), by the impulse response function, h(t), which is used in the convolution (or superposition) integral as follows:

$$z(t) = \int_{-\infty}^{\infty} h(\tau)\, F\,(t - \tau)\, d\tau \qquad (1)$$

where τ = Dummy time variable associated with the "shift" of the input F.

The FWD force and deflection time pulse data can, in principle, be used to compute the impulse response function, h(t), through a computational deconvolution procedure. This will characterize or describe the input-output relationships for the given system. Note that the response from each displacement sensor will give a different impulse response function, or a different "system."

Generally, when analyzing a relatively unknown system (such as the dynamic

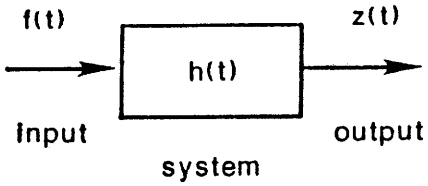

Figure 3a. Input-Output Relation in Time Domain.

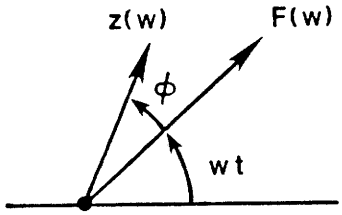

Figure 3b. Phasor Diagram of Input and Output.

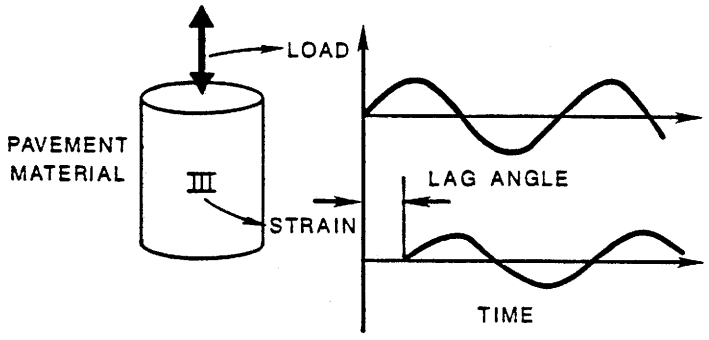

Figure 3c. Sketch Showing Lag Angle Introduced by Internal (Material) Damping.

response of a highway section), it is preferable to work in the so-called frequency domain. This is because more physical insight can be obtained on the system, even though the method appears to be less direct than working in the time domain. Another advantage of working in the frequency domain, is that the theoretical predicted responses are more readily computed in the frequency domain. Therefore, comparisons between theory and experiment can be made more readily in the frequency domain and differences can be "diagnosed" better. For example, specific phenomena such as natural frequencies, normal modes or surface waves, can be detected and damping effects can be identified directly.

To work in the frequency domain, it is necessary to perform a transformation on the time pulse data. This is done using a Fourier integral transform (Lee, 1960). If the time pulse signal is designated as f(t), its Fourier integral transform is denoted $F(\omega)$, defined as follows:

$$F(\omega) = \int_{-\infty}^{\infty} f(t)e^{-i\omega t}\, dt \tag{2}$$

where: i^2 = -1, and

ω = is the radian frequency.

The inverse transform recovers the time pulse from the frequency domain transform $F(\omega)$ as follows:

$$f(t) = \frac{1}{2\pi}\int_{-\infty}^{\infty} F(\omega)e^{i\omega t}\, d\omega \tag{3}$$

Equation (3) can be considered to be a synthesis or addition of oscillatory responses with $F(\omega)$ acting as the weighting function used to synthesize a given pulse f(t). The exponential term $e^{i\omega t}$ is the kernel of this transform and it can be expanded as follows:

$$e^{\pm i\omega t} = \cos \omega t \pm i \sin \omega t \tag{4}$$

This means the transform $F(\omega)$ is a complex number having a real and imaginary part.

In practice, the Fourier Transform (2) is performed on experimental data using a computer program with a Fast Fourier Transform (FFT) algorithm (Davis and

Rabinowitz, 1975). The FFT treats the pulse as a periodic (repeated or cyclic) function with a period T which varies with the number of sample points and the sampling interval. It is customary to use zero-packing to extend the pulse to a convenient point depending on the desired resolution of the transformed function. This will be discussed in more detail in Chapter IV.

The frequency domain counterpart to the convolution integral input-output relation in Equation (1) is written as:

$$Z(\omega) = H(\omega)\ F(\omega) \tag{5}$$

where: $Z(\omega)$ = Fourier-transformed displacement (output),
$F(\omega)$ = Fourier-transformed force (input), and
$H(\omega)$ = frequency-response function.

This relation (5) is simpler than the convolution integral relation, which is part of the reason for working in the frequency domain. The frequency response function is a complex number having a magnitude and phase angle associated with it, both defined as follows:

$$H(\omega) = H_R(\omega) + i\ H_I\ (\omega) = |H| e^{i\phi_H} \tag{6}$$

where: H_R = real part,
H_I = imaginary part,
$|H|$ = $(H_R^2 + H_I^2)^{\frac{1}{2}}$ = magnitude, and
ϕ_H = $\tan^{-1}\ (H_I/H_R)$ = phase angle.

The significance of the response function may be illustrated by taking an oscillatory cosine forcing function:

$$f(t) = F_o \cos \omega t = F_o\ R_e\ (e^{i\omega t})$$

where: R_e indicates taking the real part. From Equations (5) and (6), the time domain response z(t) is:

$$z(t) = F_o\ |H|\ R_e\{e^{\omega t+\phi_H}\} = F_o\ |H|\ \cos\ (\omega t + \phi_H\ ) \tag{7}$$

This result indicates why $H(\omega)$ is referred to as a frequency response function: for a unit cosine forcing function ($F_o = 1$), the magnitude of the response of the system is the magnitude of the frequency response function $|H|$,

and the phase shift or phase angle response is the phase angle (ϕ_H) of the frequency response function.

This can be interpreted graphically with a phasor diagram shown in Figure 3b. The oscillatory force $F(\omega)$ and the response $z(\omega)$ are drawn as rotating vectors in the complex plane, both rotating counterclockwise at an angular velocity, ω. The response leads the force by the phase angle ϕ_H while the magnitude of the response is given as:

$$|Z| = F_o |H|$$

That is, the output to an oscillatory input for a given frequency is characterized by a change in magnitude and a phase shift relative to the input, as indicated in Equation (7). The phase shift for the pavement is caused by inertia or wave effects and internal damping, as shown in Figure 3c.

The pavement system is to be characterized dynamically by the frequency response function. This is done by solving for $H(\omega)$ in Equation (5):

$$H(\omega) = Z(\omega)/F(\omega) \tag{8}$$

That is, Equation (8) indicates that the frequency response is obtained by dividing the FFT of the response at each sensor location by the FFT of the force pulse. This has been done for pavement sections and the results are shown in Chapter IV.

To this point, the discussion has treated the "system," the highway section as an unknown "black box." The response of the system can also be predicted theoretically (at least to the level of simplifying approximations made in the formulation of the theory). To illustrate what the frequency response functions should look like for a highway section, the theory of Reissner (1936), as modified by Arnold, Bycroft, and Warburton (1955) and Sung (1953), can be used. In this theory,the highway is modeled as a uniform elastic halfspace with a circular uniform oscillatory pressure distribution acting on the surface (Figure 4). The surface displacement at the center of the pressure distribution was computed. This simulates the sensor 1 data on the FWD apparatus after the pulse data is transformed using an FFT.

Reissner introduced a dimensionless representation for the response as follows:

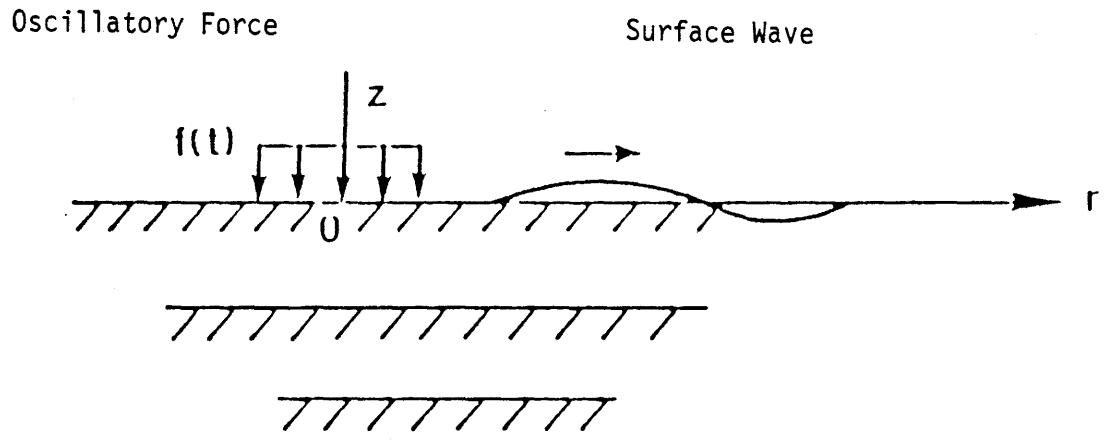

Figure 4. Sketch of Dynamic Testing of Pavements.

$$u_z = \frac{P}{Ga}(f_1 + if_2) \tag{9}$$

where: u_z = surface vertical displacement (dimensional),
P = force magnitude,
G = halfspace rigidity modulus,
a = radius of pressure distribution,
f_1 = real part of the dimensionless response, and
f_2 = imaginary part of the dimensionless response.

Equation (9) indicates that the response is proportional to the force and inversely proportional to the rigidity and the disk radius. The dimensionless functions f_1 and f_2 are in turn functions of Poisson's ratio (μ) and the dimensionless frequency (a_o) defined as:

$$a_o = \frac{\omega a}{C_T} \tag{10}$$

where: the shear wave speed (C_T) is given as
$C_T = (G/\rho)^{\frac{1}{2}}$ and
ρ = mass density ($\gamma = \rho g$).

That is,

$$f_1 = f_1(a_o, \mu)$$
$$f_2 = f_2(a_o, \mu)$$

These functions, f_1 and f_2, are plotted against a_o for various values of Poisson's ratio in Figures 5 and 6 taken from Magnuson (1988).

It is more convenient and easier to interpret the results if the dimensionless functions are expressed in magnitude and phase form as follows:

$$f_1 + if_2 = |f|e^{i\phi_f} \tag{11}$$

where: $|f| = (f_1^2 + f_2^2)^{\frac{1}{2}}$,
$\phi_f = \tan^{-1}(f_2/f_1)$.

The magnitude and phase for a Poisson's ratio of 1/3 are shown in Figures 7 and 8, respectively, taken from Magnuson (1988). Elastic results are from Sung's

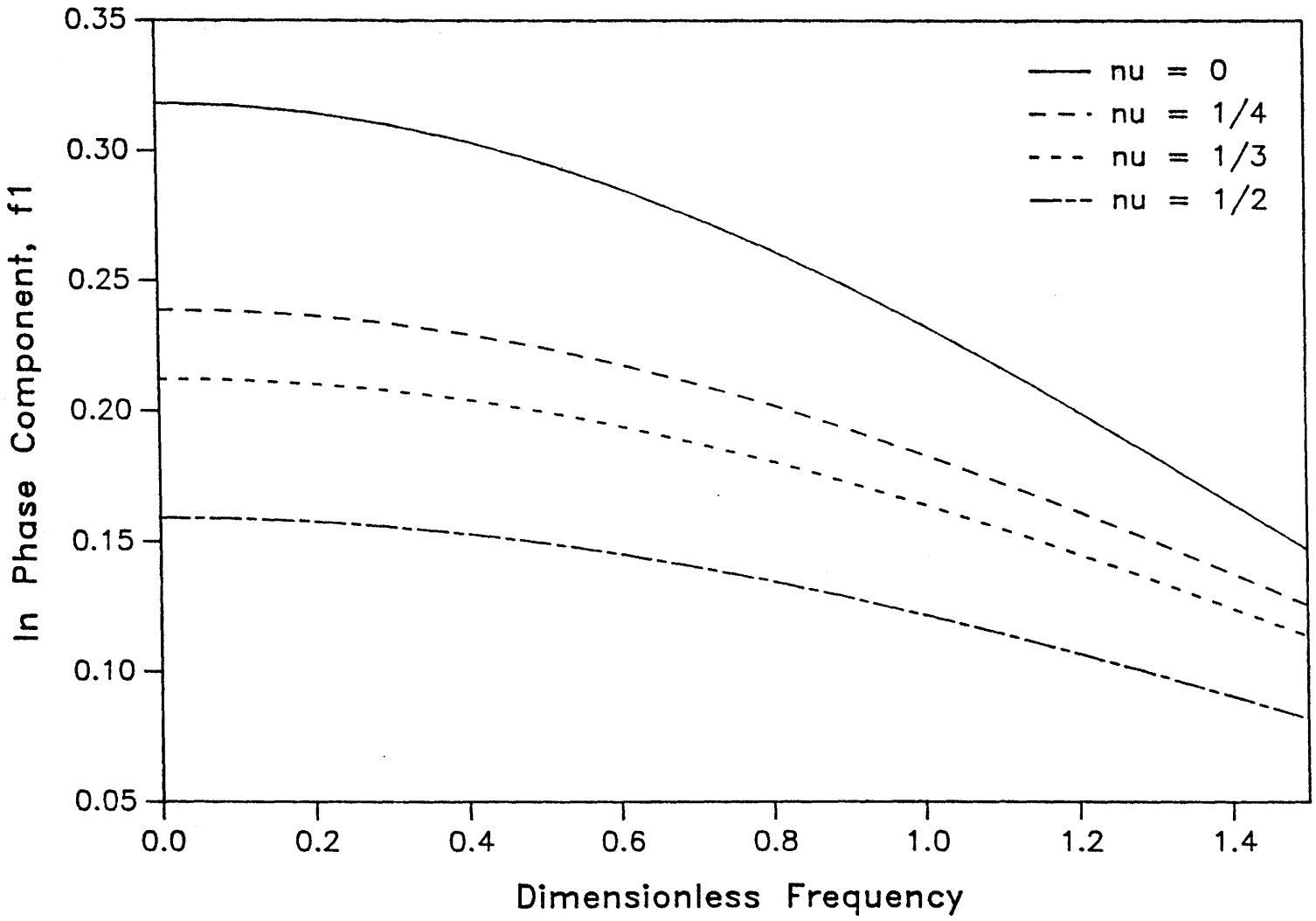

Figure 5. In-Phase Dimensionless normal Displacement for r = 0 and Uniform Pressure Distribution versus Dimensionless Frequency for Poisson's Ratio of 0, 1/4, 1/3, and 1/2 (Sung, 1954).

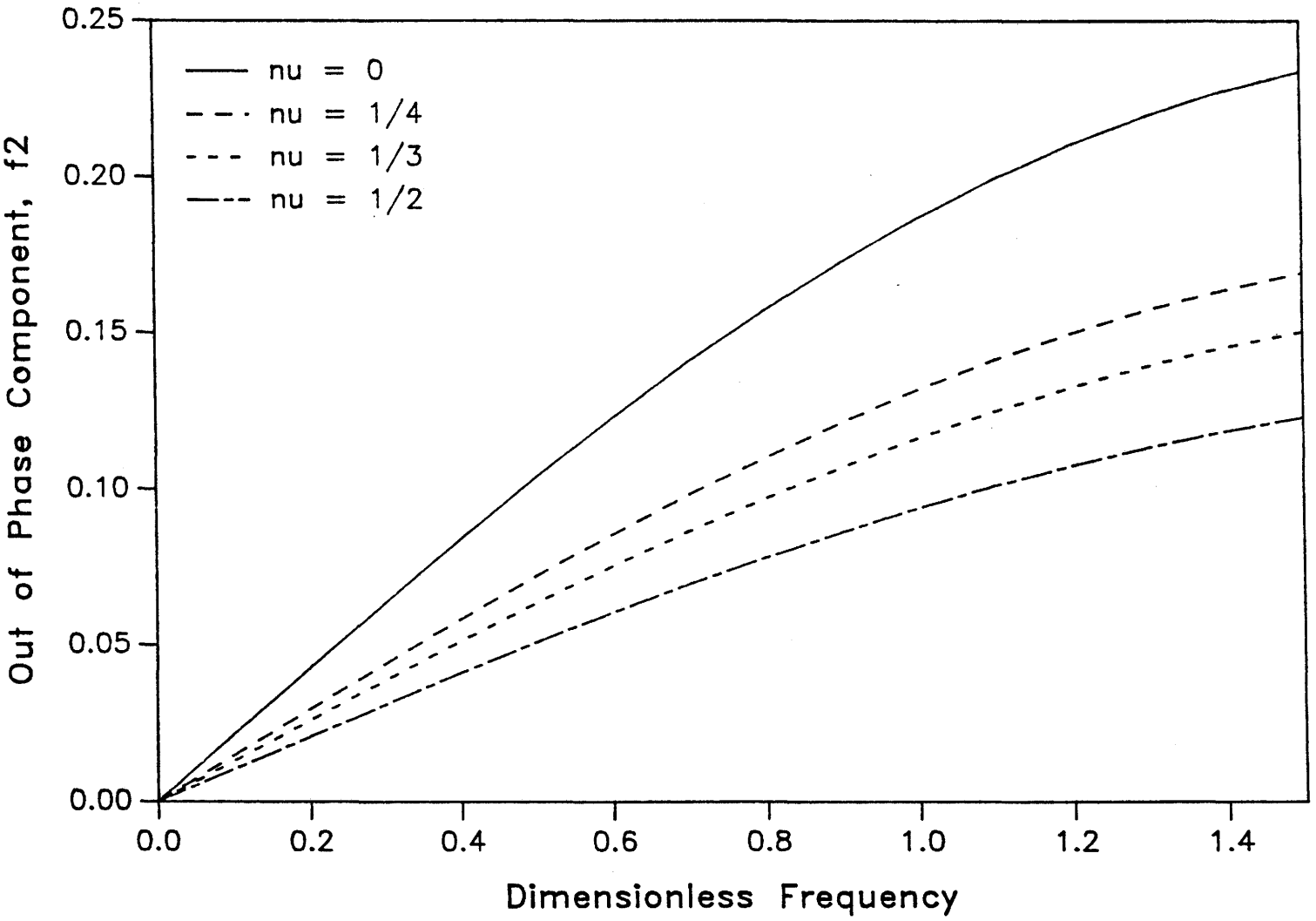

Figure 6. Out-of-Phase Dimensionless Normal Displacement for r = 0 and Uniform Pressure Distribution Versus Dimensionless Frequency for Poisson's Ratio of 0, 1/4, 1/3, and 1/2 (Sung, 1954).

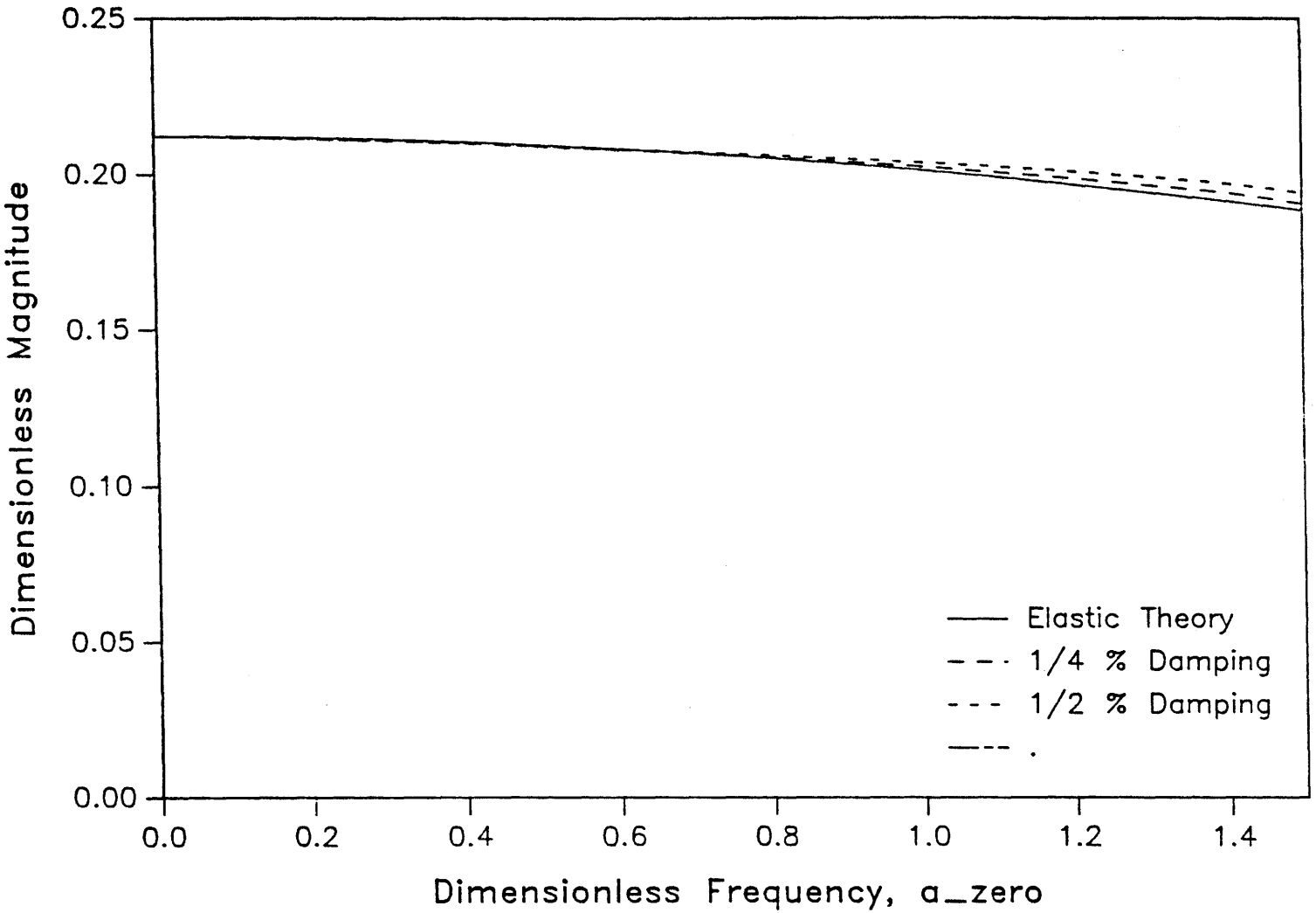

Figure 7. Dimensionless Magnitude of Normal Displacement for r = 0 and Uniform Pressure Distribution for Poisson's Ratio of 1/3: Comparison of Theory and Computed Values.

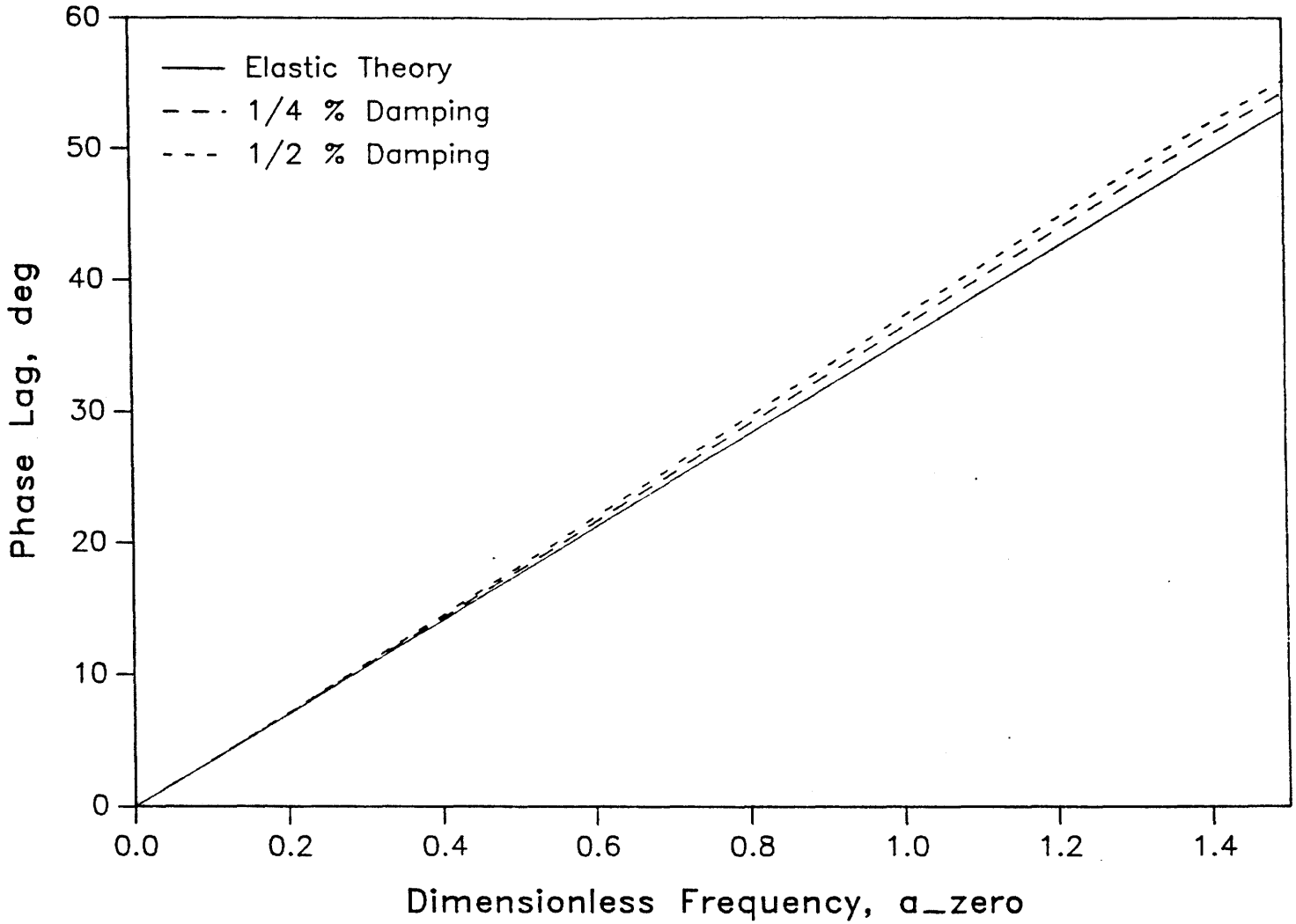

Figure 8. Phase Angle of Normal Displacement for r = 0 and Uniform Pressure Distribution for Poisson's Ratio of 1/3: Comparison of Theory and Computed Values.

(1953) computations while the damping = ½ percent, and damping = ¼ percent results were computed as part of this project by Magnuson (1988). These plots indicate that the magnitude response falls off gradually as frequency increases and the phase angle is nearly linear in frequency. Damping is seen to decrease the amplitude and increase the phase angle. In Chapter IV, Figures 7 and 8 will be shown to resemble the frequency response functions computed from FWD data. However, the FWD data includes effects of layering, inhomogeneities, etc., which are not accounted for in the Reissner-Sung theory, so a quantitative comparison cannot be made.

CHAPTER III

TIME PULSE DATA FROM THE FALLING-WEIGHT DEFLECTOMETER

Time-pulse data for SH 19 and 24 are presented and discussed in this Chapter. Appendices A and B contain similar data on FM 79 and SH 82, respectively. Characteristics of these pavement sections are given in Table 2. Test time, date, temperature and moisture content are given in Table 3. The load or force pulses are shown in Figures 9 and 10. The data is sampled every 0.2 msec and the sampling time is 60 msec. The lowest load is shown in Figure 9 and the highest load is shown in Figure 10. (Data was acquired for four load levels.) Note the double peak in the pulse. The second peak is higher than the first for the highest load. The load is given in units of kiloPascals (kPa).

Deflections are shown in Figures 11 and 12 for the lowest load and highest load, respectively. The deflections are plotted for all seven seismometer sensors. The sensors are all spaced at varying distances from the center of the dropweight as follows:

Sensor	Distance (ft.)
1	0
2	1
3	2
4	3
5	4
6	5
7	6

Note from Figures 11 and 12 how the deflections decrease as the distance increases. The pulse peaks occur at later times as the distance increases. This indicates wavelike behavior where the response is delayed the farther the distance from the dropweight.

Normal practice for static analysis is to take the peaks of each of the deflection pulses as the deflection basin. The static force is taken as the peak of the corresponding force pulse. This practice involves some approximations because the peaks do not occur at the same time and the shapes of the pulses are distorted. The time delay and the pulse distortion indicate dynamic effects are present. This will be confirmed in the frequency domain analysis in the next chapter.

Table 3. Temperature and Moisture Content Data

	Highway		
	SH 19 & 24	FM 79	SH 82
Test Date	3/30/88	3/29/88	3/30/88
Test Time	9:30 a.m.	2:00 p.m.	10:00 a.m.
Thermocouple Depth (in.)			
TC1	9	2	6
TC2	16	6	12
TC3	13	14	15
Temperature (°F)			
Surface	65	58	67
TC1	62	63	60
TC2	66	68	62
TC3	72	72	64
Moisture Content (Bars)			
Base	Saturated	Saturated	-0.167
Subbase	Saturated	Saturated	Saturated

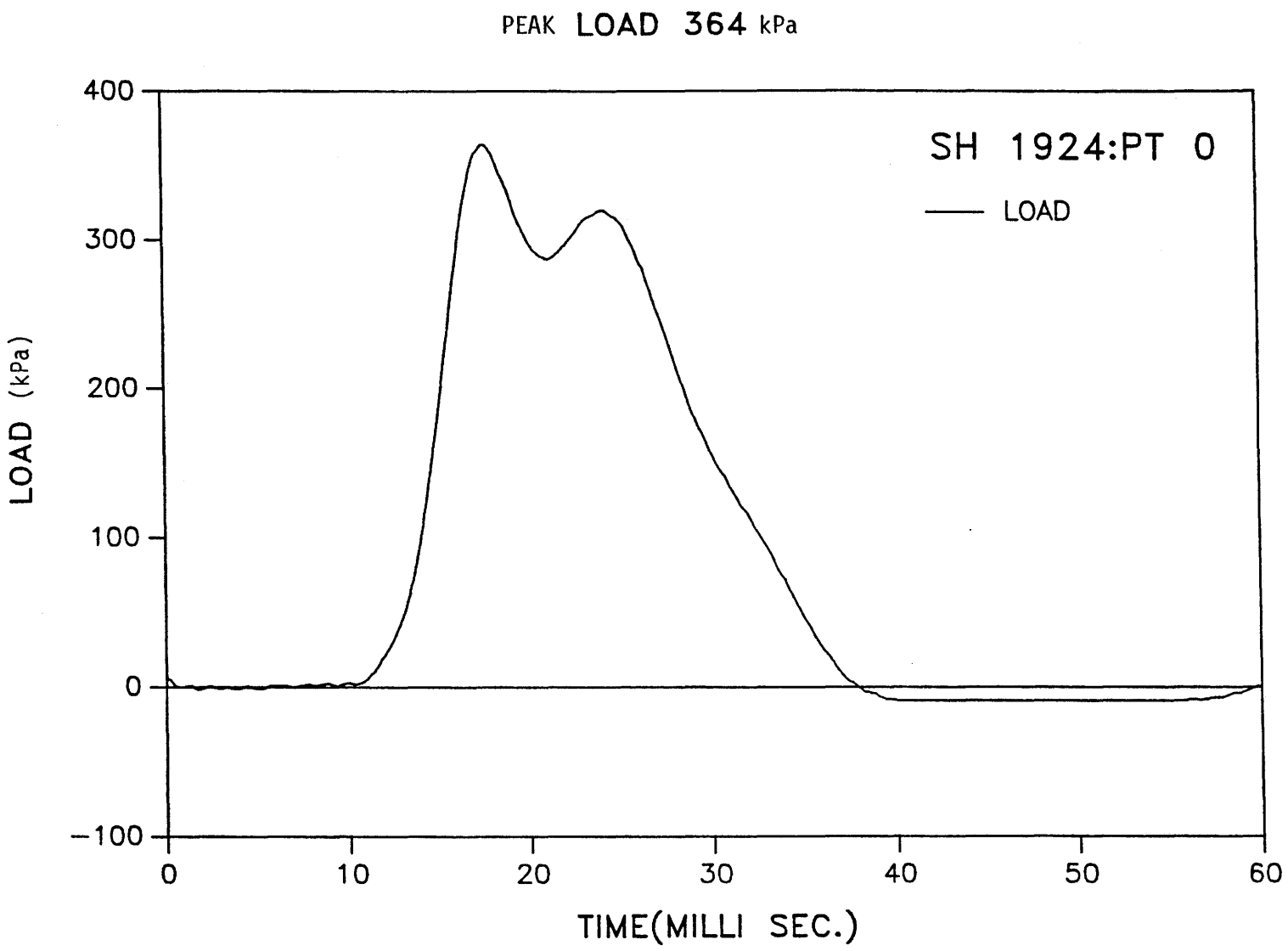

Figure 9. Load versus Time, Lowest Load (SH 19 and 24).

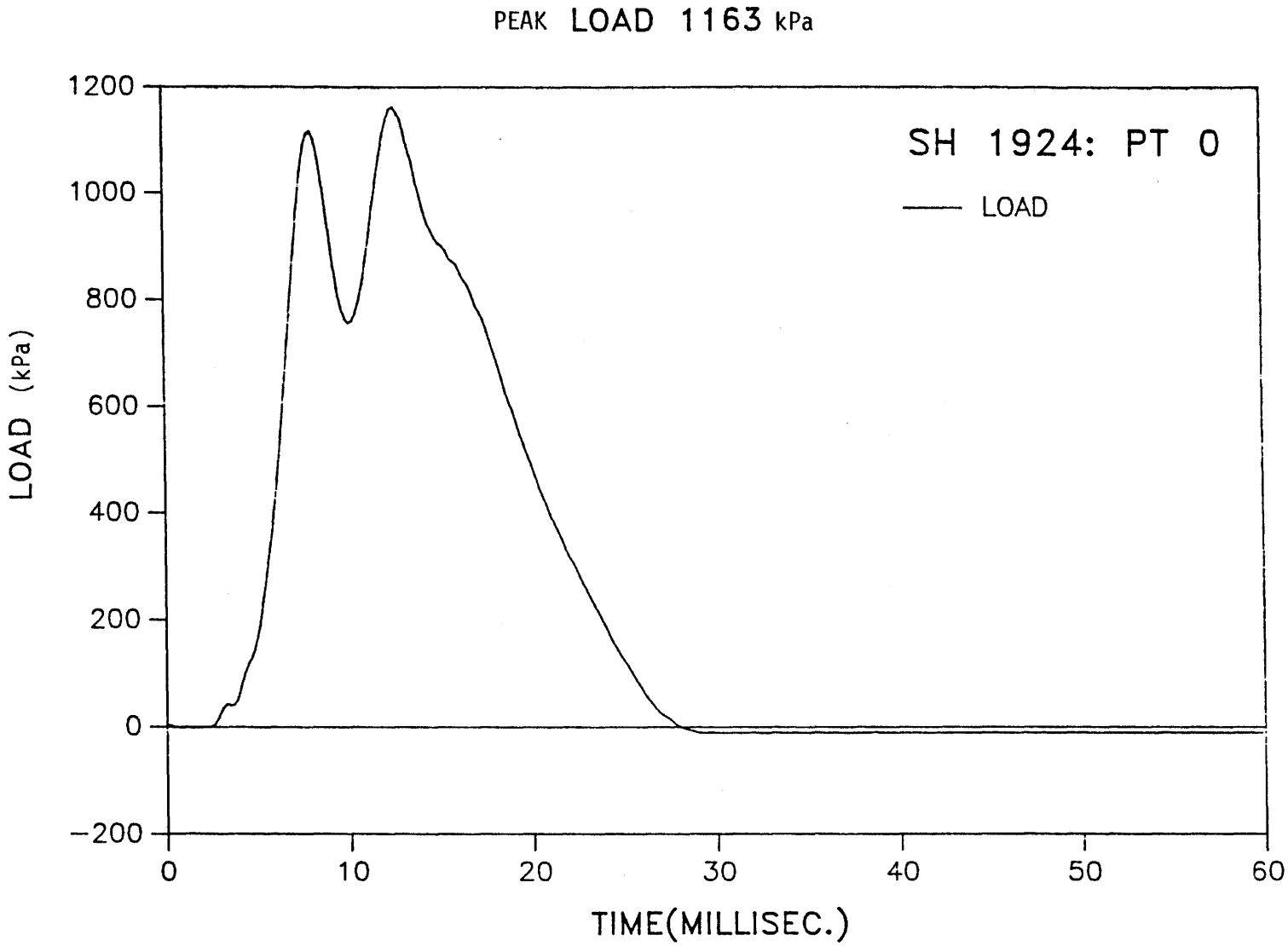

Figure 10. Load Versus Time, Highest Load (SH 19 and 24).

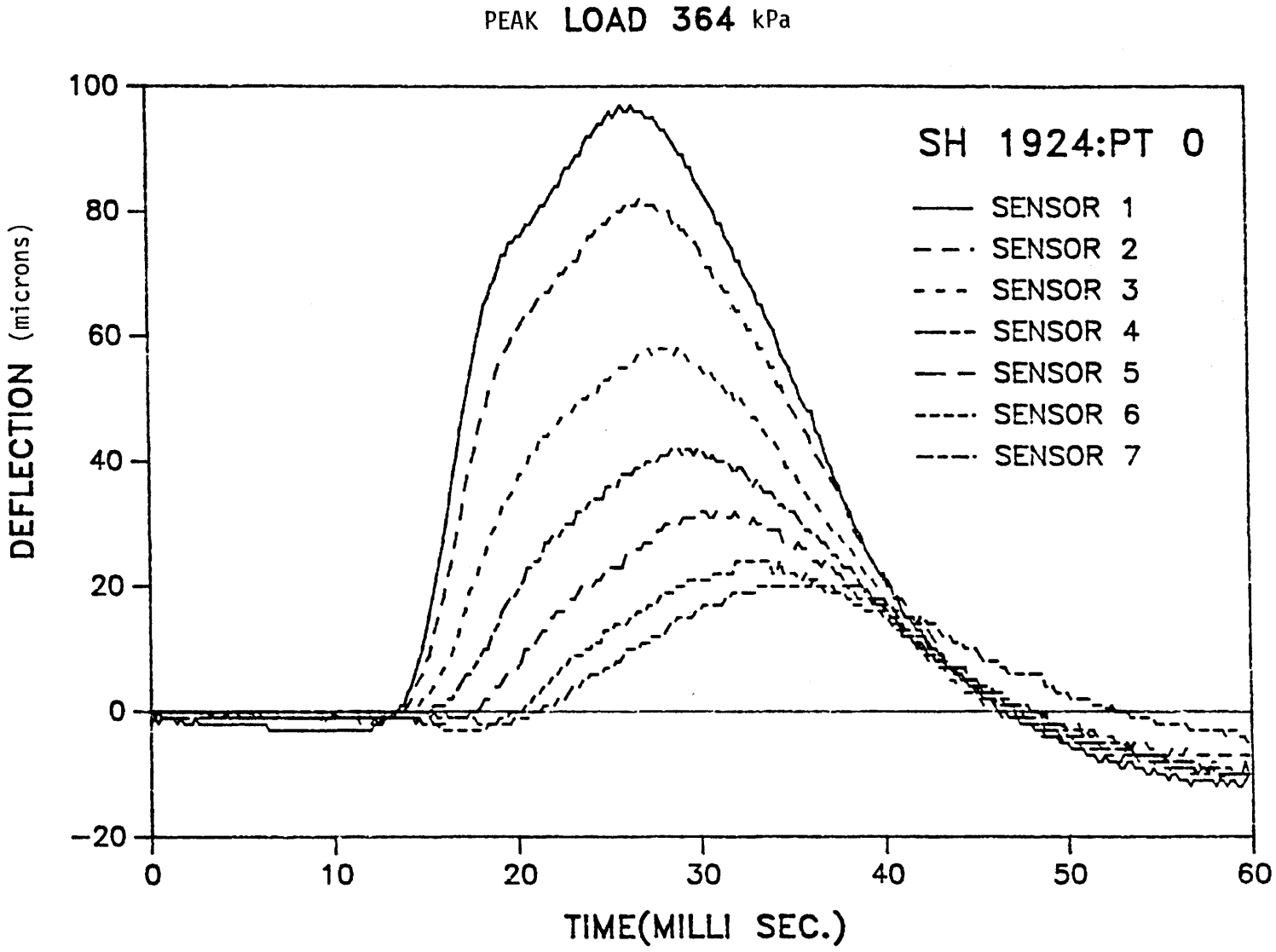

Figure 11. Deflections versus Time, Lowest Load (SH 19 and 24).

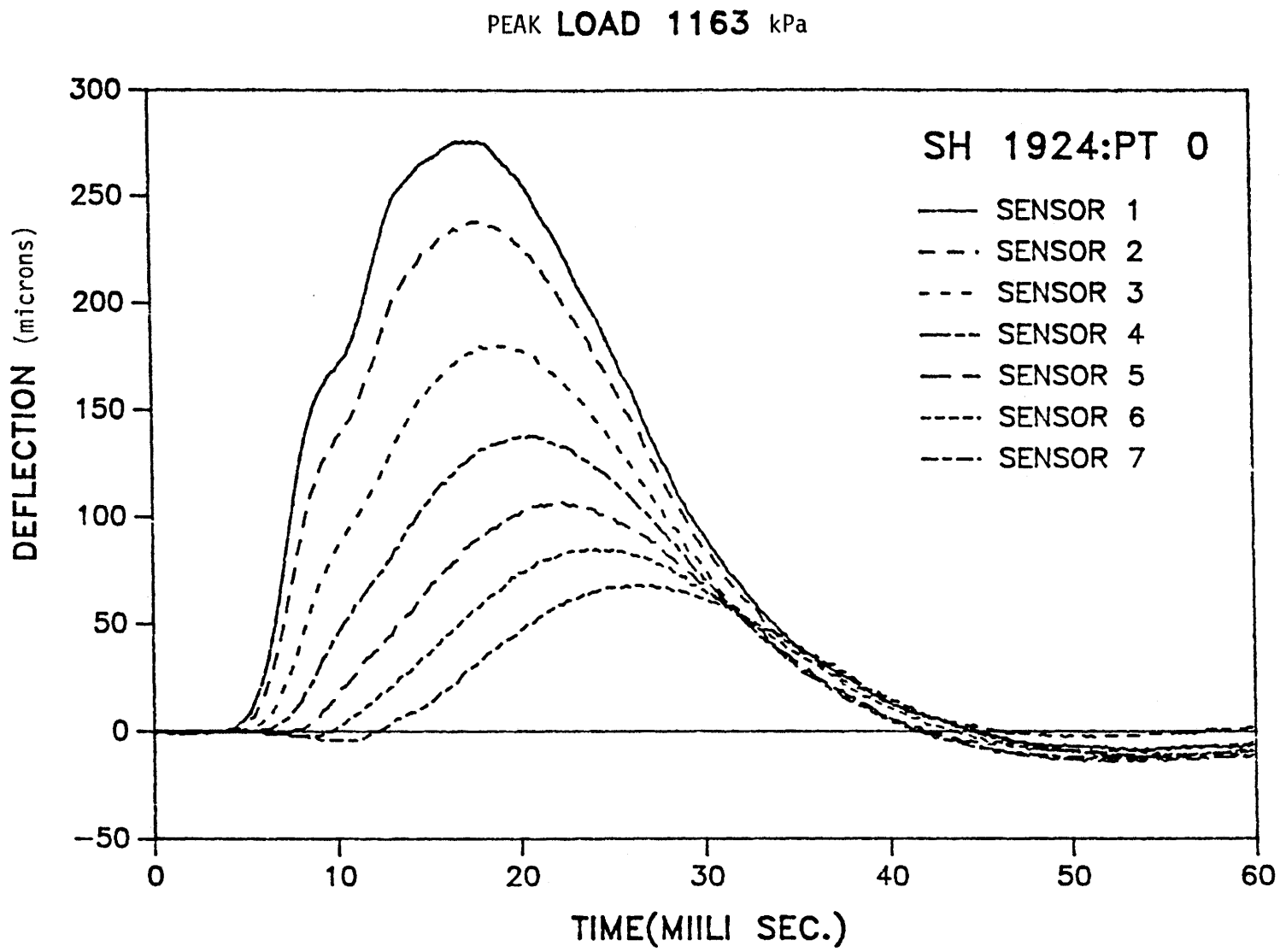

Figure 12. Deflections versus Time, Highest Load (SH 19 and 24).

Another significant feature is the truncation of the pulses at the end of the 60 msec sample time. Ideally, the pulses should "die out" or go to zero at the end of the sample period. Instead, the deflection pulses usually cross the time axis and become negative before they are truncated. What causes the truncated "tails" of the pulses is not known at this time, however one or more of the following factors are probable causes:

1. "Drift" caused by digital integration and digital filtering of the seismometer.
2. Permanent deformation caused by plastic flow of the asphaltic concrete pavement or compaction of the granular material in the base or subbase.
3. Premature truncation of the pulses before the transient response has died out. The pulses may have a damped oscillatory behavior as shown in Figure 13.

Recommendations for resolving the pulse truncation problem are given in Chapter V. The pulse truncation causes problems when the time-domain data is transformed into the frequency domain by using a Fast Fourier Transform (FFT) algorithm. Why the problem occurs and how the problem can be alleviated is discussed in the next Chapter.

Pulse data on a thin pavement (FM 79) is given in Appendix A (Figures A1 to A4) and thick pavement data is given in Appendix B (Figures B1 to B4). Comparisons of force pulses in Figures 9, 10, A1, A2, B1, and B2 show that the first peak is higher than the second for the lowest load. For the highest load, the second peak is higher than the first peak for the thicker pavements (SH 19 and 24 and SH 82). For the thin pavement (FM 79), the first peak is higher for the highest load. This indicates that the force pulse may be dynamically interacting with the pavement depending on pavement stiffness.

The pavement deflection pulses for FM 79 and SH 82 are shown in Figures A3, A4, and B3 and B4, respectively. The behavior of the pulses at truncation is summarized in Table 4 where the ratios of the pulse "tail" at truncation to pulse peak is shown for the force and all the deflection sensors. SH 82 pulse data behaved similarly to the SH 19 and 24 data discussed above whereby the relative size of the tails is higher for the lower loads. The thin pavement data (FM 79), Figures A3 and A4, showed a different pattern. The lowest load tails were moderate in size for all sensors while the first two sensors for the highest load

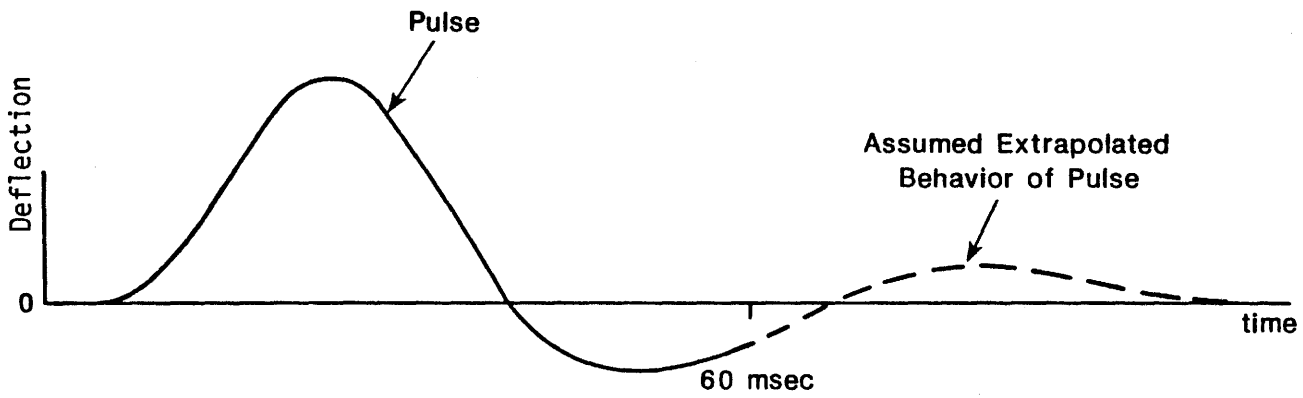

Figure 13. Possible Extrapolated Behavior of Pulse.

behaved differently. The sensor 1 pulse drops tangent to the horizontal axis and then rises again. Sensor two crosses the time axis becoming negative, then rises again and crosses a second time. The other sensors (sensors 3, 4, 5, 6, and 7) have very small "tails."

CHAPTER IV

PAVEMENT SECTION FREQUENCY RESPONSE FUNCTIONS

The time domain data in Chapter III was transformed into the frequency domain, and the results are presented here. A Fast Fourier Transform (FFT) was performed on the force pulse and on each displacement sensor for each test case. The FFT is discussed in Davis and Rabinowitz (1975). The FFT numerically performs the Fourier Transform in Equation (2) on digitized data.

The FFT's are computed in the program listed in Appendix C. The FFT works on a digitized signal which is a series of discrete values sampled at fixed intervals of time. The sampling rate of the Dynatest FWD is 0.2 msec, giving 300 samples for the 60 msec pulse. The FFT sample size must be a power of two. The normal sample size is 2^{10} = 1024. To obtain this sample size, the FWD data is supplemented by a series of zeroes. This process is called zero-packing. When the data pulse has a truncated tail, which is usually the case for FWD data, the full pulse has a discontinuity as shown in Figure 14a. It will be shown shortly that the pulse discontinuity produces an undesirable effect on the FFT of the pulse. It will also be shown that the effect can be alleviated (if not totally eliminated) by adjusting the pulse with a linear correction, as shown in Figure 14b. The corrected deflection pulse data eliminating the tail discontinuity is shown in Figure 15.

The FFT of the force pulse for the lowest load (SH 19 and 24) is shown in Figures 16 and 17 for the real and imaginary components, respectively. The FFT algorithm sets the FFT frequency range as the reciprocal of the sampling rate, or 1/0.0002 = 5000 Hz. The normal frequency resolution Δf is given as:

$$\Delta f = \frac{1}{(0.0002 \times 1024)} = 4.8828 \text{ Hz}$$

Note in Figures 16 and 17 that most of the energy of the force pulse is in the 0-250 Hz range. The real and imaginary components of the sensor 1 deflection for the lowest load (SH 19 and 24) are given in Figures 18 and 19.

The frequency response functions are obtained by dividing the FFT of the deflections [$Z(\omega)$] by the FFT of the force [$F(\omega)$]. Since the FFT's are complex numbers, the frequency response function is also a complex number. If the frequency response function is denoted $H(\omega)$, one has:

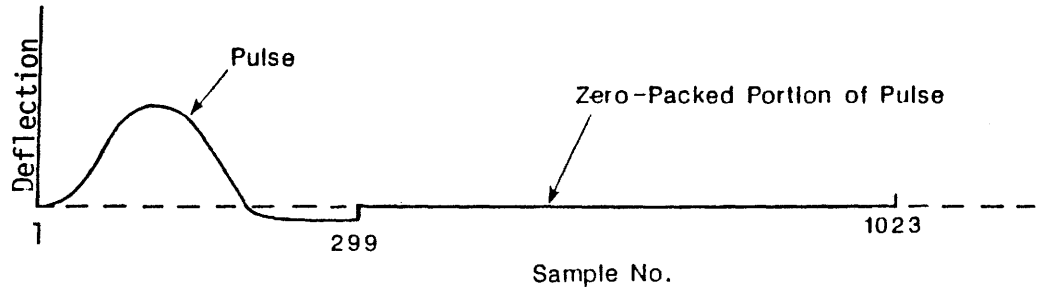

Figure 14a. Truncated Pulse With Zero-Packing Showing Discontinuity.

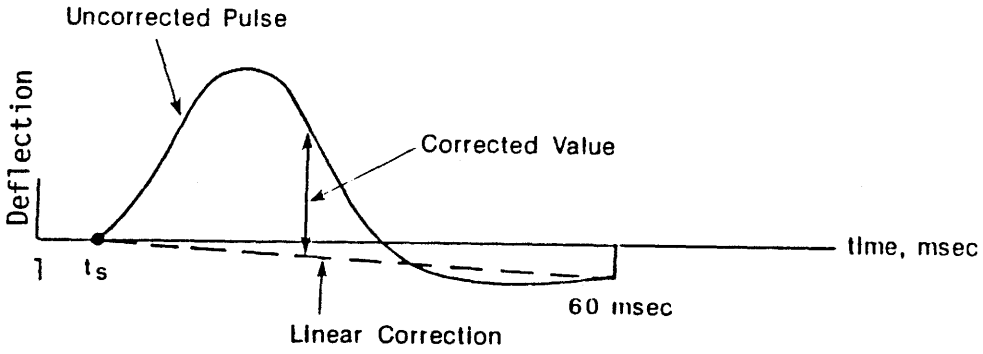

Figure 14b. Linear Correction to Pulse to Eliminate Tail Discontinuity.

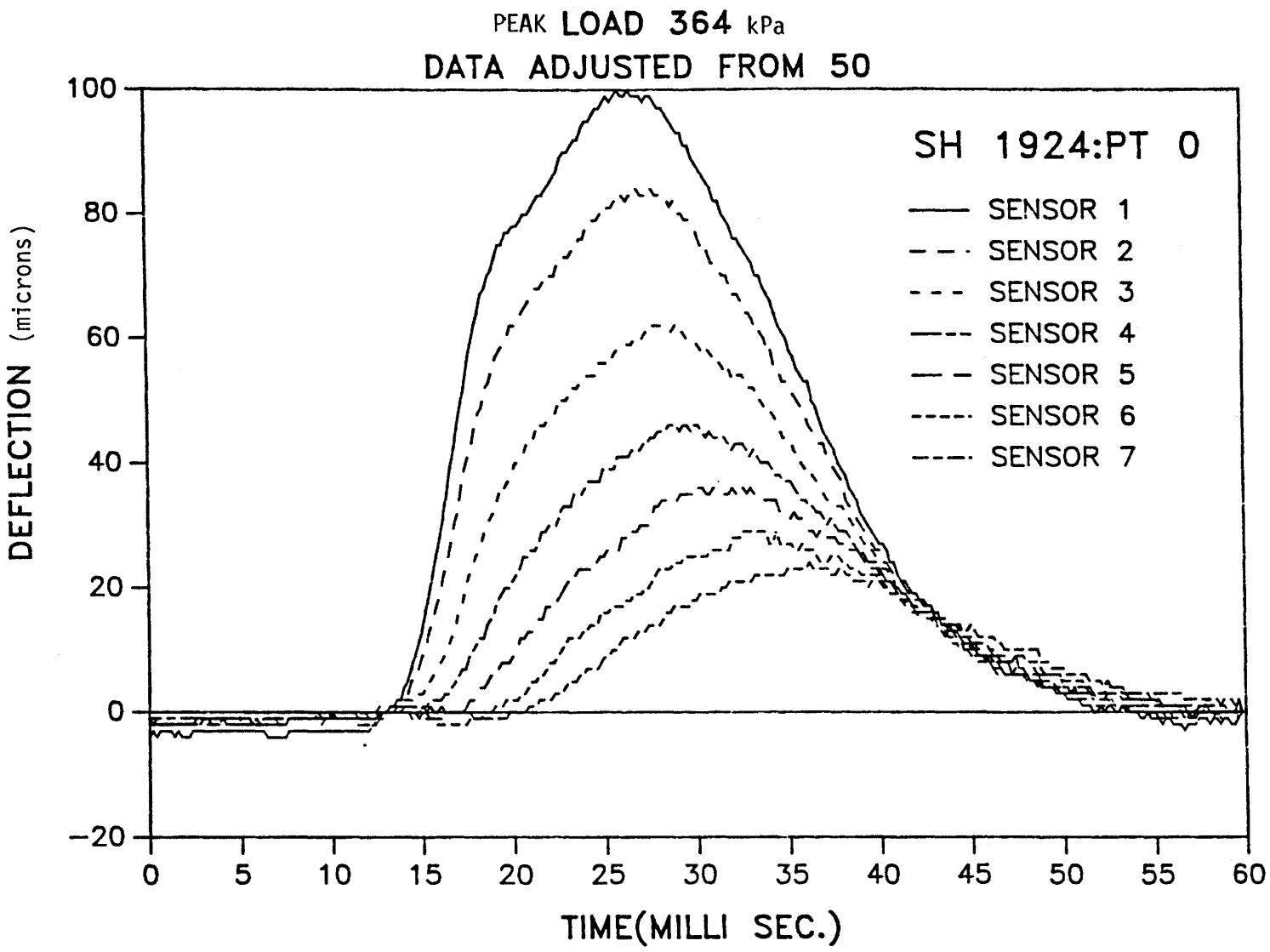

Figure 15. Corrected Deflection versus Time, Lowest Load (SH 19 and 24).

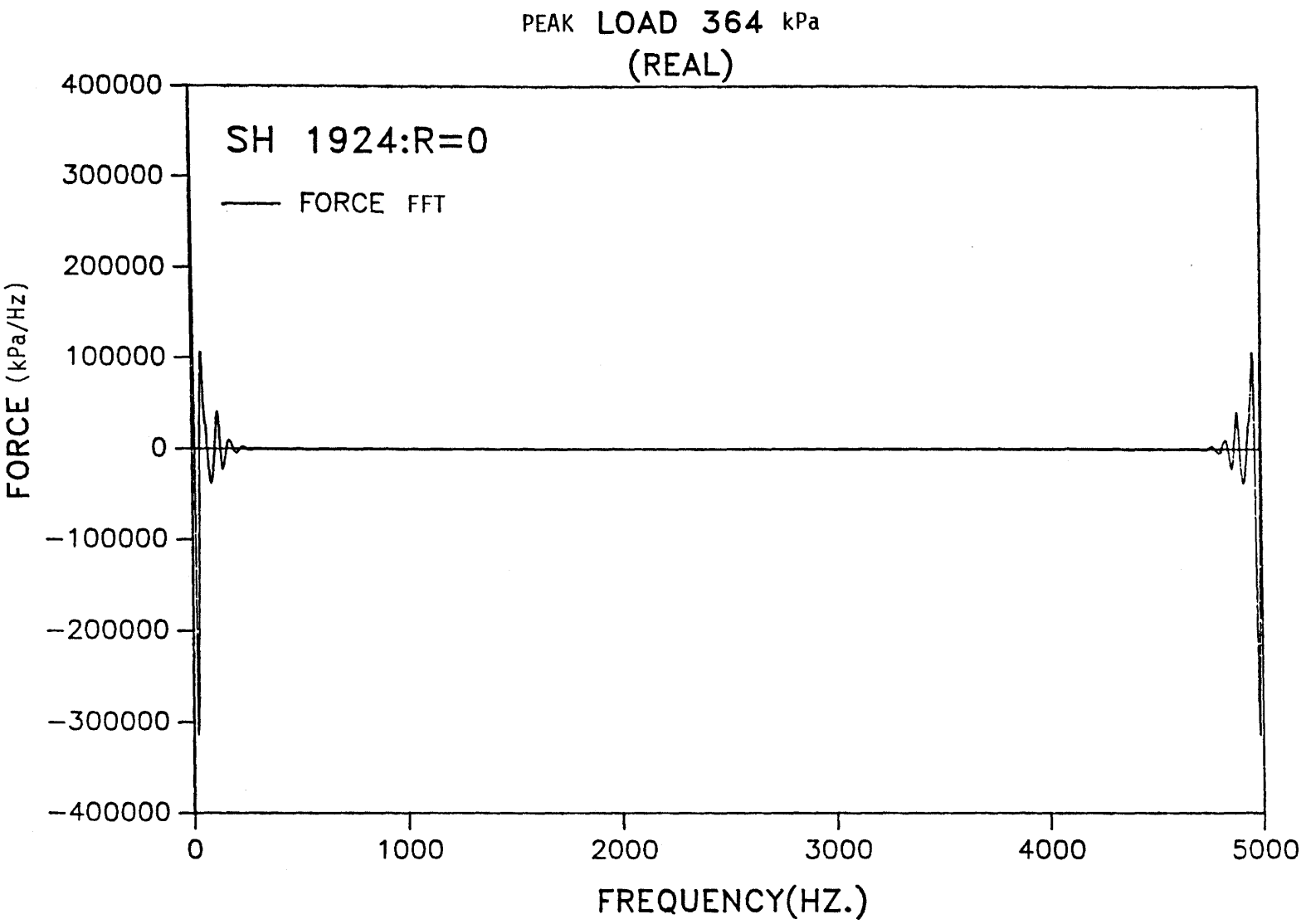

Figure 16. Real Part of Fast-Fourier Transform of Force Pulse, Lowest Load (SH 19 and 24).

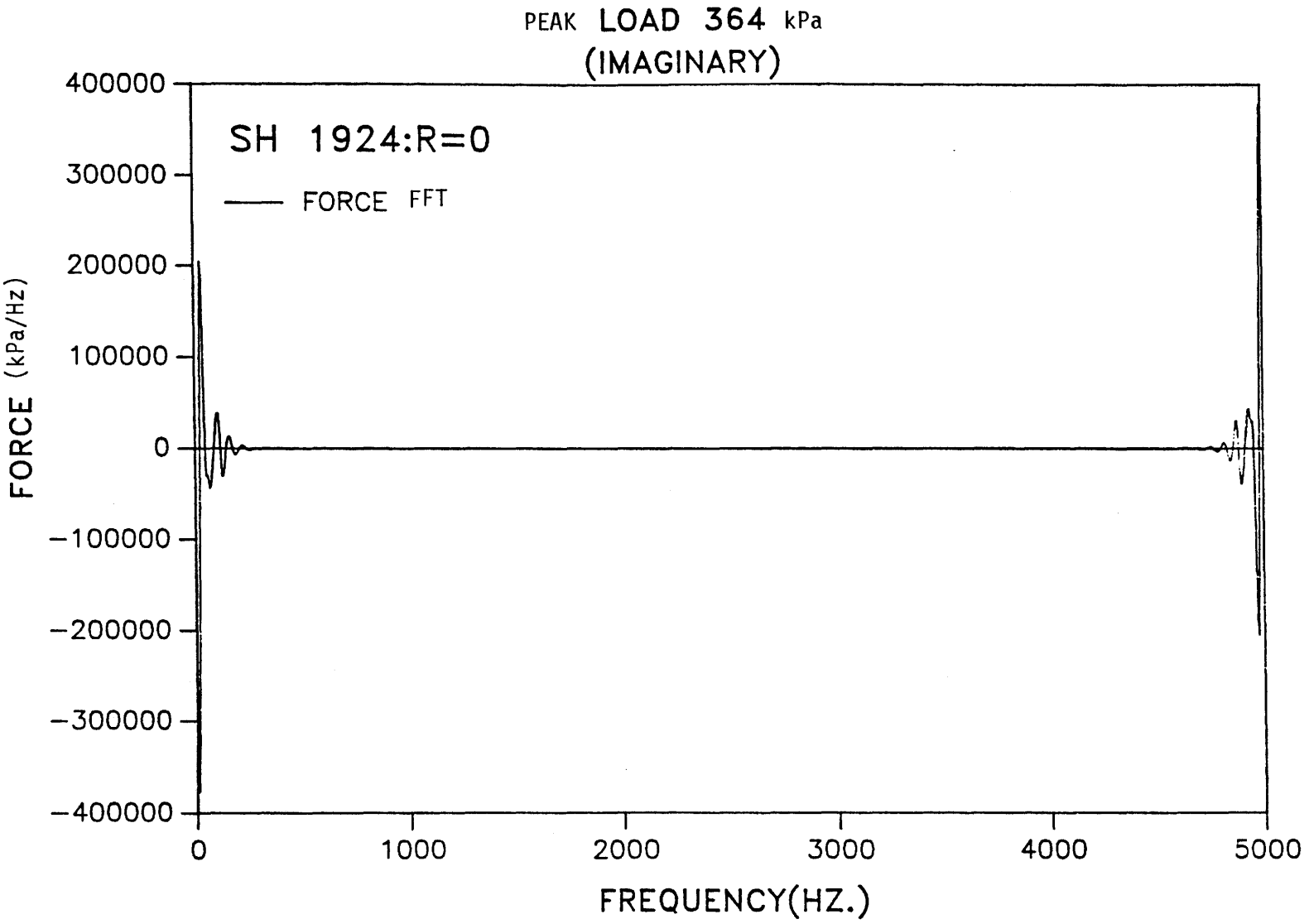

Figure 17. Imaginary Part of Fast-Fourier Transform of Force, Pulse Lowest Load (SH 19 and 24).

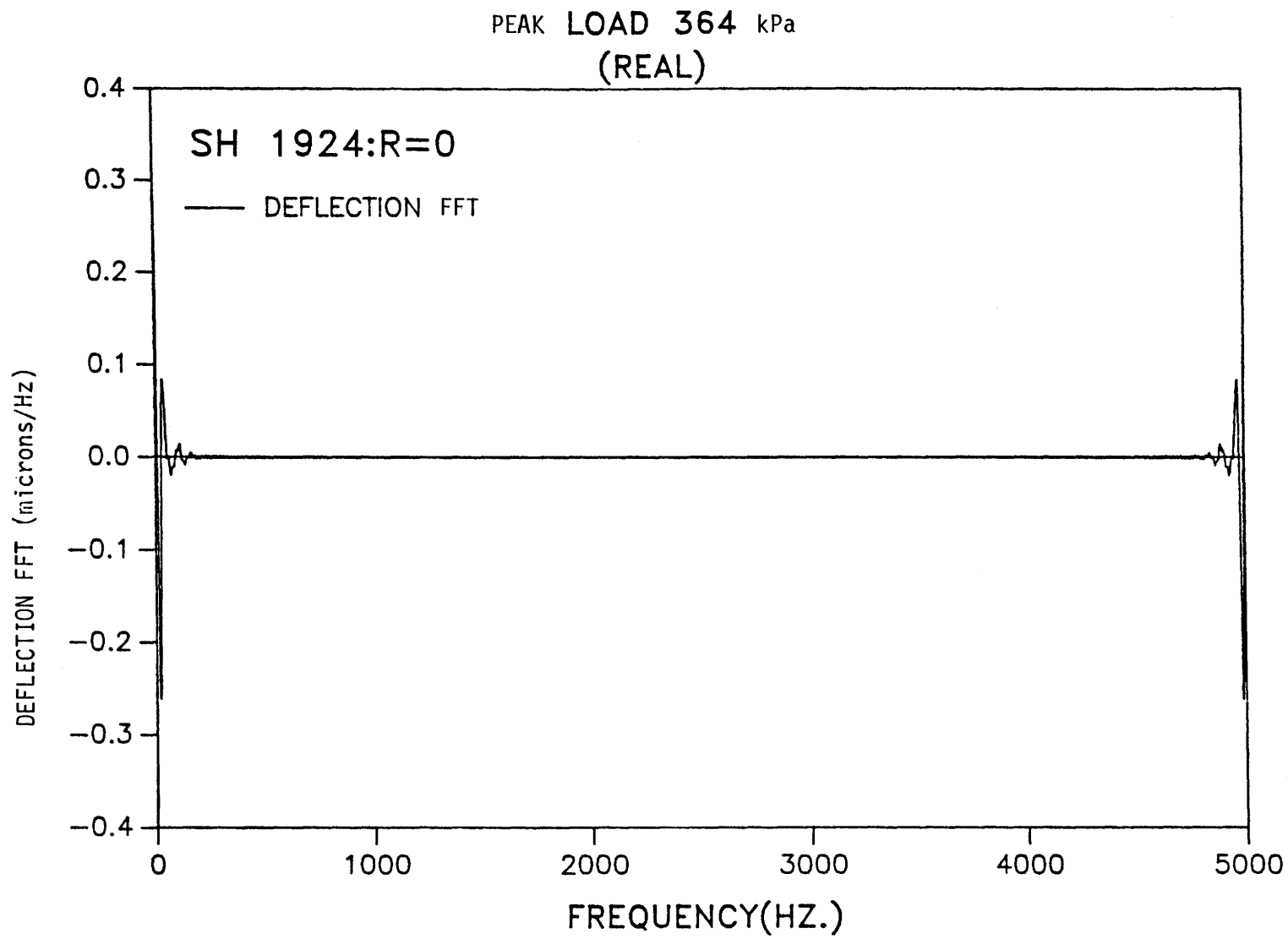

Figure 18. Real Part of Fast-Fourier Transform of Deflection Sensor 1, Lowest Load (SH 19 and 24).

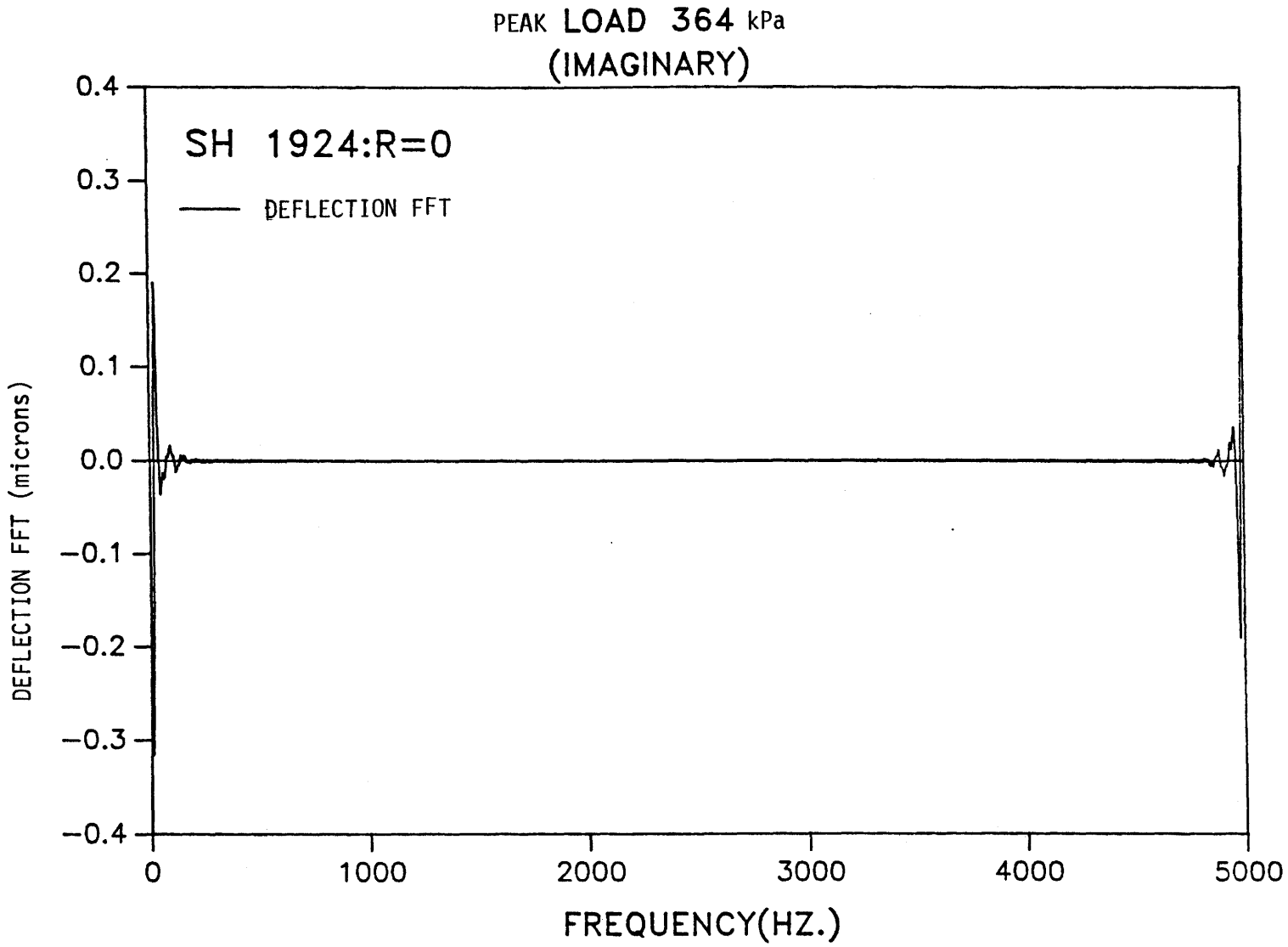

Figure 19. Imaginary Part of Fast-Fourier Transform of Deflection Sensor 1, Lowest Load (SH 19 and 24).

$$H(\omega) = \frac{Z(\omega)}{F(w)1} = H_R + iH_I = |H|e^{i\phi_H} \qquad (12)$$

where the magnitude $|H|$ and the phase ϕ_H are given by:

$$|H| = (H_R^2 + H_I^2)^{\frac{1}{2}}$$

$$\phi_H = \arctan\left[\frac{H_I}{H_R}\right]$$

The magnitude $|H|$ has dimensions of in./lb.

Figures 20 and 21 show magnitudes of the frequency response functions for the lowest load (SH 19 and 24) for frequency ranges of 0-300 Hz and 0-125 Hz, respectively. For a given sensor, one expects the magnitude response to decrease with frequency similar to the theoretical result in Figure 7. One sees from Figure 20 that the noise apparently takes over at about 120 to 150 Hz, where the magnitude starts to increase. The noise becomes dominant when the FFT of the force pulse becomes small because of the division indicated in Equation 12. The dominance of numerical "noise" starts at about 250 Hz, as can be seen from Figures 16 and 17 where the FFT of the force is seen to be small. Figure 21 shows the magnitude response over the relatively noise-free range. One sees from Figure 21 that (despite the marked oscillation), on the average, the response decreases with distance as well as with frequency. Later, the frequency oscillation will be shown to be associated with the truncation of the pulse and the resulting discontinuity.

A study of the effect of the responses to the resolution of the FFT was made by taking a sample size of $2^{11} = 2048$ (higher resolution) and $2^9 = 512$ (lower resolution). The results are shown in Figures 22 and 23 for higher and lower resolutions, respectively. Figure 22 shows improved resolution relative to the "normal" FFT in Figure 21. Figure 23 shows an unacceptable deterioration of resolution, as the frequency step size was about 10 Hz, which was too crude to characterize the oscillations which had a "period" of about 20 Hz. The same oscillation was present regardless of the resolution.

Figure 24 shows the responses for the adjusted pulses with no discontinuity, using the correction scheme shown in Figure 14b. The oscillations present in the previous four plots have all but disappeared, giving a smooth, well-behaved,

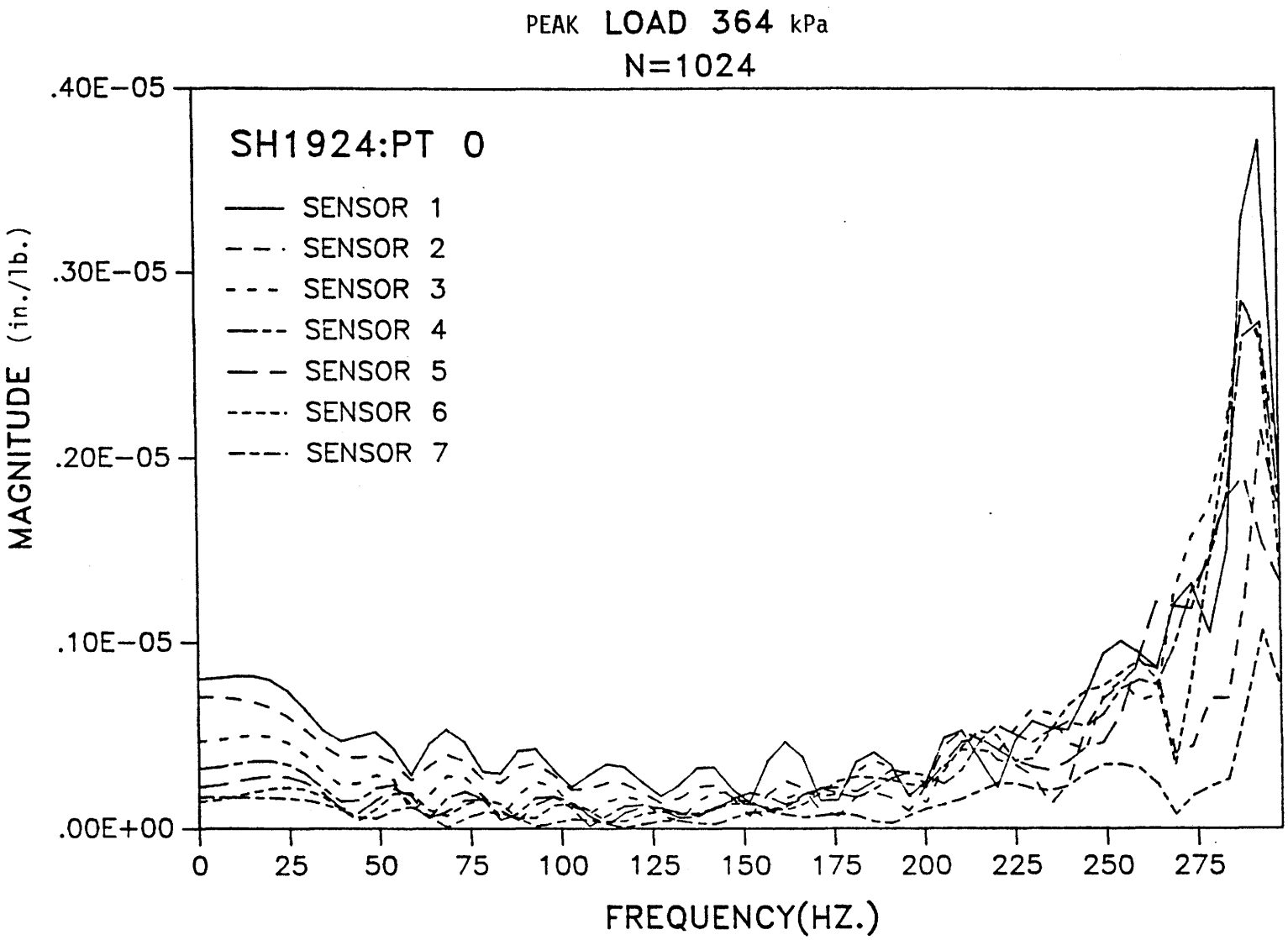

Figure 20. Magnitude of Frequency Response Function versus Frequency, Lowest Load, 0-300 Hz (19 and 24).

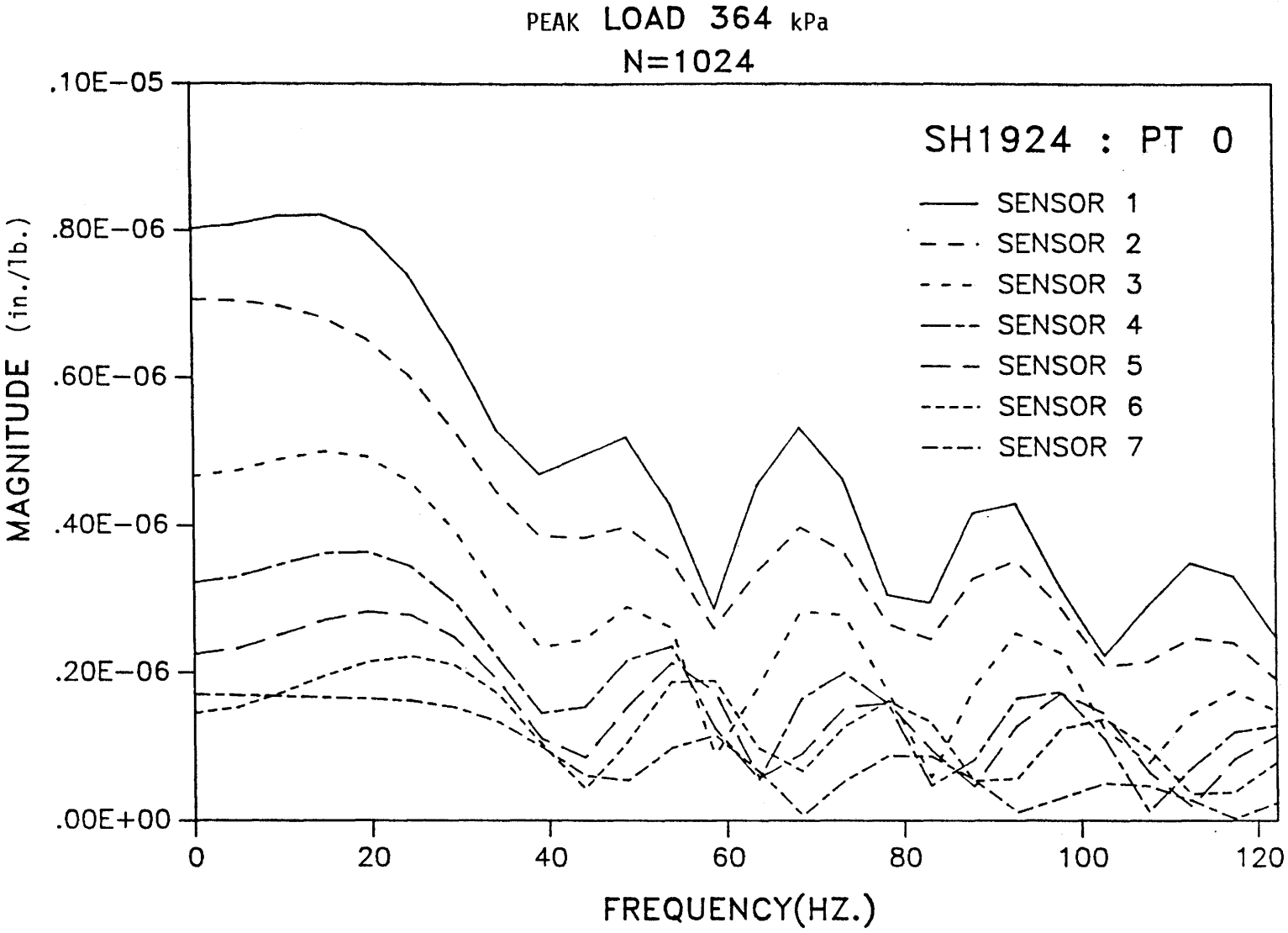

Figure 21. Magnitude of Frequency Response Function versus Frequency, Lowest Load, 0-125 Hz (SH 19 and 24).

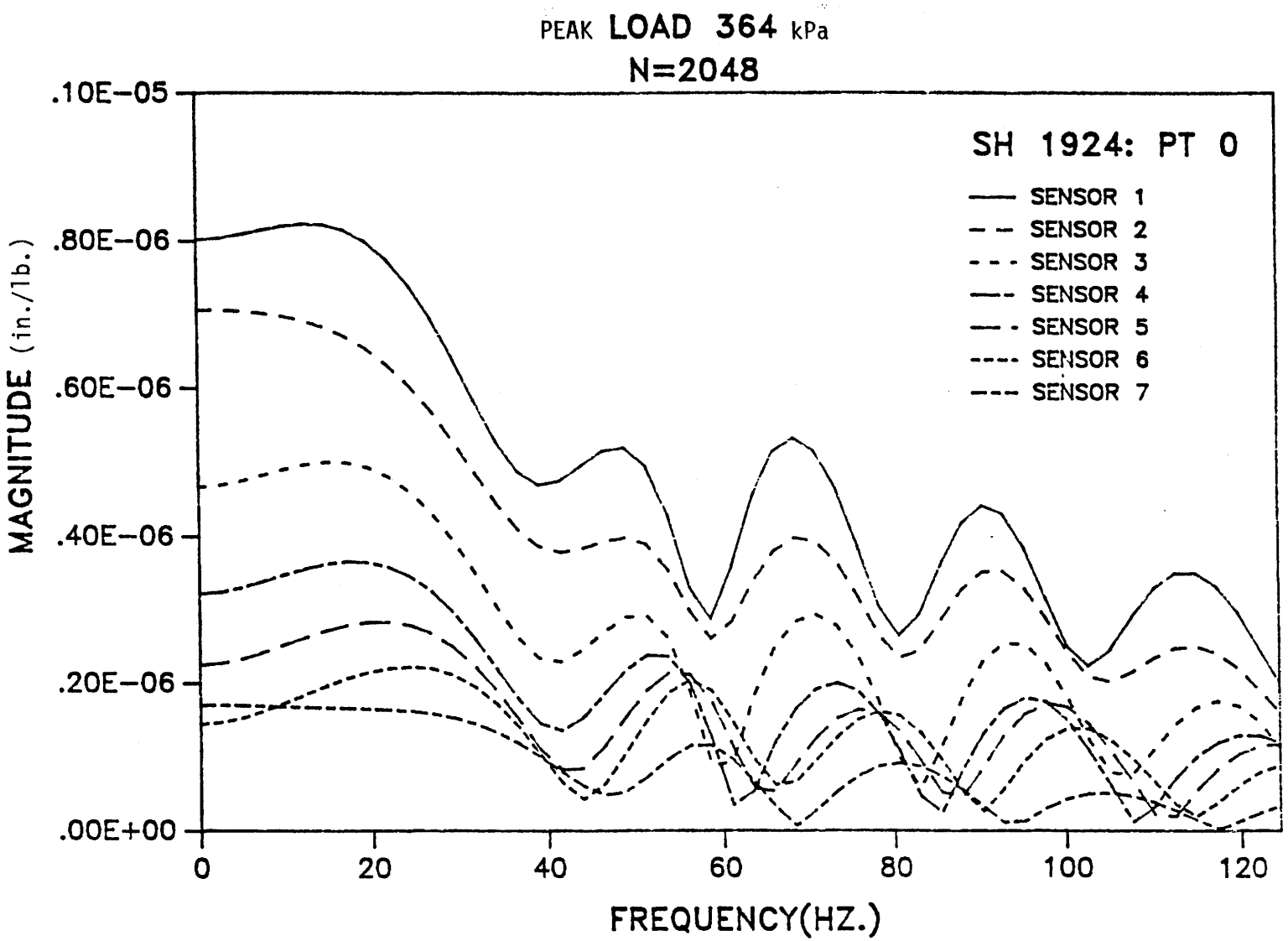

Figure 22. Magnitude of Frequency Response Function versus Frequency, Lowest Load N = 2048 (higher resolution), 0-125 Hz (SH 19 and 24).

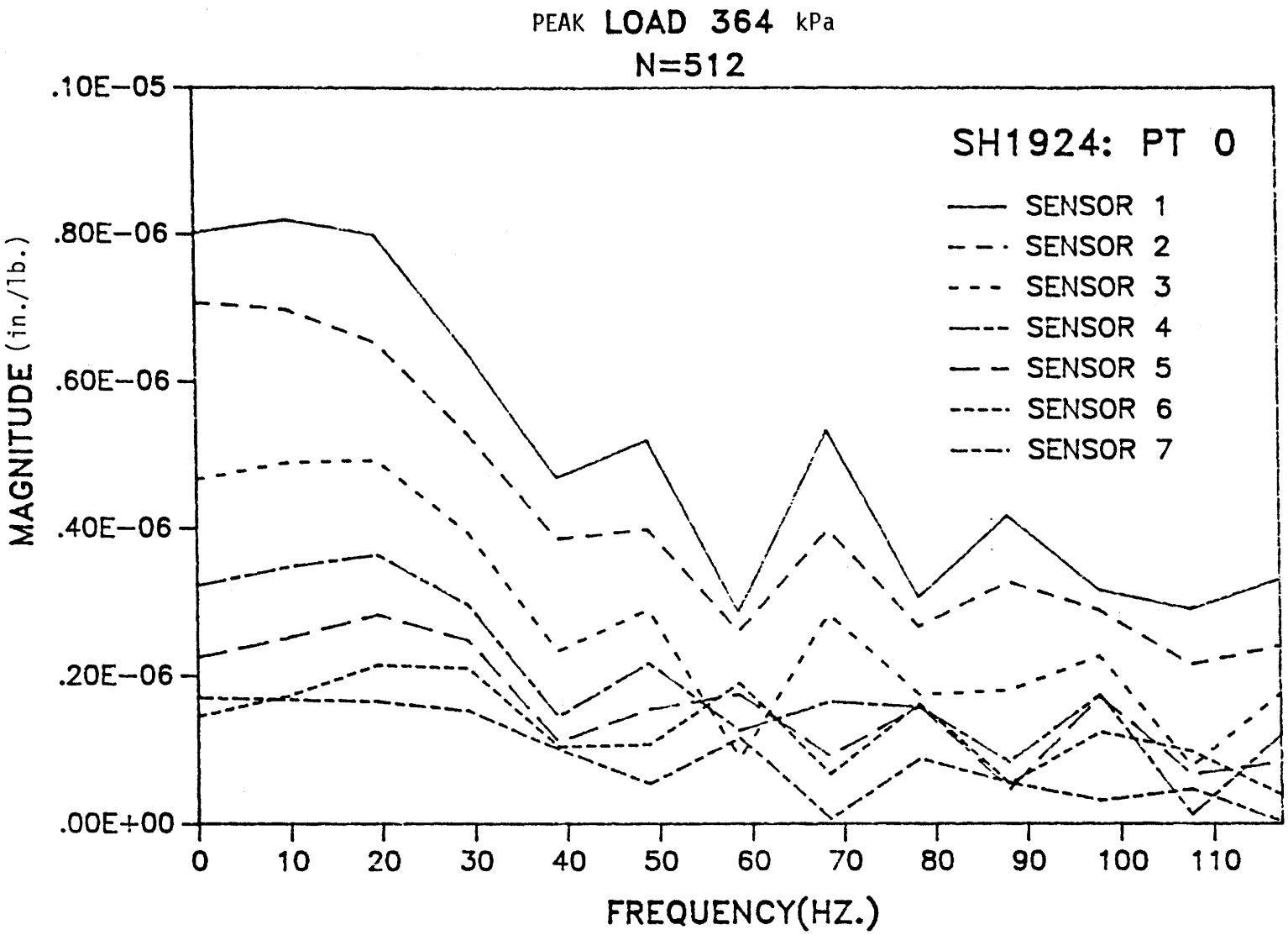

Figure 23. Magnitude of Frequency Response Function versus Frequency, Lowest Load N = 512 (lower resolution), 0-115 Hz (SH 19 and 24).

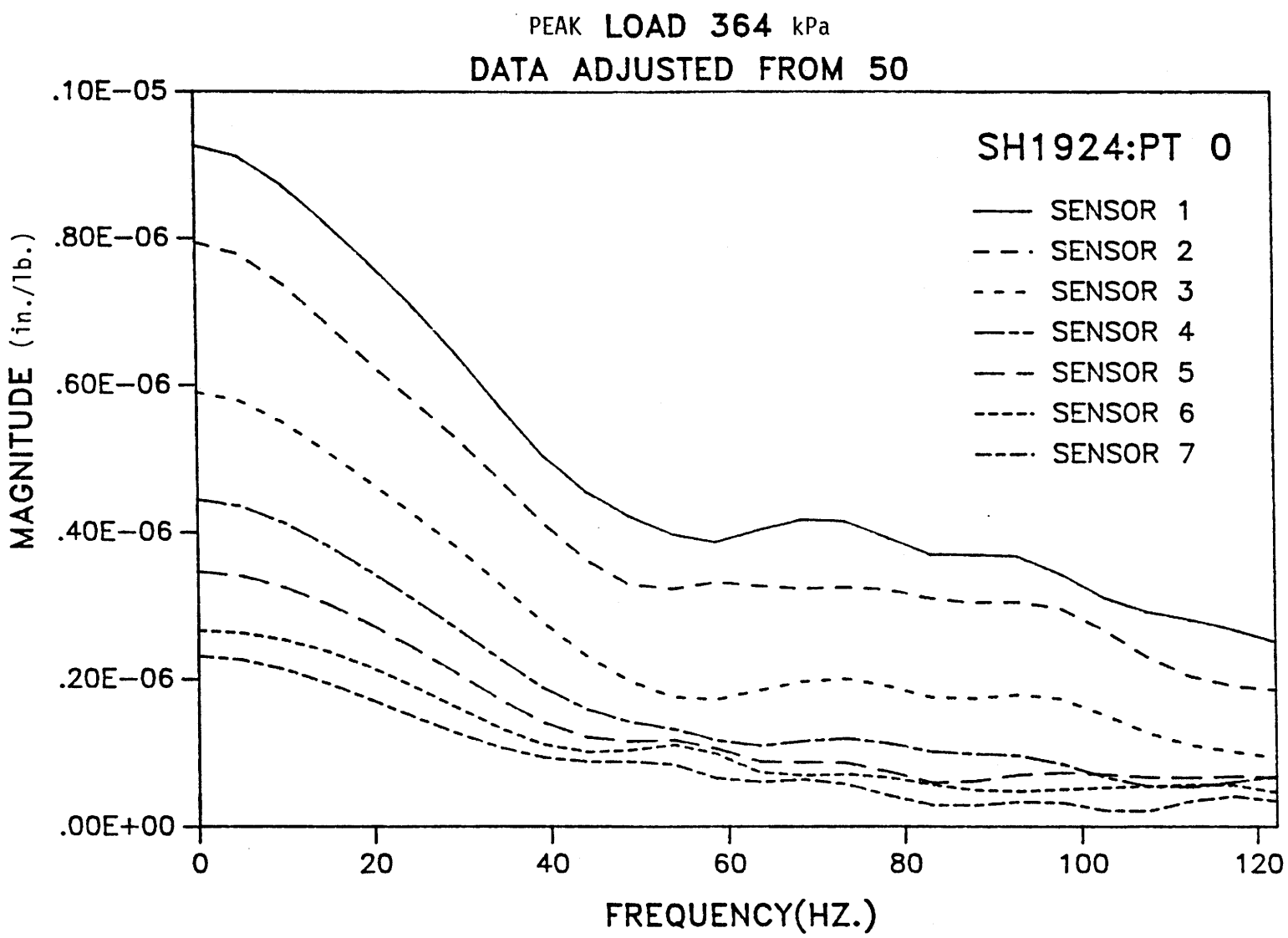

Figure 24. Magnitude of Frequency Response Function versus Frequency, Lowest Load, Corrected Pulse with No Discontinuity, 0-125 Hz (SH 19 and 24).

almost monotonic decrease in response with frequency and distance. This response is more consistent with computed responses from models based on elasto-dynamic or viscoelastic theory (Figure 7 for example).

The response magnitude for the highest load (SH 19 and 24) is shown in Figure 25 for a frequency range of 0-300 Hz. Comparison of Figure 25 with Figure 20 (lowest load) shows that noise effects (as manifested by an increase of response magnitude with frequency) are less pronounced for the highest load case, where noise effects are apparent only at the highest frequencies (250-300 Hz). The highest load response also exhibits much less oscillation than the lowest load. The noise effects are smaller for higher loads, probably because the noise is independent of load. This reduces the effect of division by a small number (containing random noise), as indicated in Equation 12.

The correlation between the discontinuity caused by the truncated pulse tail and the oscillations can be seen more readily by referring to Table 4, which shows the ratio of the pulse "tail" discontinuity to the pulse peak for the force pulse and all the displacement sensors. High values of the "tail ratio" in Table 4 consistently indicate severe oscillations in the magnitude and phase of the frequency response functions. The "tail ratio" is consistently higher for the lowest load cases, apparently because the pulse tail is relatively independent of load. Therefore, low load cases will have relatively large "tails."

Nonlinear effects in the magnitude responses can be determined by a frequency-by-frequency comparison of Figures 24 and 25. If the pavement response system is linear, the responses in Figure 24 and 25 for a given frequency and sensor (distance) should be equal, since the frequency response function is defined on a per unit load basis.

Phase angle data for the lowest level (SH 19 and 24) is shown in Figures 26-31. The uncorrected phase angle data in Figures 26-29 is difficult to interpret because of "jumps" or discontinuities caused by the arctangent function, which is restricted to the range between -180° and +180°. The jumps occur when the phase angle gets more negative than -180°, causing the arctangent to go to the next "branch" starting at +180°. In Figure 26, the "jumps" start at about 35 Hz, with the outermost sensors jumping first. The first three sensors show no jumps at all because the phase angle never gets more negative than -180°. The "jumps" are so numerous in Figure 27 (which shows the extended 0-300 Hz frequency range) that it would be impractical to try to correct the data. The improved resolution seen in Figure 28, with sample size of 2048, helps in interpreting the

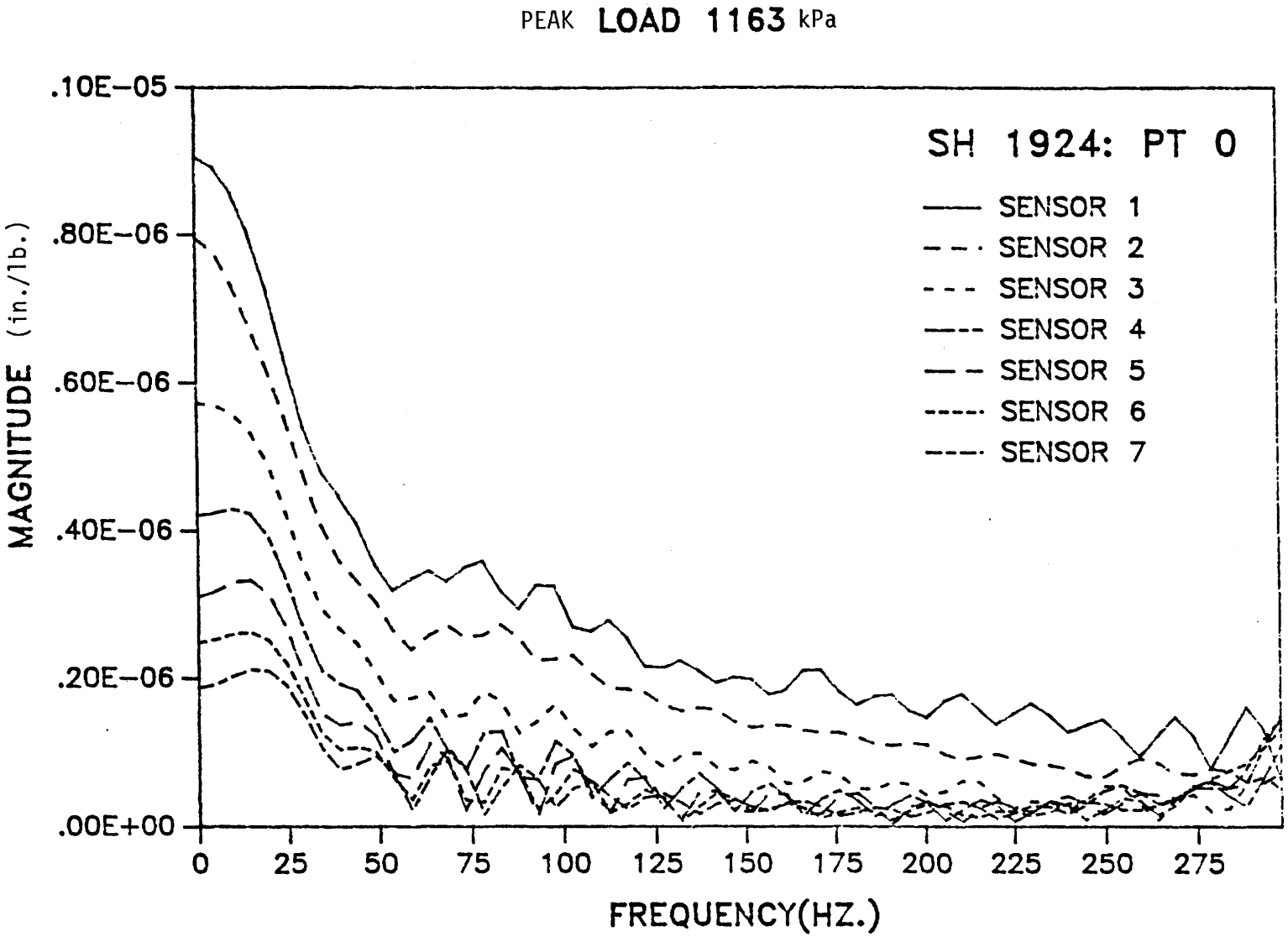

Figure 25. Magnitude of Frequency Response Function versus Frequency, Highest Load, 0-300 Hz (SH 19 - 24).

Table 4. Tail Ratio for Three Pavements and Two Load Levels.

Highway	Load Level	Force Load	Sensor						
			1	2	3	4	5	6	7
SH 19 & 24	Lowest	0.0027	-0.104	-0.0864	-0.172	-0.238	-0.3125	-0.4167	-0.25
	Highest	-0.0094	-0.0218	-0.0084	-0.017	-0.0652	-0.103	-0.117	-0.1617
FM 79	Lowest	-0.016	-0.190	-0.138	-0.174	-0.194	-0.258	-0.35	-0.375
	Highest	-0.037	-0.055	-0.010	-0.032	-0.065	-0.083	-0.121	-0.172
SH 82	Lowest	-0.032	-0.051	-0.064	-0.156	-0.192	-0.192	-0.175	-0.161
	Highest	-0.009	+0.048	0.161	0.00787	-0.0078	-0.027	-0.0511	-0.091

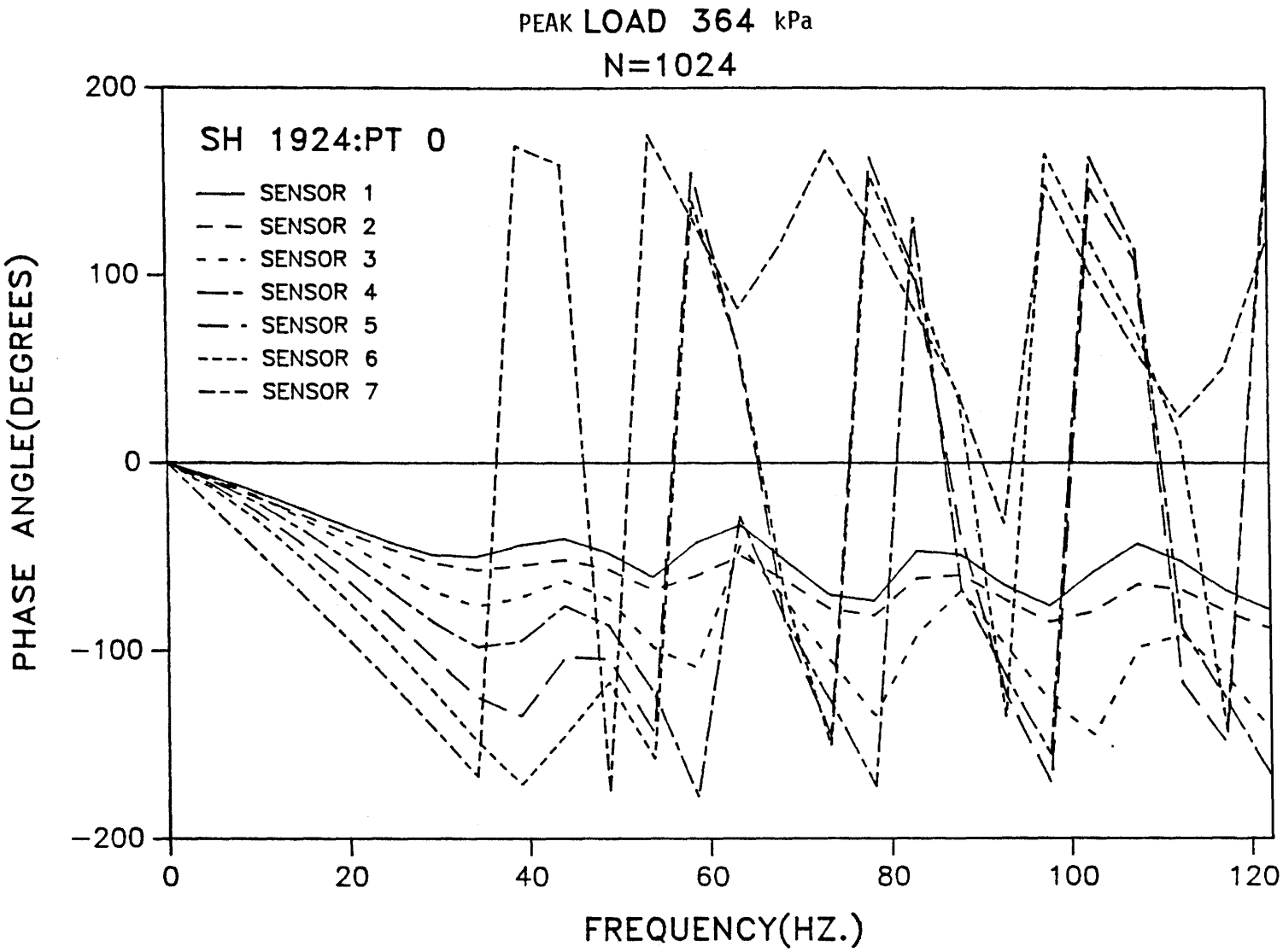

Figure 26. Phase Angle versus Frequency, Lowest Load, 0-125 Hz (SH 19 - 24).

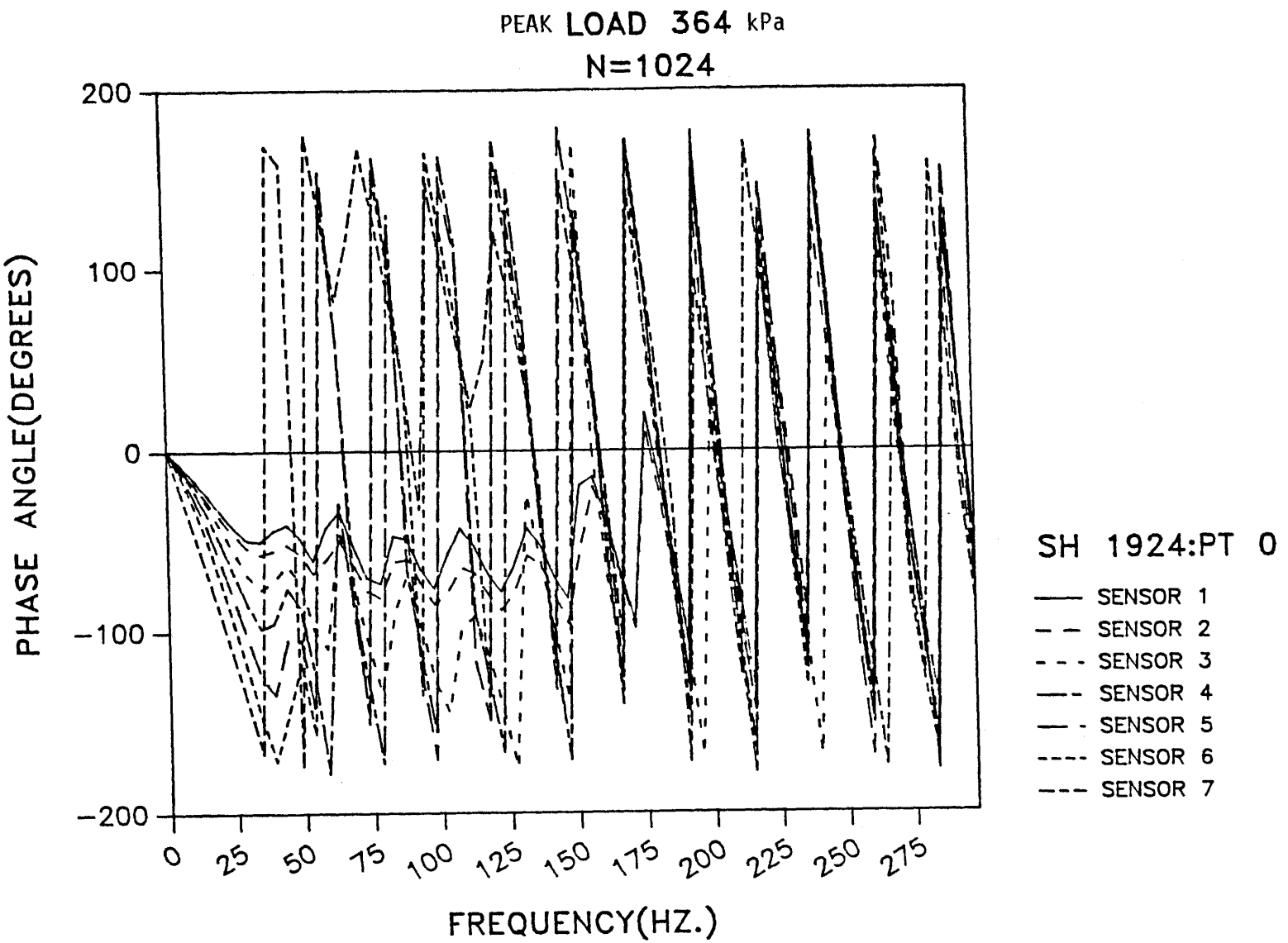

Figure 27. Phase Angle versus Frequency, Lowest Load, 0-300 Hz (SH 19 and 24).

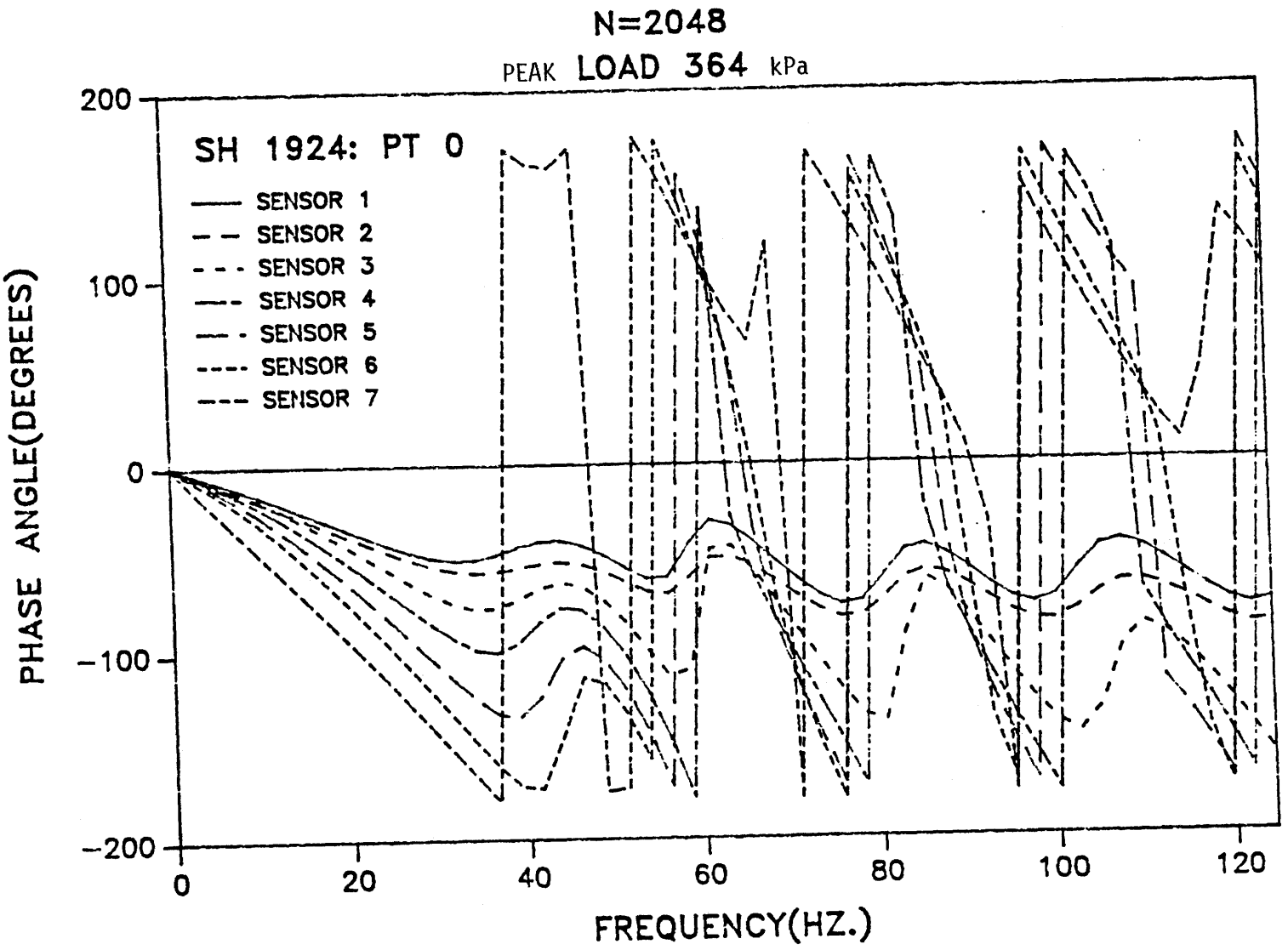

Figure 28. Phase Angle versus Frequency, Lowest Load, 0-125 Hz, N = 2048 (higher resolution), (SH 19 and 24).

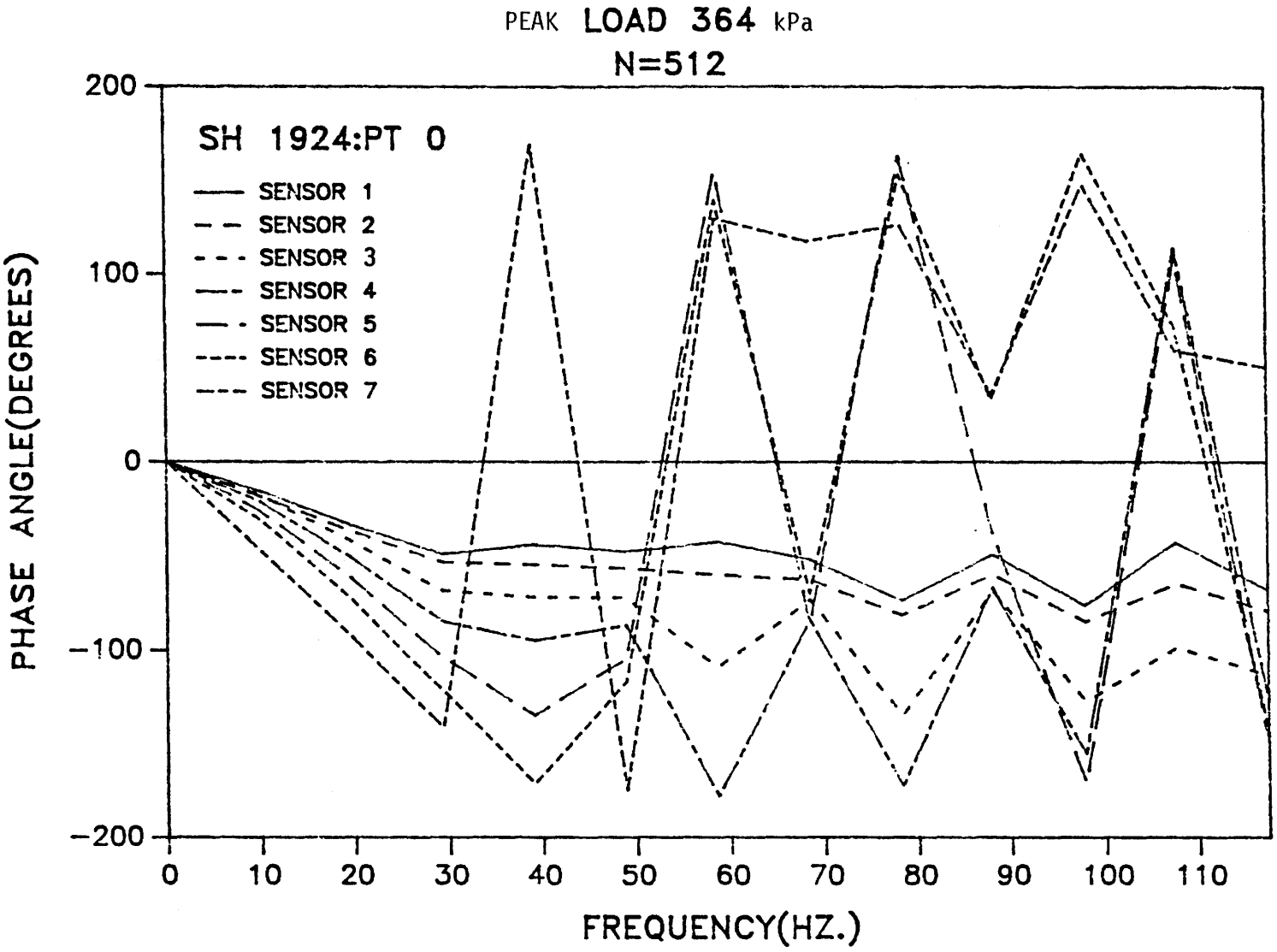

Figure 29. Phase Angle versus Frequency, Lowest Load, 0-115 Hz, N = 512 (lower resolution), (SH 19 and 24).

discontinuities, but interpretation is still difficult. The poor resolution in Figure 29 with sample size of 512, makes interpretation impossible. The phase data in Figure 30 shows the effect of applying the linear correction to the pulse to eliminate the tail discontinuity, as indicated in Figure 14b. Figure 30 shows a single jump for each of the last three sensors.

The jumps in the last three sensors were eliminated by subtracting 360° from the phase angles immediately after the jump. The results are seen in Figure 31. The phase angle data is seen to behave regularly, with the phase angle for each sensor increasing with frequency and the phase angles increasing with distance. The phase angles are nearly linear with frequency for the first 20-30 degrees. Some irregularity is present in the phase data for the higher frequencies and the outer sensors. This is probably due to noise in the sensor or force signal. A comparison of the uncorrected phase data in Figures 26 and 28 to the corrected data in Figure 31 shows the dramatic improvement made possible by the correction.

The phase angle data for the highest load (SH 19 and 24) is shown in Figure 32. Except for the first three sensors, the phase angle data has many discontinuities due to branch jumps and is therefore difficult to interpret. The oscillations are not as pronounced as they were for the lowest load, again because the tail discontinuity was moderate due to the high load level (Table 4).

Frequency response data on a thin pavement (FM 79) is given in Appendix A (Figures A5 to A9), and thick pavement data (SH 82) is given in Appendix B (Figures B5 to B9). No frequency resolution studies or pulse corrections were made on the data in Appendices A and B. The data is presented for comparison purposes to illustrate the changes in pavement thickness. The most interesting comparison is the correlation of the pulse tail ratio (Table 3) to the oscillations. The frequency response functions for SH 82 behaved similarly to SH 19 and 24, whereby the oscillations are worse for the lowest load. The thin pavement (FM 79) behaved differently; the moderate "tails" in the lowest load pulses resulted in moderate oscillations in the frequency response functions in Figures A5 and A6. The highest load data in Figure A7 showed severe oscillations by sensor 2 which had the worst tail. Sensors 3 through 7 had very little oscillation because the "tails" were small (Table 4). The phase angle data for the FM 79 highest load (Figure A9) had the least number of discontinuities, or jumps from -180° to +180°, of any of the uncorrected data in the frequency range of 0 to 125 Hz because the oscillations were small for the outer sensors. All of the other phase data for SH 82 and FM 79 is very difficult to interpret because

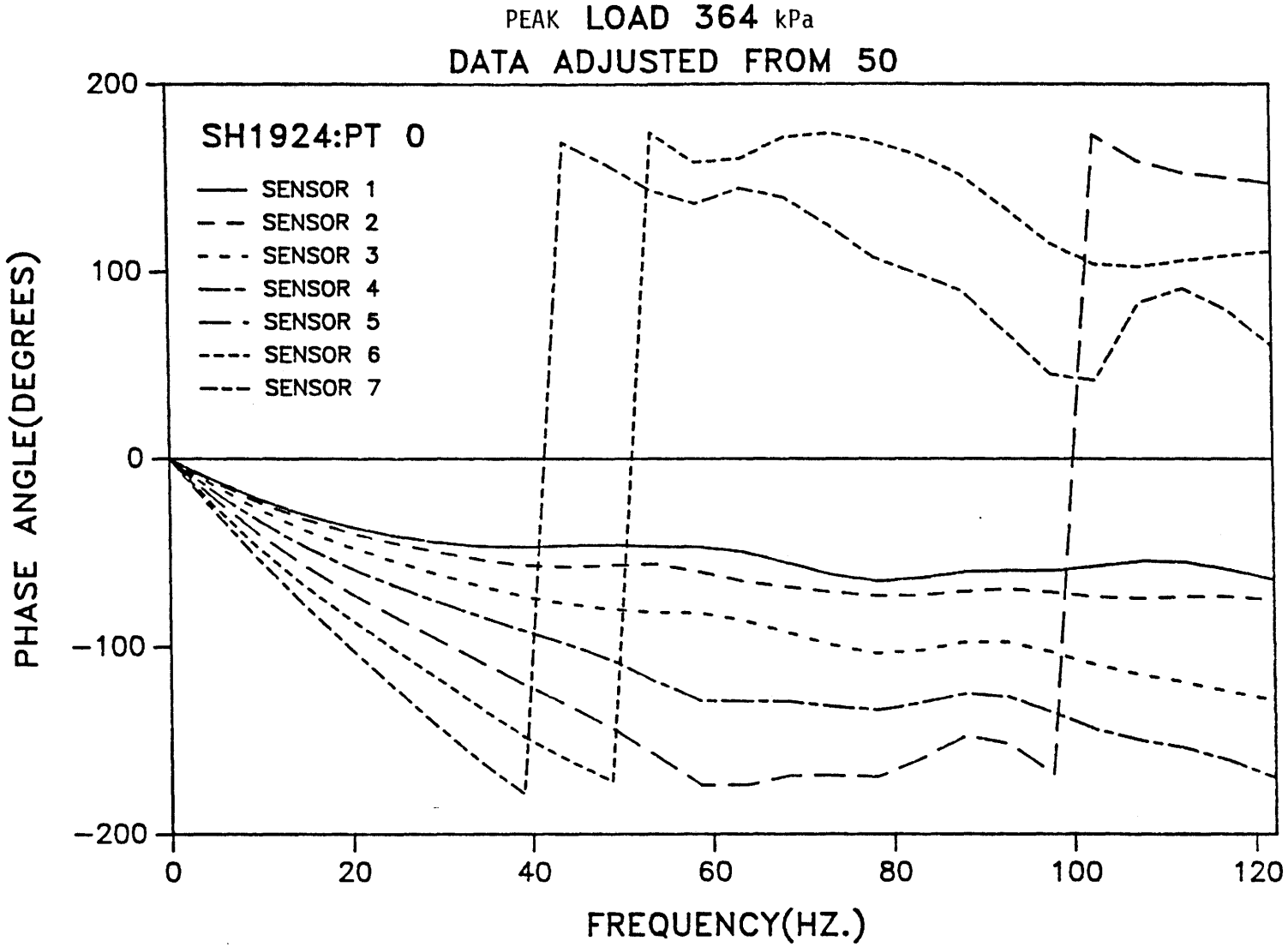

Figure 30. Phase Angle versus Frequency, Lowest Load, 0-125 Hz Corrected Pulse with No Discontinuity (SH 19 and 24).

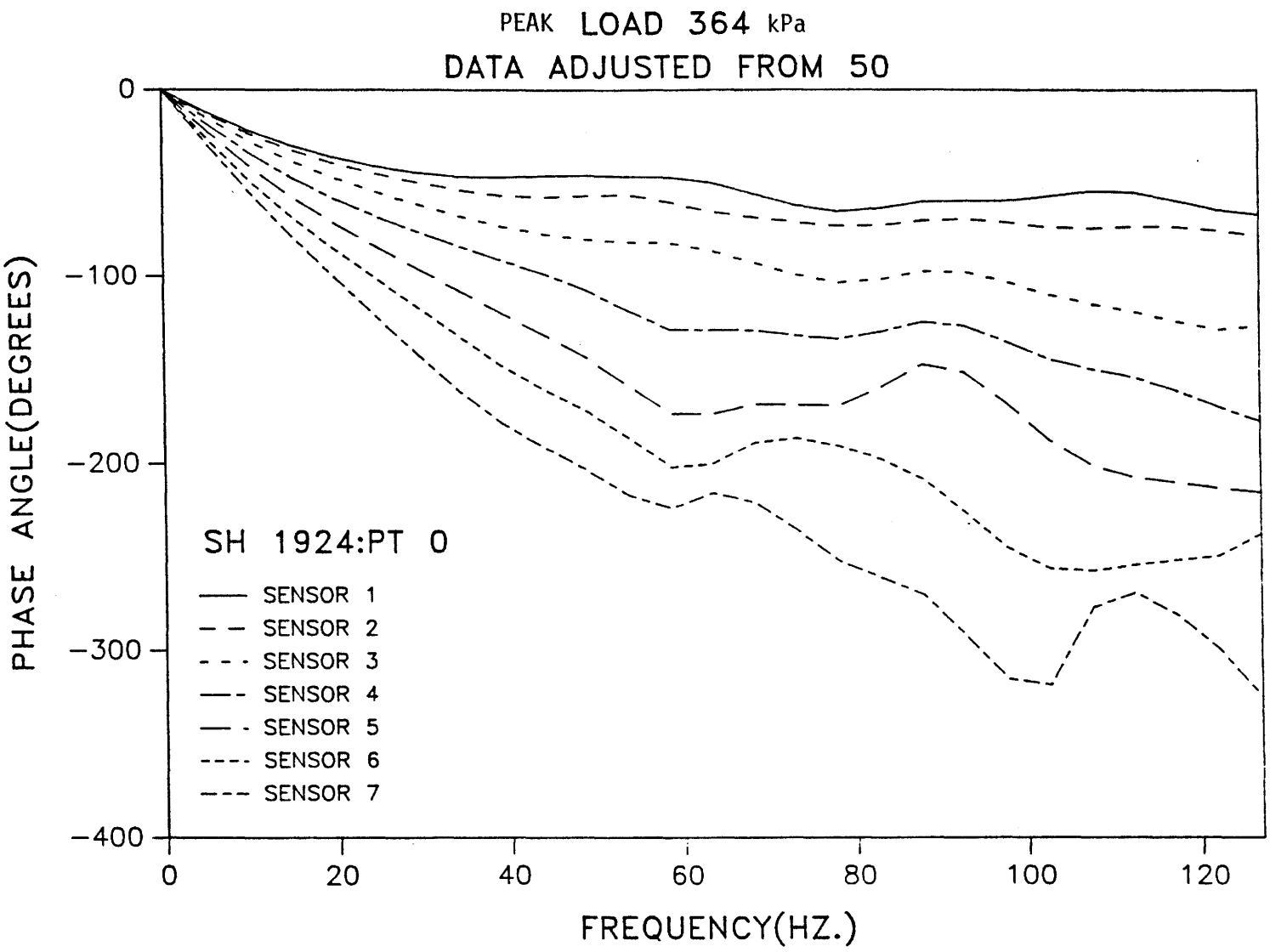

Figure 31. Phase Angle versus Frequency, Lowest Load, 0-125 Hz Using Corrected Pulse with Branch Jumps Eliminated (SH 19 and 24).

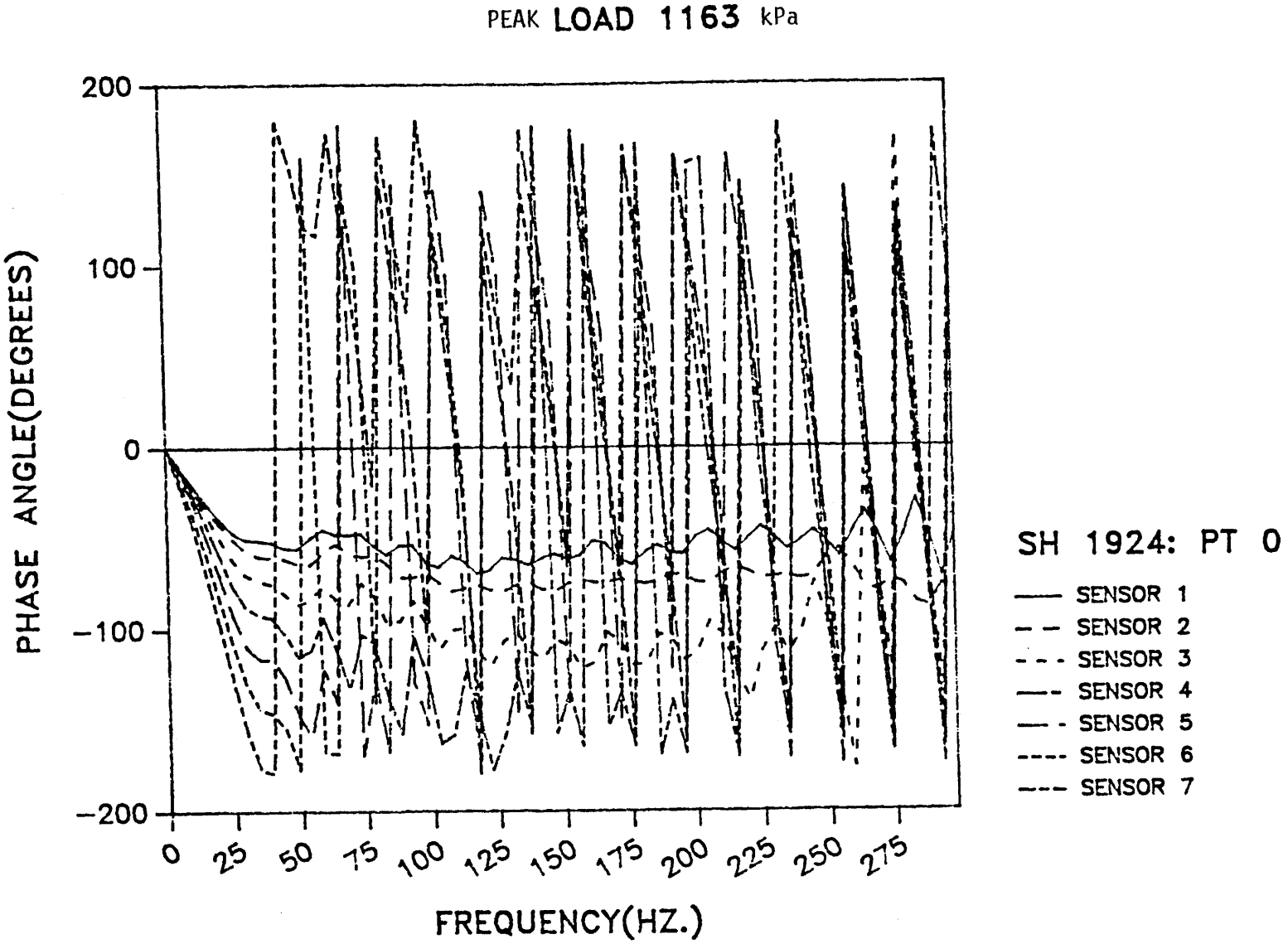

Figure 32. Phase Angle versus Frequency, Highest Load, 0-300 Hz (SH 19 and 24).

of the phase discontinuity problem. Whether this behavior is typical of thin pavements will not be known until more thin pavement data is analyzed.

CHAPTER V

SUMMARY, CONCLUSIONS, AND RECOMMENDATIONS

Falling-Weight Deflectometer (FWD) full-pulse data from three in-service highway sections have been analyzed to obtain dynamic response information. The three sections analyzed have thin (1.5"), medium (9") and thick (12" asphaltic concrete pavements. Data for two load levels for each pavement have also been analyzed. The time series data for the force pulse and the seven seismometer surface deflection pulses at r = 1, 2, 3, 4, 5, and 6 ft. are presented. The force and deflection pulse data were Fourier transformed using a Fast Fourier Transform (FFT) algorithm and pavement frequency response functions were computed. The frequency response functions are the FFT deflections divided by the FFT force. They are preseOnted in the form of separate magnitude and phase angle plots versus frequency for each displacement. These plots have an oscillatory component superimposed on them that is not predicted by the elasto-dynamic or viscoelastic theory. The oscillation makes the phase angle data for the outer sensors extremely difficult to interpret because it produces many "jumps" or discontinuities between -180° and +180°. This will make the phase angle data reduction very expensive and time-consuming. In general, the severity of the oscillations is higher for the low load levels. The oscillation is attributed to the truncation of the pulses at 60 msec. This results in a discontinuity in the pulse because of zero-packing of the data in the FFT algorithm. The discontinuity occurs because the pulses do not decay out to zero at the end of the fixed sample time. The pulse "tails" may be due to one or more of the following factors:

1. Drift from digital integration and filtering of the raw seismometer data,
2. Permanent deformation of the pavement, or
3. Premature truncation before the transient response has decayed out.

The relationship between the "tail" and the load level is shown by taking ratios of the "tails" to the peaking of the respective pulses. The results are shown in tabular form. A definite correlation between the "tail ratio" and the severity of oscillatory behavior of the frequency response functions is evident

by visually comparing the frequency plots to the "tail" ratios for both load levels.

To verify if the discontinuity in the displacement pulses was causing the oscillations, the pulses were adjusted by introducing a linear (in time) correction such that the discontinuity at 60 msec was eliminated. For the SH 19 and 24 lowest load data, the frequency response functions were recalculated using the corrected pulses. The result was that the superimposed oscillations were virtually eliminated for both magnitude and phase responses, giving the data a much smoother, regular variation with frequency. This greatly simplified interpretation of the phase angle data which without the correction has many discontinuities (from -180° to +180°) due to branch interchanges of the arctangent function. Making this correction to the data will enable investigators to make more accurate comparisons of computed responses to measured FWD responses. The improvement will make it economical and practical to interpret phase angle data for the full frequency range of 0-125 Hz.

Recommendations

1. For use in back-calculation studies to be performed later in the project, FWD full-pulse data should be presented in the form of frequency-response functions as defined in this report. The results should be presented in magnitude and phase-angle format. This format for presenting the data is similar to the format used in the computer programs developed for this project. The phase angle data (as shown, for example, in Figure 31) is particularly sensitive to damping effects, which are directly related to rutting and cracking properties of pavements.
2. As an interim measure to eliminate oscillations in frequency response functions, the FWD full-pulse data should be corrected to eliminate the "tail" discontinuity by using a linear correction in time as described in this report.
3. An investigation of the cause or causes of the pulse "tail" should be conducted and means of improving measurements for dynamic data analysis should be developed to reduce or eliminate the "tail." This investigation requires:
    a. Dynatest FWD software and/or hardware modification so that a 100 msec or 120 msec pulse sampling period can be used as an option.

b. Time-domain synthesis of responses should be computed from a linear layered viscoelastic media computer program using actual force pulse data as input (for comparison with extended time pulses).

c. The manufacturer of the Dynatest units should investigate possible causes of drift and recommend ways to reduce or correct for drift.

d. The possibility of pavement permanent deformation as a contributing cause of the pulse "tail" should be investigated. This will require analysis of responses using nonlinear stress-strain relationships locally, using finite element analysis.

REFERENCES

Arnold, R.N., G.N. Bycroft, and G.B. Warburton. "Forced Vibrations of a Body on an Infinite Elastic Solid." Journal of Applied Mechanics, Transportation ASME Vol. 77, 1955, pp. 391-401.

Bendat, J.S. and A.G. Piersol. Random Data: Analysis and Measurement Procedures. Wiley-Interscience, New York, 1971.

Bendat, J.S. and A.G. Piersol. Engineering Applications of Correlation and Spectral Analysis. Wiley-Interscience, New York, 1980.

Davis, P.J. and P. Rabinowitz. Methods of Numerical Integration. Academic Press, New York, 1975.

Lee, Y.W. Statistical Theory of Communication. John Wiley and Sons, Inc., New York, 1960.

Lytton, R.L., F.L. Roberts, and S.M. Stoffels. "Determination of Asphaltic Concrete Pavement Structural Properties by Nondestructive Testing." Final Report, Phase I, NCHRP Project 10-27, July 1986.

Lytton, R.L. "Backcalculation of Pavement Layer Properties." Presented at the First Symposium on Nondestructive Testing of Pavements and Backcalculation of Moduli. ASTM, Baltimore, Maryland, 1988.

Magnuson, A.H. "Computer Analysis of Falling-Weight Deflectometer Data, Part I: Vertical Displacement Computations on the Surface of a Uniform (One-Layer) Halfspace Due to an Oscillating Surface Pressure Distribution." Texas Transportation Institute Research Report 1215-1, October 1988.

Reissner, E. "Stationare, Axialsymmetrische Durch Eine Schuttelnde Masseerregte Schwingugen Eines Homogenen Elastischen Halbraumes." Ingenieur-Archives, Vol. 8, No. 6, 1936, pp. 381-396.

Sung, T.Y. "Vibration in Semi-Infinite Solids Due to Periodic Surface Loadings." Symposium on Dynamic Testing of Soils, ASTM, STP 156, 1953, pp. 35-68.

Uzan, J., R.L. Lytton, and F.P. Germann. "General Procedure for Backcalculating Layer Moduli." First Symposium on NDT of Pavements and Backcalculation of Moduli, ASTM, 1988.

APPENDIX A

DATA FOR FM ROAD 79

Figure:

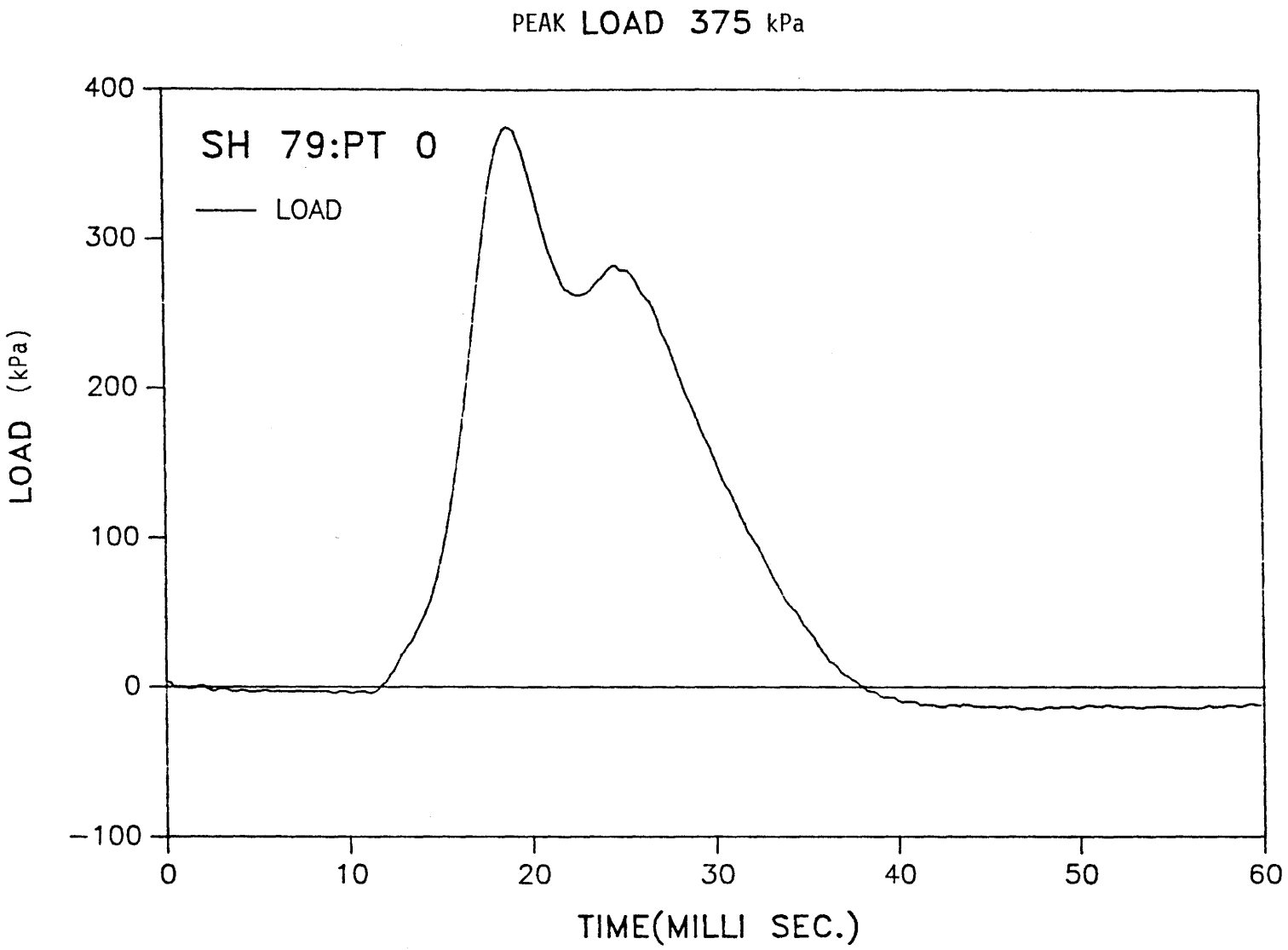

Figure A-1. Force pulse, lowest load.

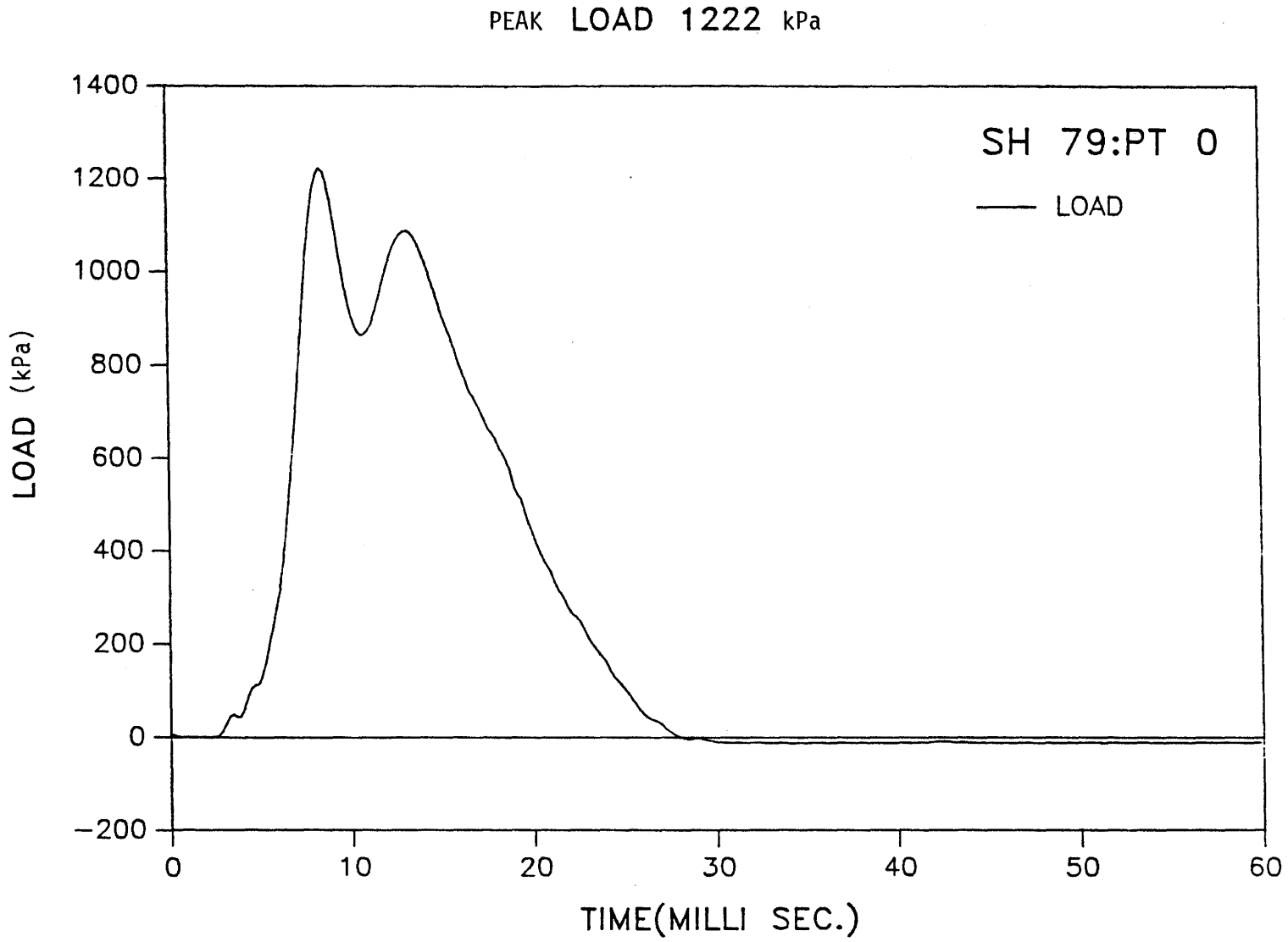

Figure A-2. Force pulse, highest load.

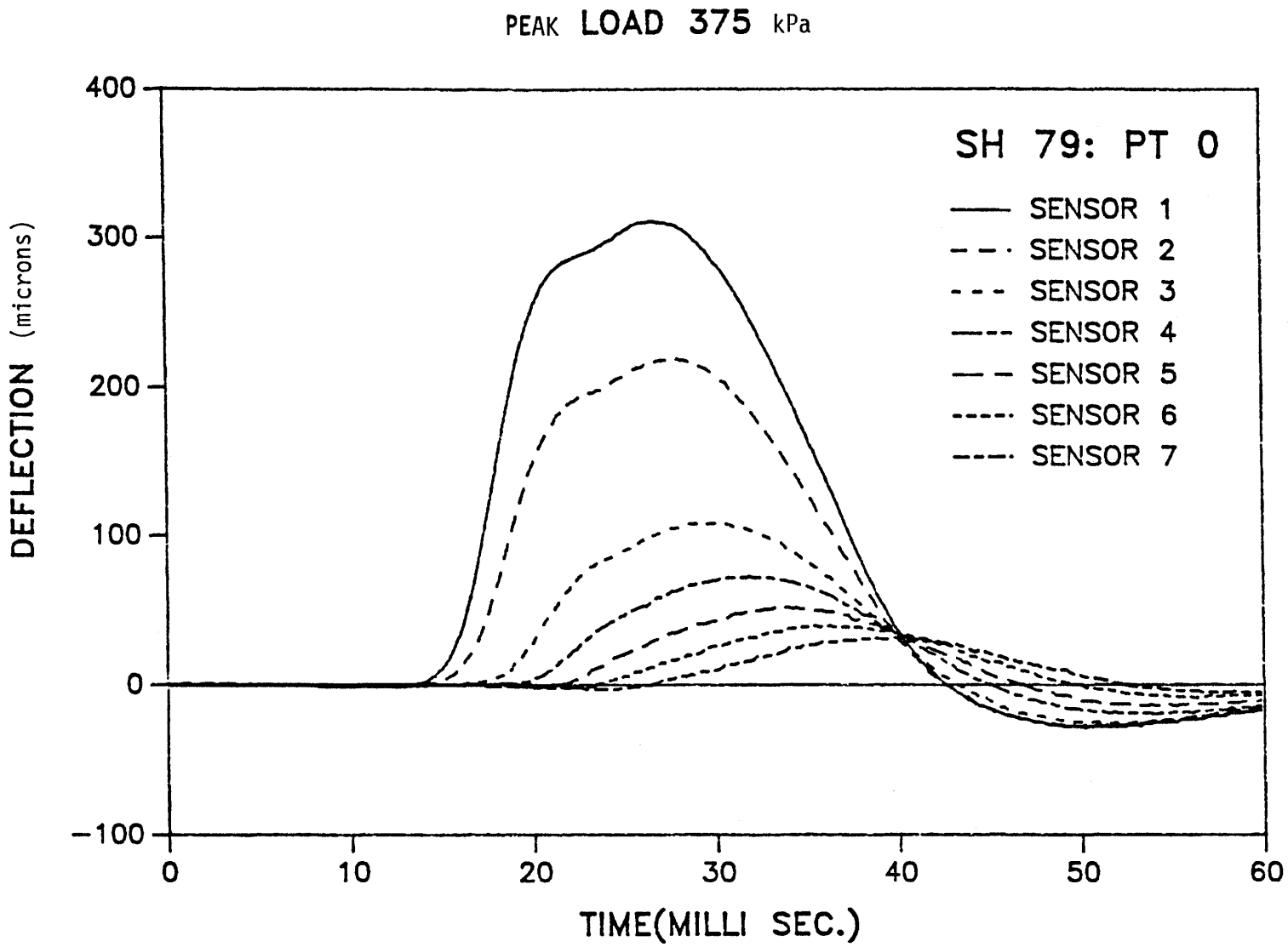

Figure A-3. Deflection pulses, lowest level.

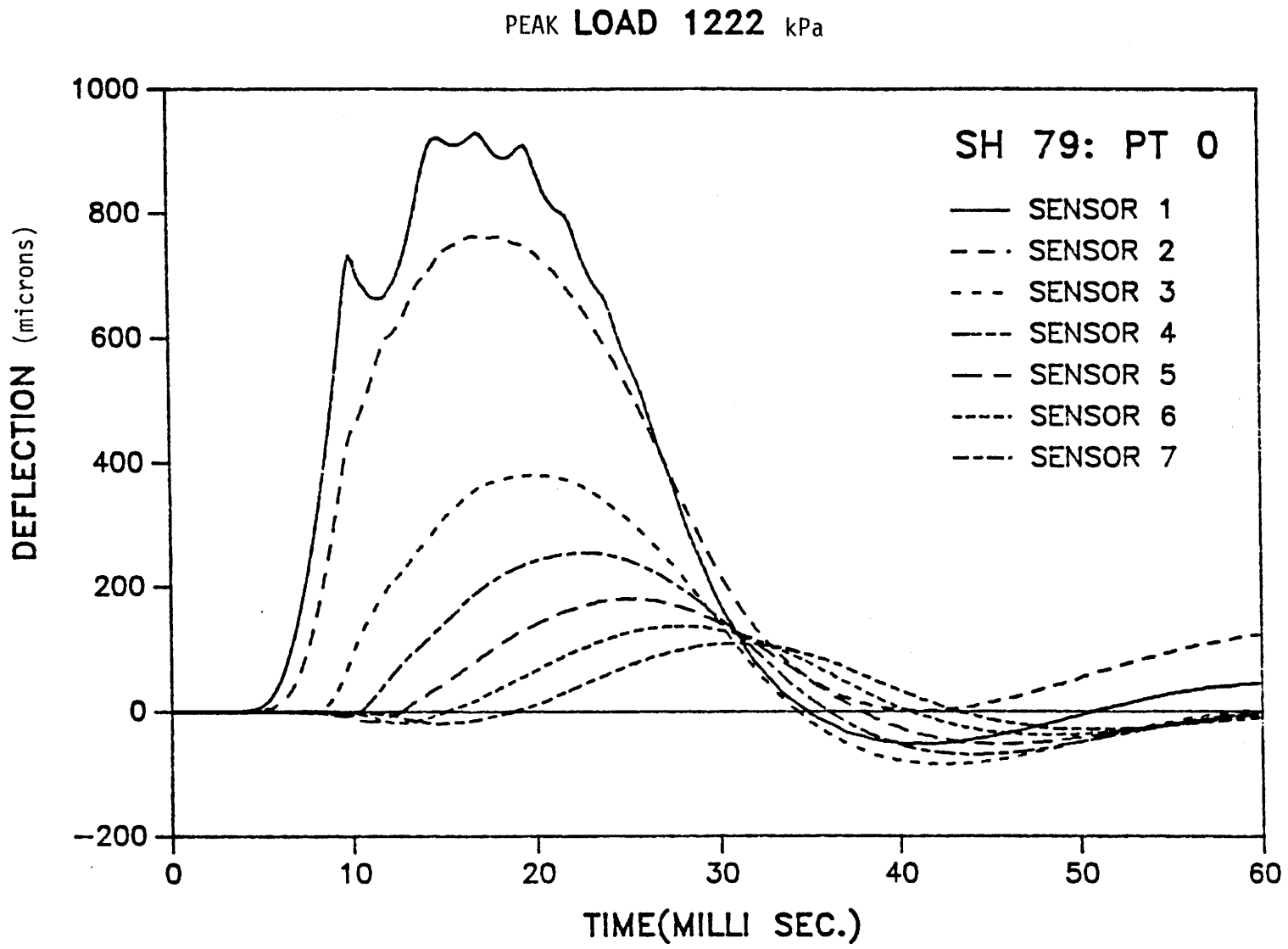

Figure A-4. Deflection pulses, highest load.

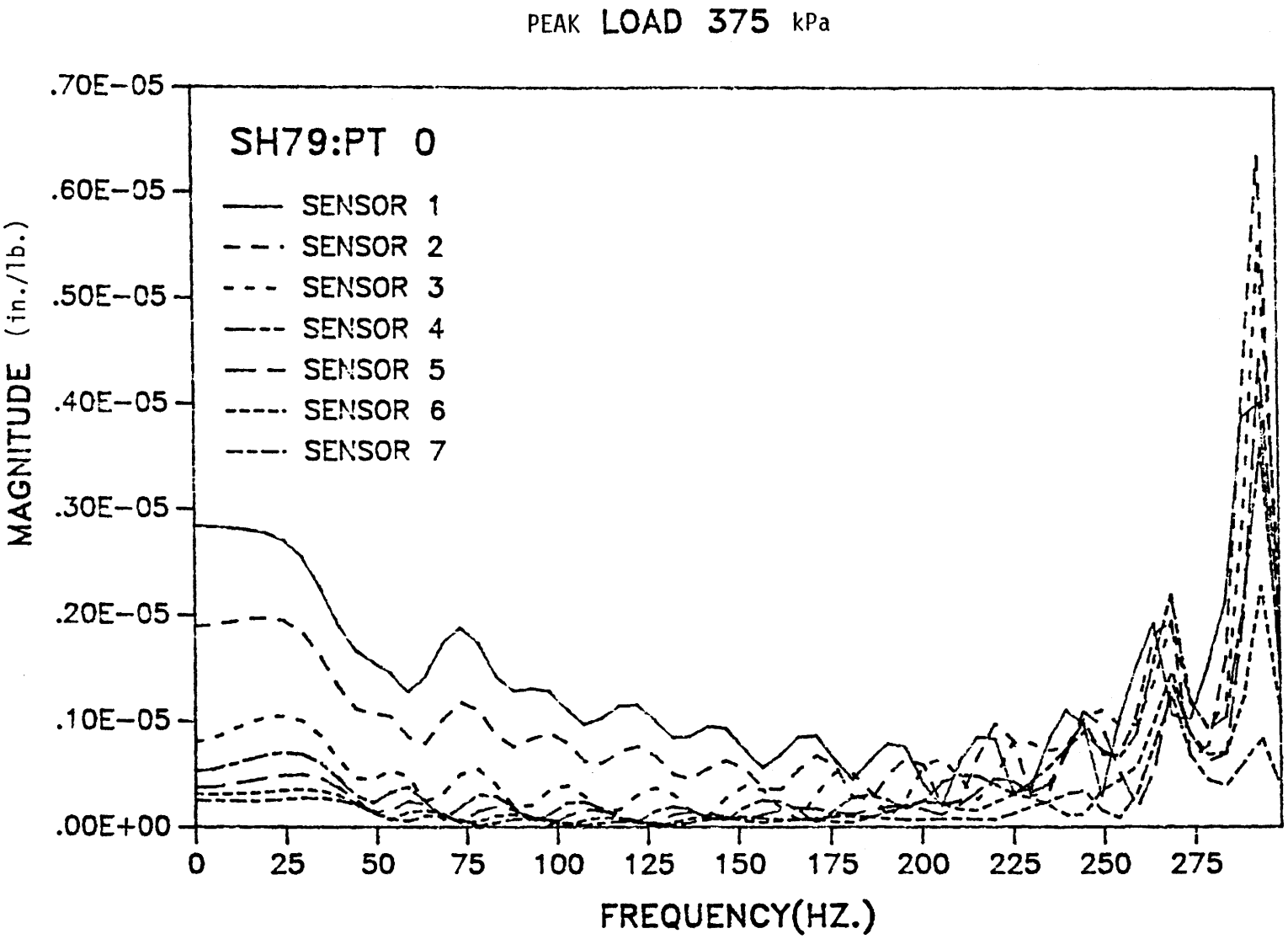

Figure A-5. Magnitude of frequency response function, 0-300 Hz, lowest load.

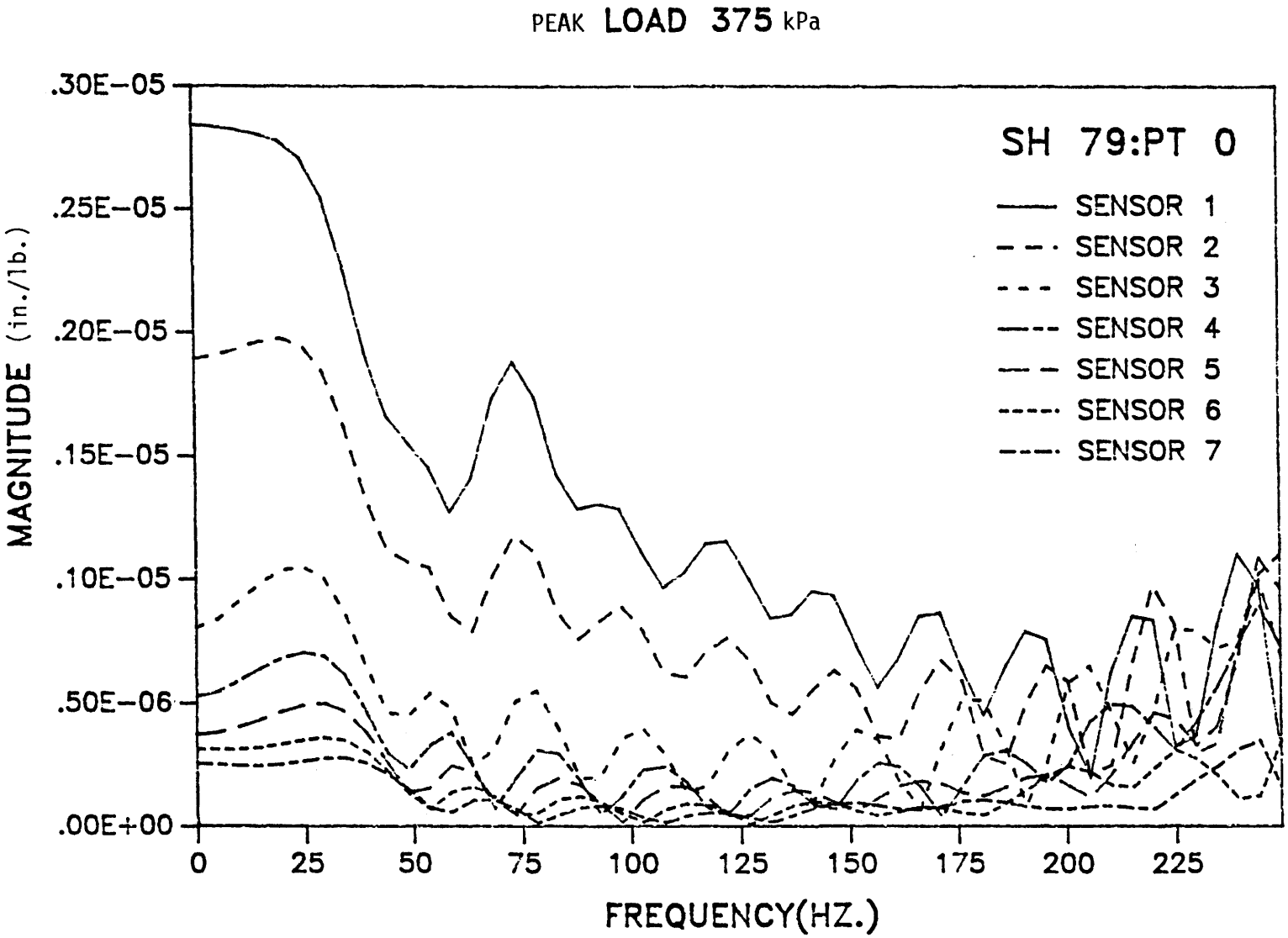

Figure A-6. Magnitude of frequency response function, 0-250 Hz, lowest load.

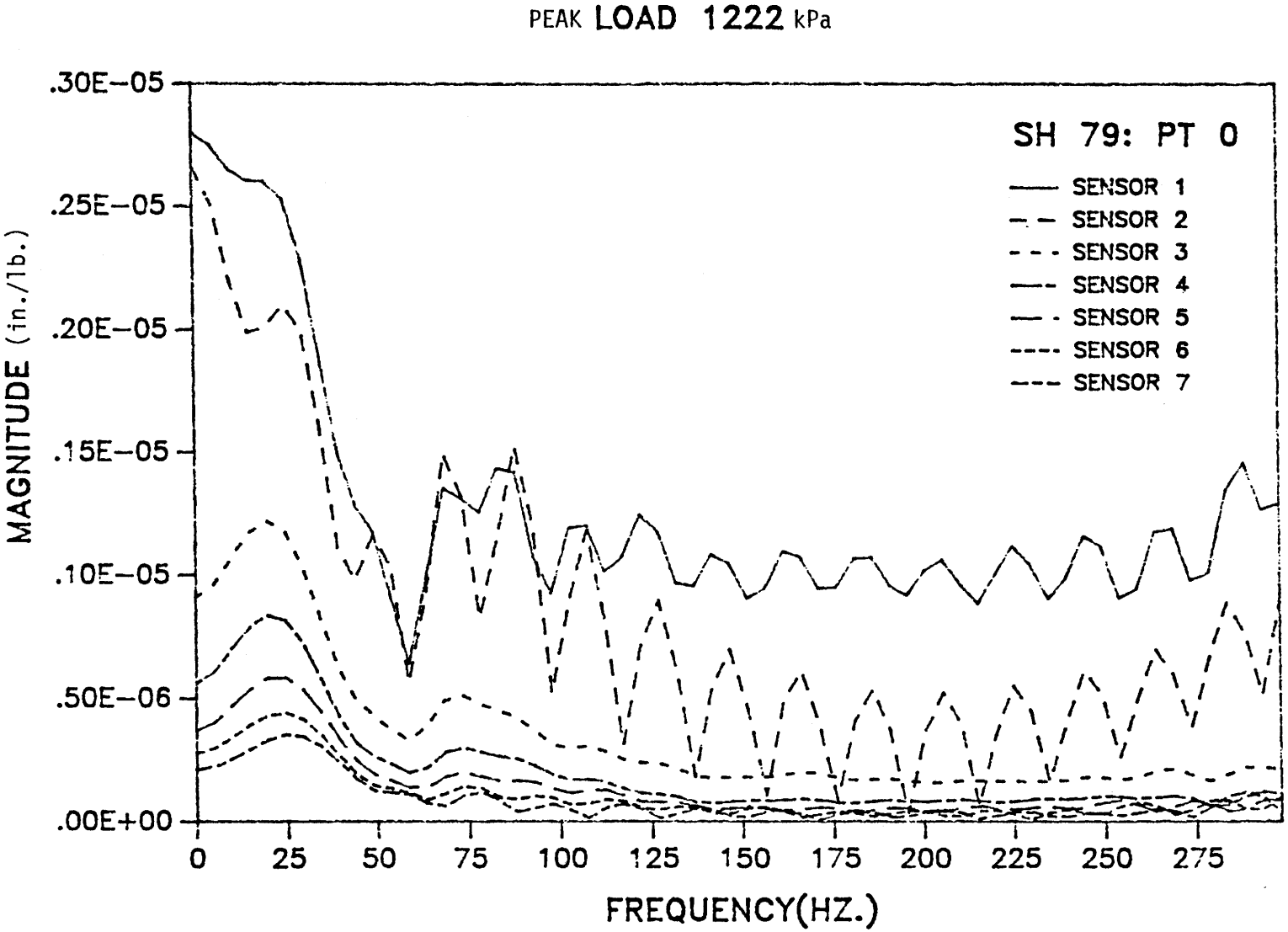

Figure A-7. Magnitude of frequency response function, 0-300 Hz, highest load.

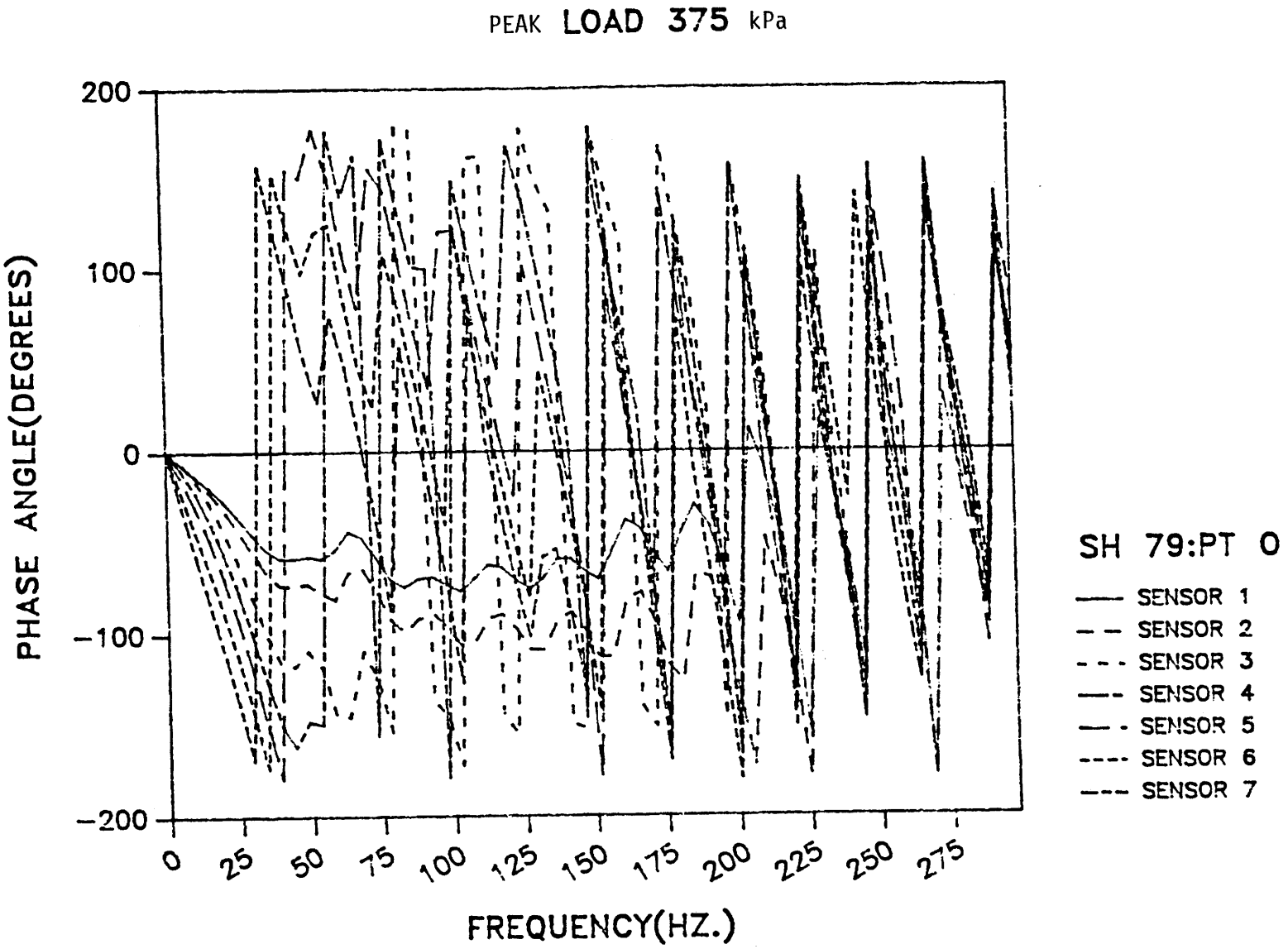

Figure A-8. Phase angle of response, 0-300 Hz, lowest load.

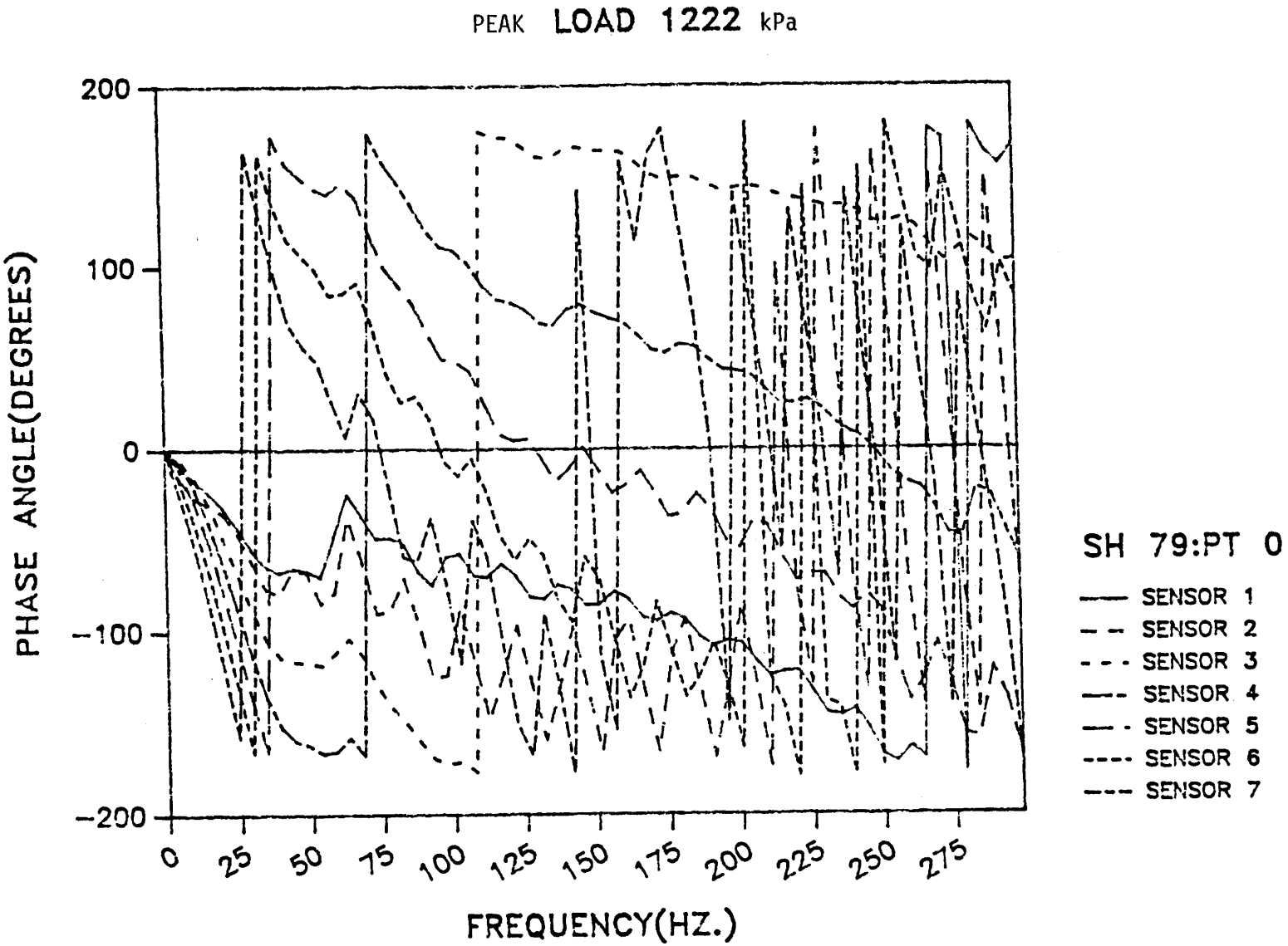

Figure A-9. Phase angle of response, 0-300 Hz, highest load.

APPENDIX B

DATA FOR STATE HIGHWAY 82

Figure:

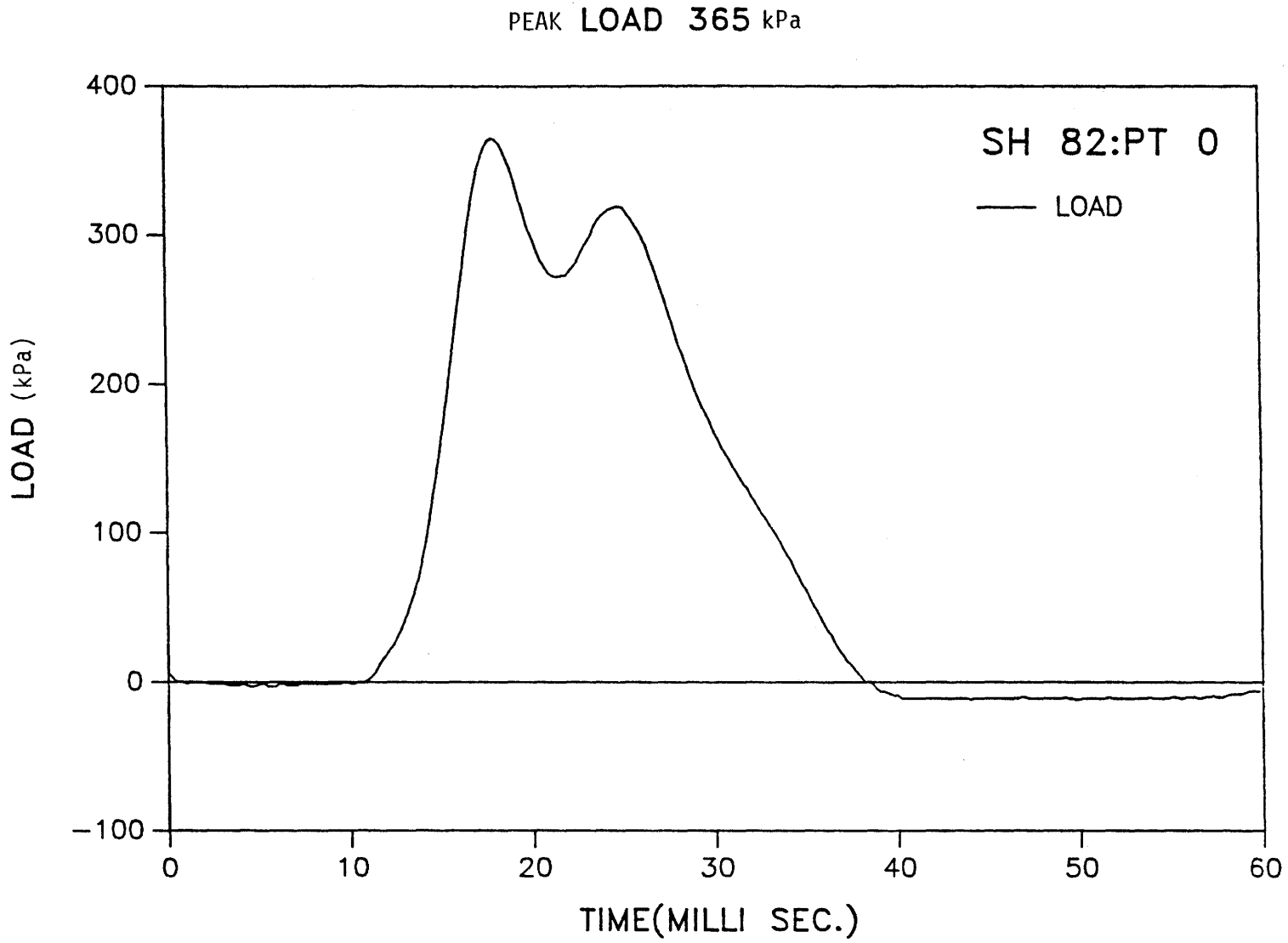

Figure B-1. Force pulse, lowest load.

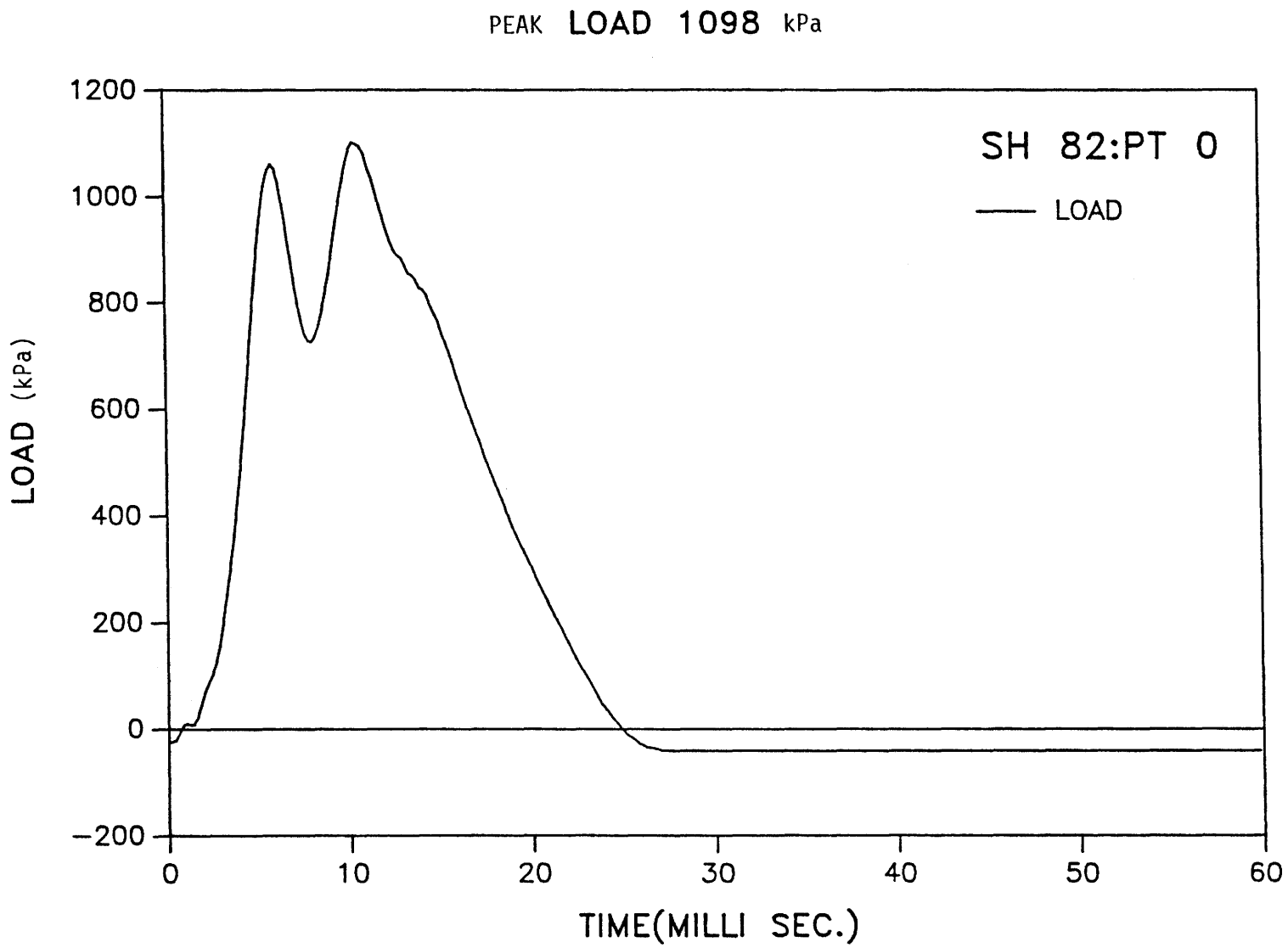

Figure B-2. Force pulse, highest load.

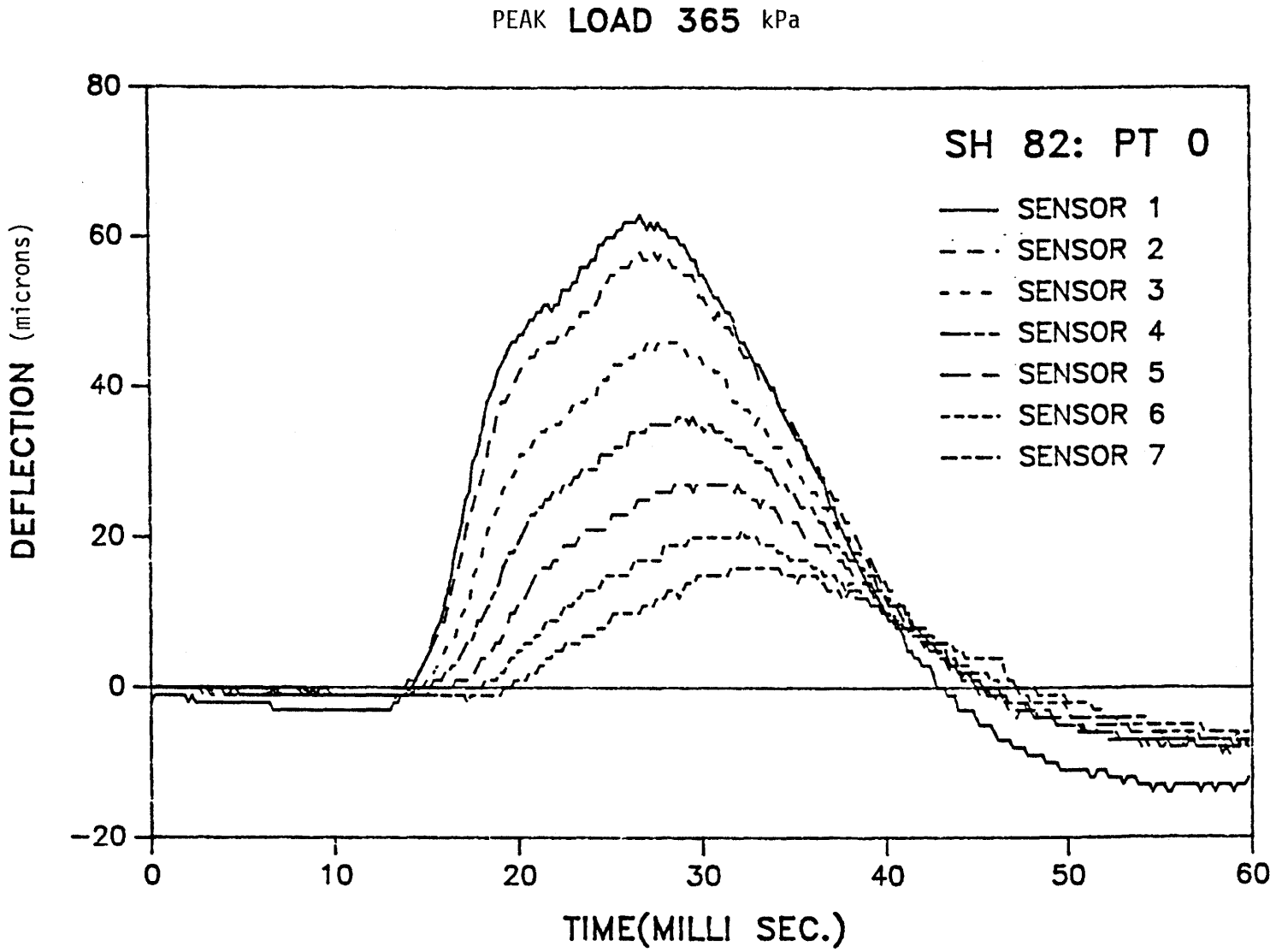

Figure B-3. Deflection pulses, lowest load.

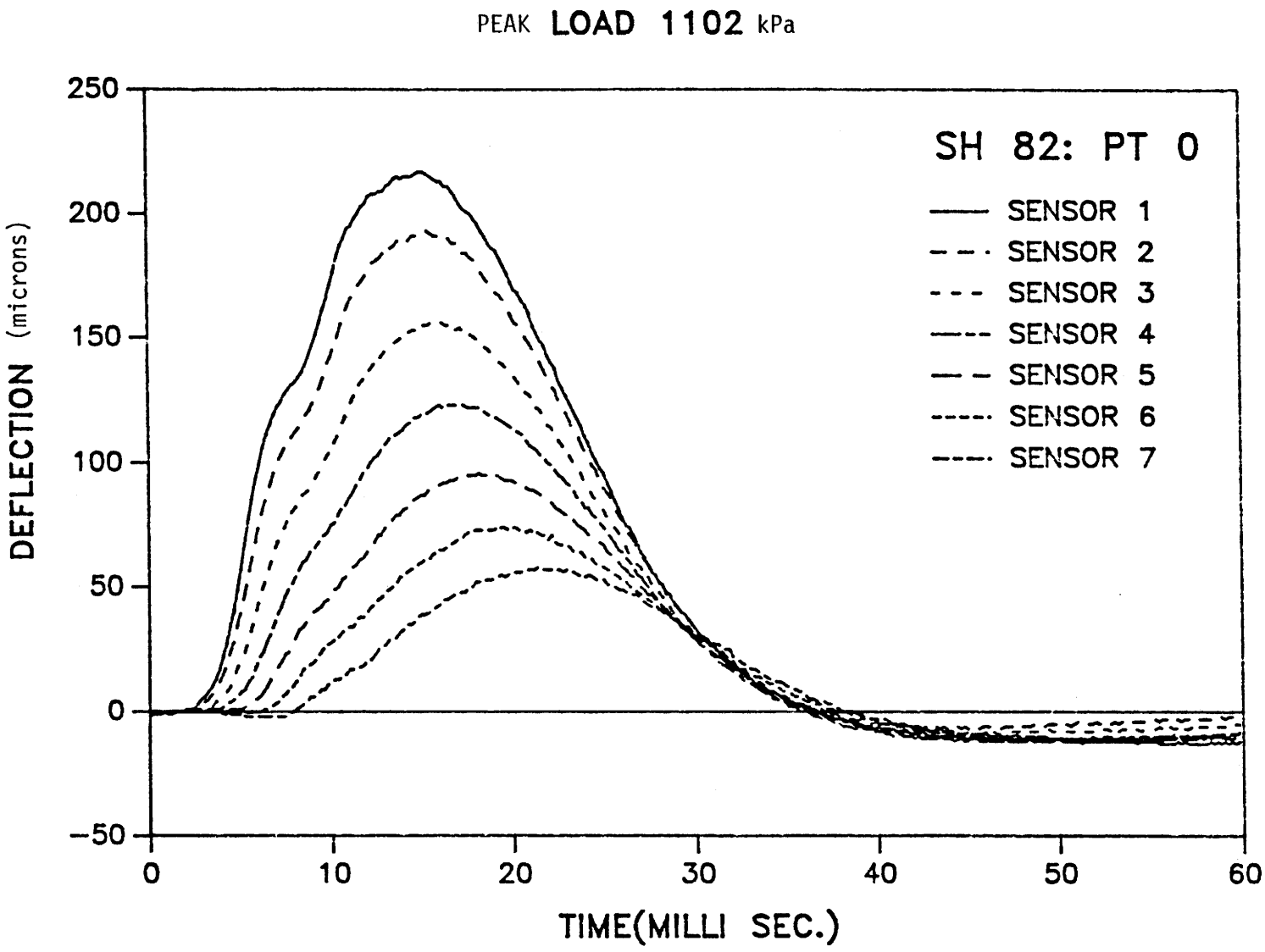

Figure B-4. Deflection pulses, highest load.

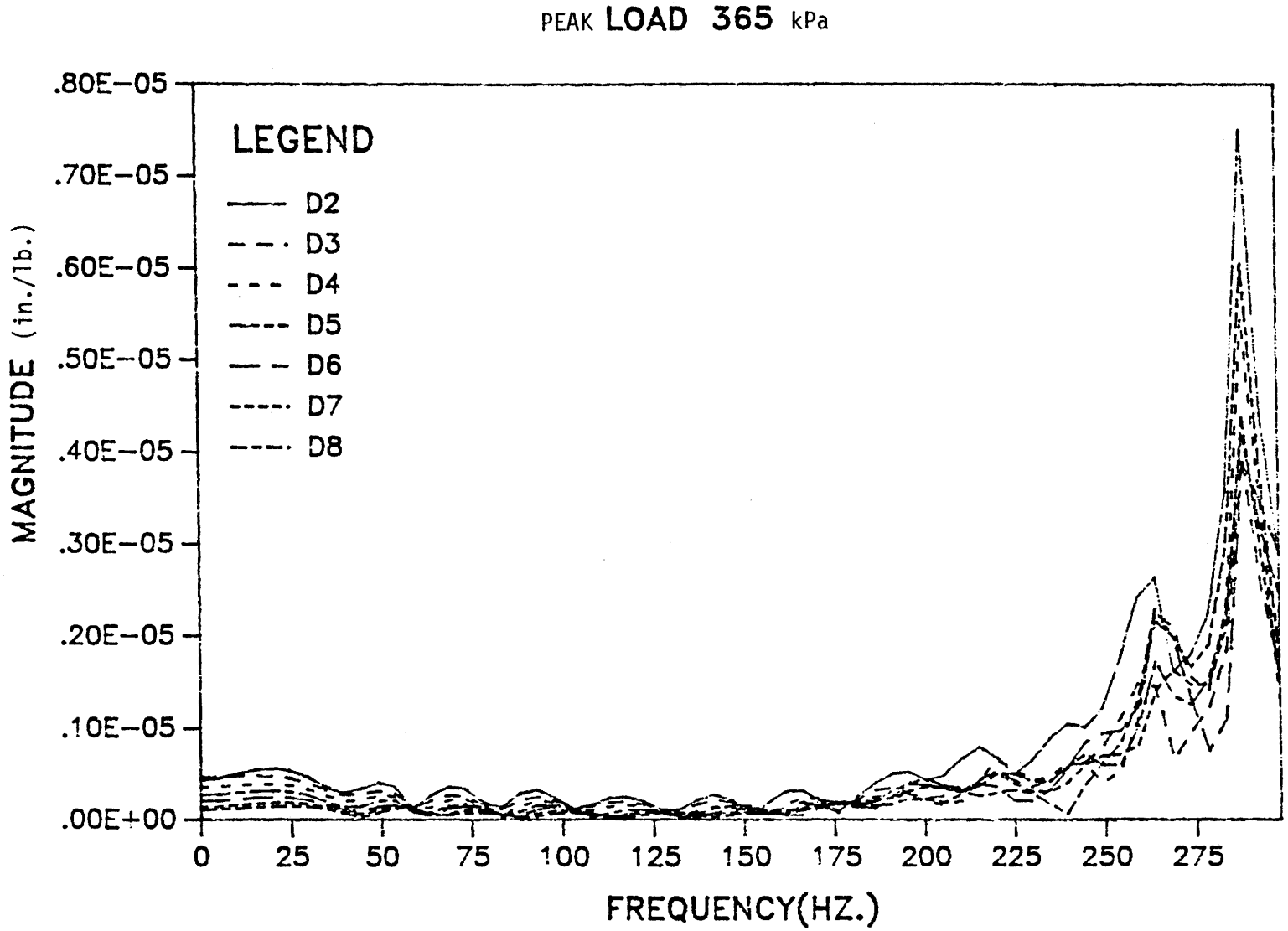

Figure B-5. Magnitude of frequency response function, 0-300 Hz, lowest load.

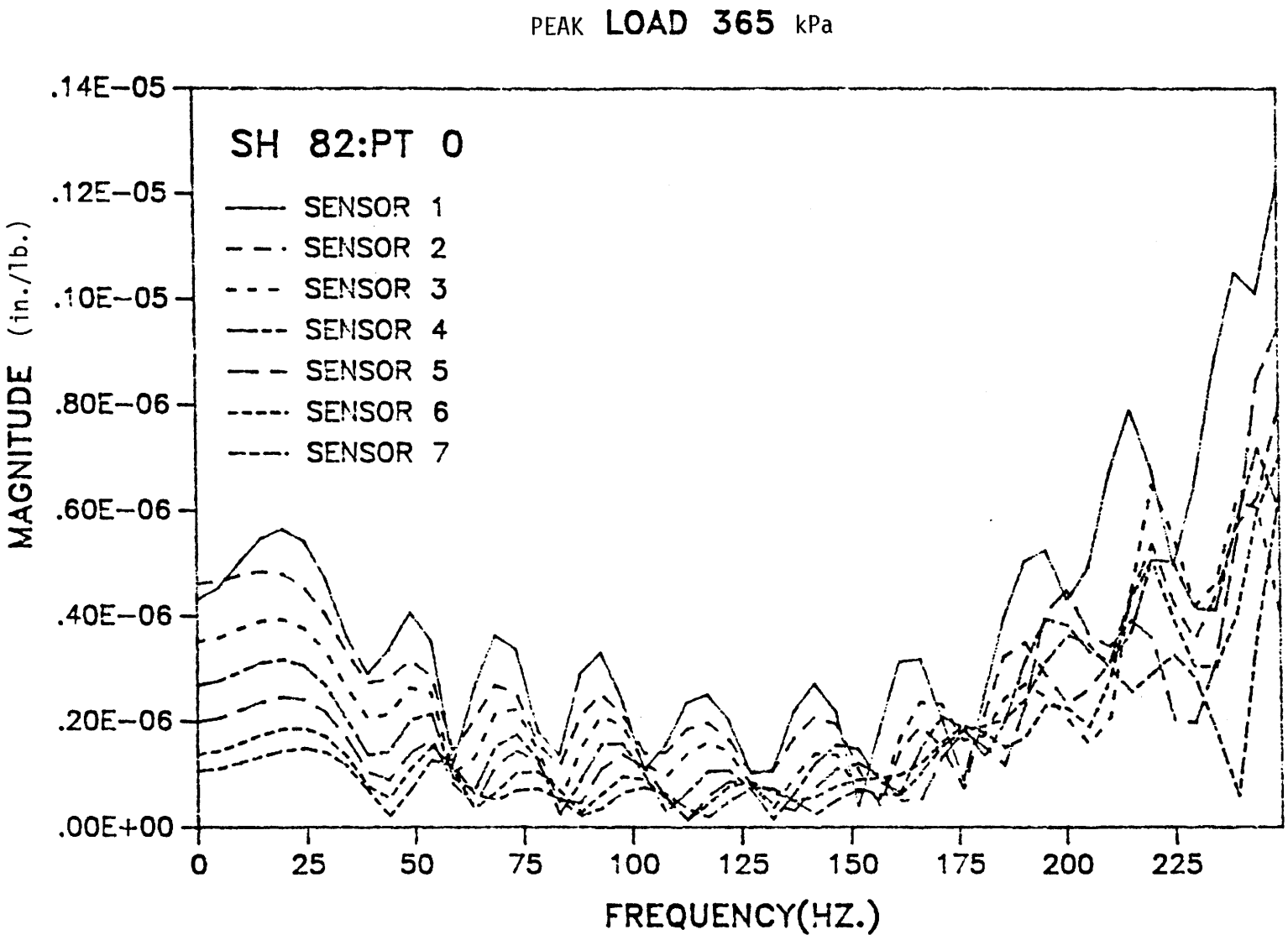

Figure B-6. Magnitude of frequency response function, 0-250 Hz, lowest load.

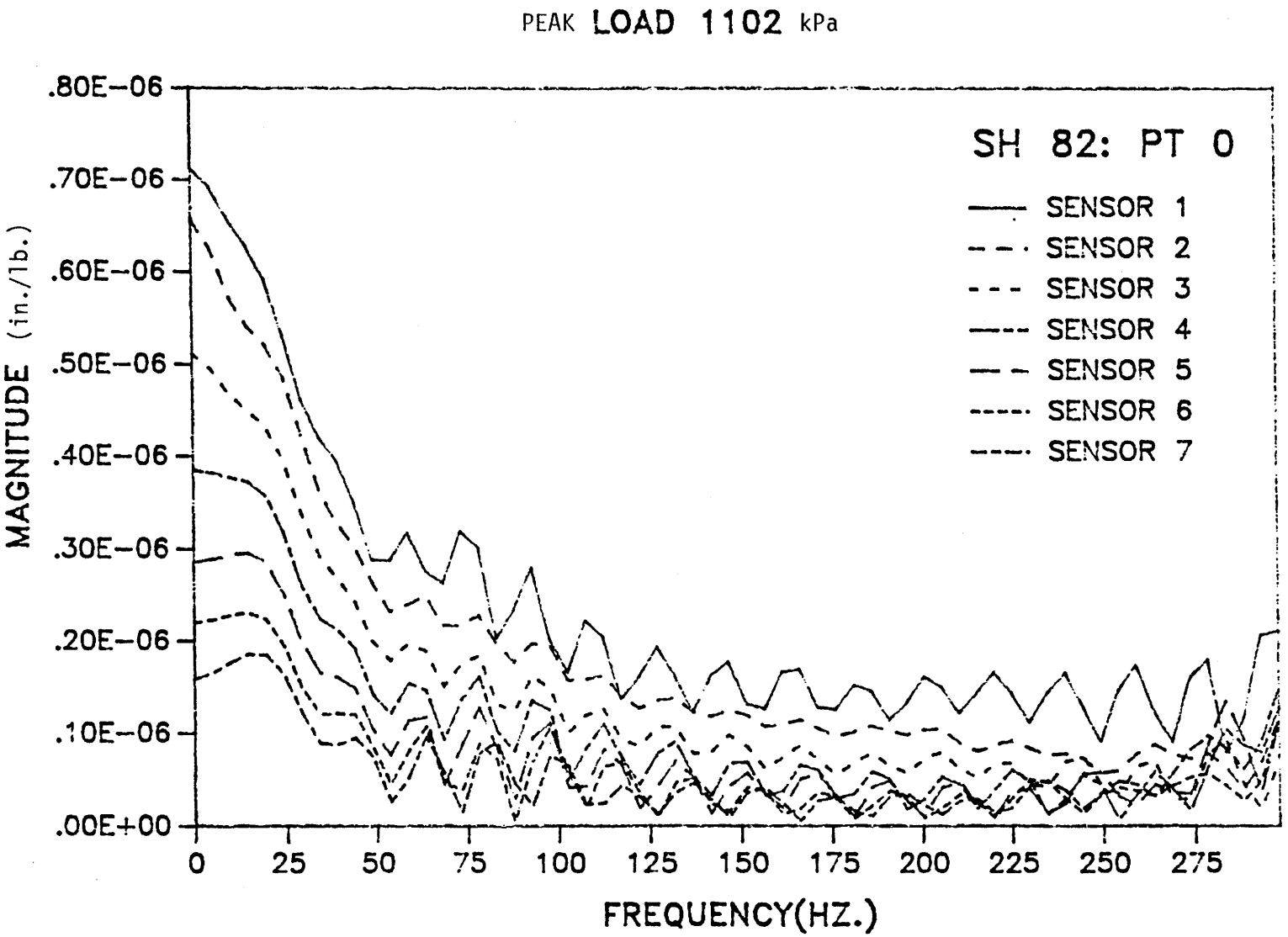

Figure B-7. Magnitude of frequency response function, 0-300 Hz, highest load.

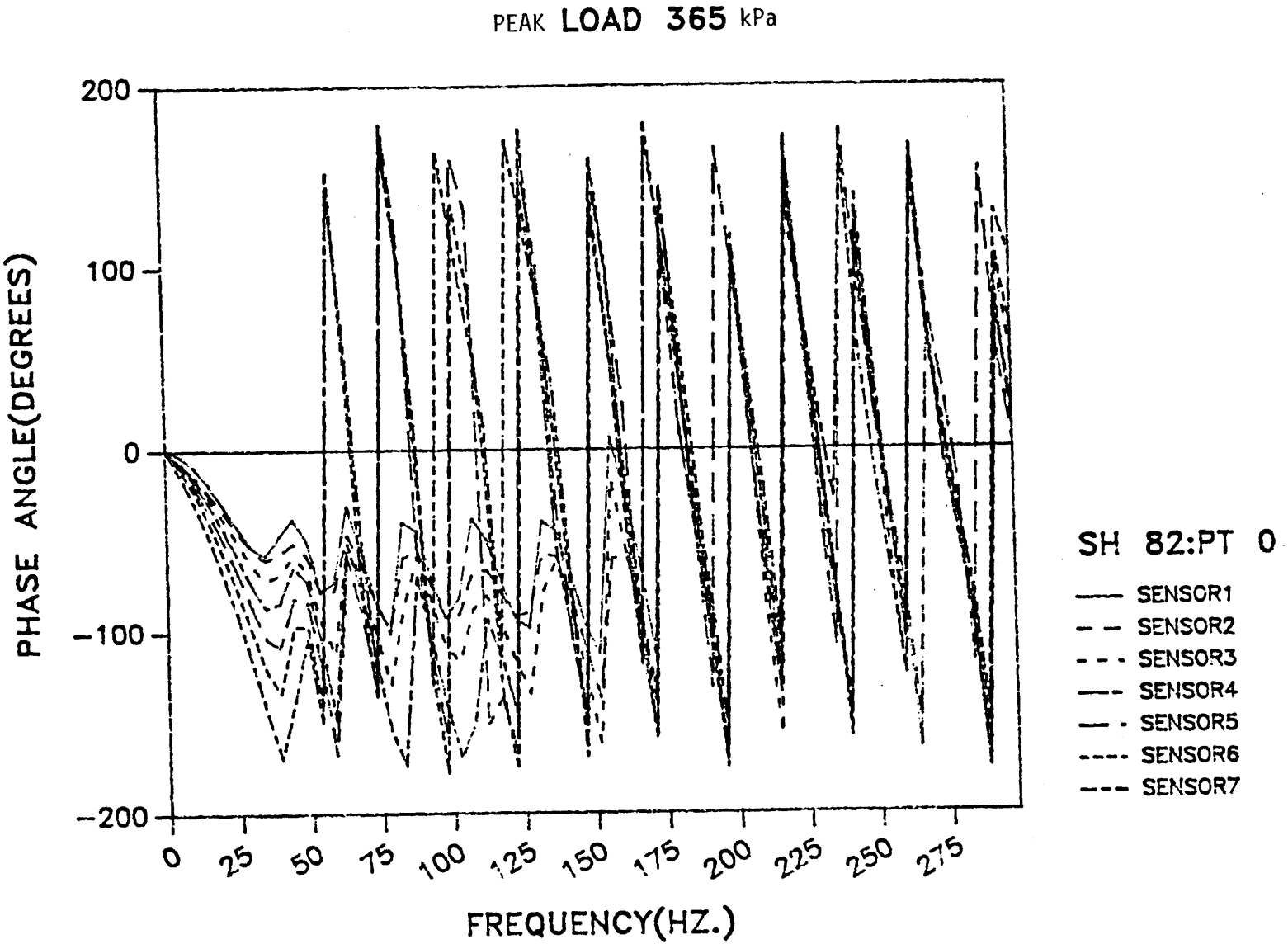

Figure B-8. Phase angle of response, 0-300 Hz, lowest load.

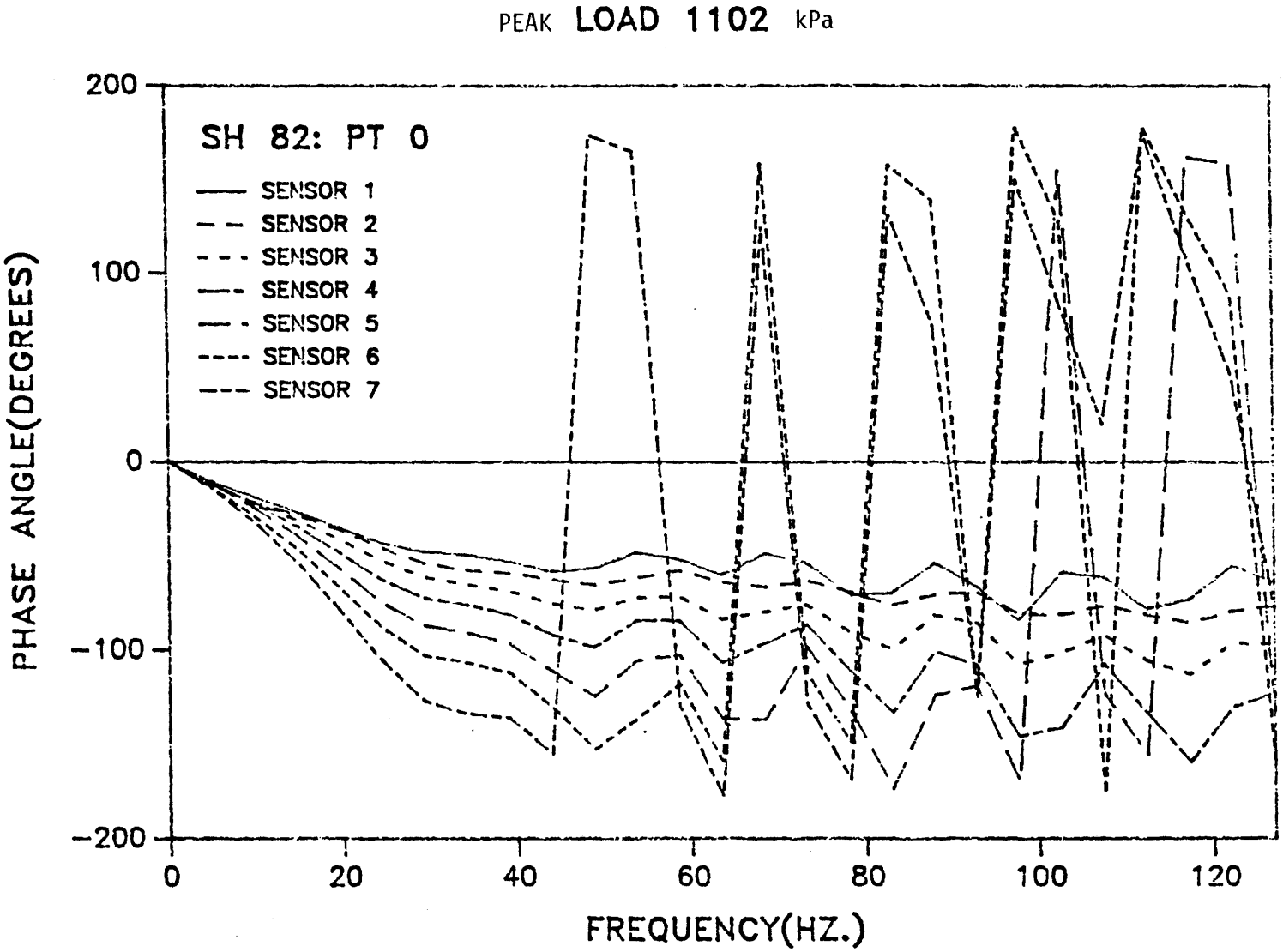

Figure B-9. Phase angle of response, 0-125 Hz, highest load.

APPENDIX C

LISTING OF DATA ANALYSIS PROGRAM

FOR FFT AND FREQUENCY-RESPONSE FUNCTIONS

```
C       THIS PROGRAMME IS TO COMPUTE FAST FOURIER TRANSFORMS AND
C       TRANSFER FUNCTIONS OF THE RAW FWD DATA
C_____________________________________________________________________
C
C       * DEFLECTPHASE.FOR
        COMPLEX TEMPX1(1024),TEMPX2(1024),TEMPX3(1024)
        REAL MAX,NTAN,MAG(1024,7),PHASE(1024,7),SENSOR(0:1023,7)
        REAL PI,R,T,TT
        DIMENSION ALOAD(0:1023),
     *  XIM(1024),X(0:1023),A(0:1023),TEMP(0:1023),XRE(1024),
     *  B(0:1023),TEST(0:1023)
        INTEGER ILOAD(0:1023),IENSOR(0:1023,7)
        OPEN(UNIT=5,FILE='S1H1924.DAT',STATUS='OLD')
        OPEN(UNIT=6,FILE='LLM1924.DAT',STATUS='NEW')
        OPEN(UNIT=7,FILE='LLP1924.DAT',STATUS='NEW')
        OPEN(UNIT=8,FILE='LLFT1924.DAT',STATUS='NEW')
C       OPEN(UNIT=9,FILE='D1924.DAT',STATUS='NEW')
C       OPEN(UNIT=10,FILE='S1924.DAT',STATUS='NEW')
C-----------------------------------------------------------------------
C       AK1 is to convert micron to 'mu' i.e. milliseconds i.e. 1/1000
c       AK2 is to convert KPa to Psi
c-----------------------------------------------------------------------
         N = 1024
        PI=3.1415926535891924
        MAX = -1.
        AK1 = .0001/2.54
        AK2 = 109.73/6.894757
        XMAX = 1023.
        XMIN = 0.
        YMIN = 0.
        YMAX = 1.
        r=0.
        t=0
        tt=0
        WRITE(6,*)'SH1924.DAT:point=0:LOWEST LOAD:N=1024'
        WRITE(7,*)'SH1924.DAT:point=0:LOWEST LOAD:N=1024'
        WRITE(8,*)'DATA FOR SH1924.DAT :point=0 :LOWEST LOAD:N=1024'
C       WRITE(9,*)'SH1924.DAT:point=0:LOWEST LOAD:N=1024'
C       WRITE(10,*)'SH1924.DAT:point=0:LOWEST LOAD:N=1024'
C       WRITE(6,111)
C111    FORMAT(2X,'FREQUENCY',10X,'FFTLOAD',10X,'FFTDEFLECTION')
        DO 220 I=0,299,2
C
          READ(5,*)ILOAD(I),IENSOR(I,1),IENSOR(I,2),IENSOR(I,3),
     *    IENSOR(I,4),IENSOR(I,5),IENSOR(I,6),IENSOR(I,7),ILOAD(I+1),
     *    IENSOR(I+1,1),IENSOR(I+1,2),IENSOR(I+1,3),IENSOR(I+1,4),
     *    IENSOR(I+1,5),IENSOR(I+1,6),IENSOR(I+1,7)
220           CONTINUE
C-----------------------------------------------------------------------
C       THE FOLLOWING STEP IS TO WRITE ALL THE DATA IN A SYSTEMATIC FASHION
C       IN A FILE
C-----------------------------------------------------------------------
C       DO 221 I=0,299
C       write(10,113)ILOAD(I),IENSOR(I,1),IENSOR(I,2),IENSOR(I,3),
C    *        IENSOR(I,4),IENSOR(I,5),IENSOR(I,6),IENSOR(I,7)
C113            FORMAT(5X,8(I6,3X))
C221    CONTINUE
C               ALOAD(299)=FLOAT(ILOAD(299))
C       DO 114 J=1,7
C114    SENSOR(299,J)=FLOAT(IENSOR(299,J))
C       WRITE(*,*)(ALOAD(299),SENSOR(299,J),J=1,7)
C-----------------------------------------------------------------------
C_____________________________________________________________________
C       ADJUSTING TAIL OF THE PULSE
C_____________________________________________________________________
        DO 223 I=0,299
```

```
        DO 222 K=1,7
C       T=(I-50)
C       TT=(299-50)
C       R=T/TT
        ALOAD(I)=FLOAT(ILOAD(I))
        SENSOR(I,K)=FLOAT(IENSOR(I,K))
C               ALOAD(I)=(ALOAD(I)-(ALOAD(299)*R))
C                       SENSOR(I,k)=(SENSOR(I,k)-(SENSOR(299,k)*R))
222        CONTINUE
C             write(9,111)ALOAD(I),SENSOR(I,1),SENSOR(I,2),SENSOR(I,3),
C     *        SENSOR(I,4),SENSOR(I,5),SENSOR(I,6),SENSOR(I,7)
C111          FORMAT(5X,8(F6.0,3X))
223     CONTINUE
c-------------------------------------------------------------------------------
C       ZERO PACKING:
C       -------------
c       the following loop is to put zeroes for load & sensor values after 300
c       i.e. after sixty milliseconds value,since we have data only until
c       sixty m.sec and we have defined n value to be larger than 300
c_______________________________________________________________________________
        DO 240 I = 300,N-1
           DO 230 J=1,7
                ALOAD(I) = 0.
                SENSOR(I,J)= 0.
230        CONTINUE
240     CONTINUE
C_______________________________________________________________________________
        DO 500 I=0,N-1
                TEMP(I)=ALOAD(I)*AK2
                TEMPX2(I+1)=CMPLX(TEMP(I),0.)
500     CONTINUE
        CALL FFT(TEMPX2,10)
C
        DO 110 J=1,7
        DO 120 I=0,N-1
                TEMP(I)=SENSOR(I,J)*AK1
                TEMPX1(I+1)=CMPLX(TEMP(I),0.)
120     CONTINUE
         CALL FFT(TEMPX1,10)
C-------------------------------------------------------------------------------
C       THE NEXT STEP IS TO WRITE TRANSFER FUNCTIONS OF LOAD AND
C       DISPLACEMENT FOR RAW DATA
C_______________________________________________________________________________
         DO 160 I=0,1023
                X(I+1)=I/.0002/1023
160     CONTINUE
        do i=1,1024
        write(8,*)x(i),tempx2(i),tempx1(i)
        end do
        DO 140 I=0,1023
C       IF (tempx1(i).EQ.0)  THEN
        IF (tempx2(i).EQ. 0) THEN
        GO TO 140
C       end if
        end if
        TEMPX3(I)=TEMPX1(I)/TEMPX2(I)
C_______________________________________________________________________________
              MAG(I,J)=CABS(TEMPX3(I))
        D1=AIMAG(TEMPX3(I))
        D2=REAL(TEMPX3(I))
C       MAY BE THIS:--  WRITE(7,*)D1,D2
        IF (D1.EQ.0)  THEN
        IF (D2 .EQ. 0) THEN
        GO TO 140
        END IF
        END IF
```

```
          PHASE(I,J)=ATAN2(D1,D2)
          PHASE(I,J)=(180.0*PHASE(I,J))/PI
140     CONTINUE
110     CONTINUE
C
C       THE MAX VALUE 'N' FOR I DEPENDS ON
C       (5000/1024)=(100/N)
C       E.G.FOR A FR OF 100, N=(100*1024/5000)
C
        DO 122 I=1,1024
                X(I+1)=I/.0002/1023
122      CONTINUE
         DO I=1,62
C        FOR MAGNITUDES
                 WRITE(6,900)X(I),(MAG(I,J),J=1,7)
900              FORMAT(F10.4,2X,7(E10.4,1X))
C        NOW FOR THE PHASE ANGLES
                 WRITE(7,920) X(I),( PHASE(I,J),J=1,7)
920              FORMAT(F10.4,2X, 7(F8.2, 1X))
         END DO
               STOP
         END
C
         SUBROUTINE FFT(X,M)
         COMPLEX X(1024),U,W,T
         N=2**M
         PI=3.1415926535891924
         DO 20 L=1,M
         LE=2**(M+1-L)
         LE1=LE/2
         U=(1.0,0.0)
         W=CMPLX(COS(PI/FLOAT(LE1)),-SIN(PI/FLOAT(LE1)))
         DO 20 J=1,LE1
         DO 10 I=J,N,LE
         IP=I+LE1
         T=X(I)+X(IP)
         X(IP)=(X(I)-X(IP))*U
10       X(I)=T
20       U=U*W
         NV2=N/2
         NM1=N-1
         J=1
         DO 30 I=1,NM1
         IF(I.GE.J) GO TO 25
         T=X(J)
         X(J)=X(I)
         X(I)=T
25       K=NV2
26       IF(K.GE.J) GO TO 30
         J=J-K
         K=K/2
         GO TO 26
30       J=J+K
         RETURN
         END
```